CYCLONE SCALE-UP AND RADIAL GAS CONCENTRATION PROFILES

BY

RANDY W. ENGMAN

B.A.Sc., The University of Calgary, 1986

A THESIS SUBMITTED IN PARTIAL FULFILLMENT OF

THE REQUIREMENTS FOR THE DEGREE OF

MASTER OF APPLIED SCIENCE

in

THE FACULTY OF GRADUATE STUDIES

Department of Chemical Engineering

We accept this thesis as conforming

to the required standard

THE UNIVERSITY OF BRITISH COLUMBIA

September 1990

In presenting this thesis in partial fulfilment of the requirements for an advanced degree at the University of British Columbia, I agree that the Library shall make it freely available for reference and study. I further agree that permission for extensive copying of this thesis for scholarly purposes may be granted by the head of my department or by his or her representatives. It is understood that copying or publication of this thesis for financial gain shall not be allowed without my written permission.

Department of Chemical Engineering

The University of British Columbia
Vancouver, Canada

Date 18/09/90

DE-6 (2/88)

ABSTRACT

A two part study was undertaken to explain the performance of cyclones operated in circulating fluidized bed combustion (CFBC) systems.

In the first part, collection efficiency tests were performed on a one-ninth scale polyacrylic cyclone model of the industrial scale cyclone at the 22 MWe CFBC facility at Chatham, New Brunswick. Emphasis was placed on scale-up considerations, loading effects, inlet geometry effects, and flow visualization trials. Experiments were performed at room temperature with inlet velocities between 3.7 and 5.5 m/s, solids loading between 0.05 and 7.5 mass solids/mass air with two different solids systems. There was disappointing agreement between the results from the Chatham unit, scaled according to Stokes Number scaling, and the findings obtained from the cold model unit. There was a minimum in the particle collection efficiency for particles of diameter 2.5 to 3.0 μm, apparently associated with agglomeration effects in the cyclone. Particle collection efficiency was found to increase with increased particle loading for the conditions studied. Changes in the inlet geometry gave inconclusive results. The experimental results were limited by problems associated with feeding and recycling the fines solids system used.

In the second part radial gas concentration profiles of a secondary cyclone serving the UBC pilot scale Circulating Fluidized Bed Combustor were performed at temperatures of about 870 °C. Concentrations of O_2, CO_2, NO_x, CH_4, CO and SO_2 were measured. An increase in [CO], and to a lesser extent [CO_2], was measured near the cyclone wall. There appeared to be little radial variation in the concentration of other species.

Further work is required to allow the cold model to operate continuously, with particles which can be fed more freely, and to obtain radial gas concentration profiles within the primary cyclone of the UBC CFBC system.

TABLE OF CONTENTS

List of Tables

LIST OF FIGURES

ACKNOWLEDGMENTS

I would like to acknowledge the immense help of my advisors Dr. John R. Grace, Dr. C. J. Lim, and Dr. Clive M.H. Brereton. Their time, energy, and personal commitment was central to the completion of this work. As well the staff of the Department of Chemical Engineering, The Pulp and Paper Center and other employees of the University of British Columbia provided colorful support throughout the progress of this work.

The financial support of Energy, Mines and Resources, and The New Brunswick Electric Power Commission is greatly acknowledged.

Finally I would like to thank my parents without whom this thesis would not have been completed.

INTRODUCTION

Cyclonic separators, generally simply called cyclones, have been used in gas cleaning operations for well over a century largely because they offer good particle collection efficiencies under extreme and varying conditions and are simple to design, fabricate, and operate. A good overview of various designs, applications can be found in reference 33. Although they have been replaced by more efficient devices in many pollution control applications, cyclones have been the subject of renewed interest for high temperature solids-gas separation in combined power cycles and within Circulating Fluidized Bed Combustor (CFBC) applications. It was because of particle collection efficiency problems encountered in one such application (1), the Chatham Circulating Fluidized Bed Demonstration Project, a 22 MWe CFBC electric generation facility in New Brunswick, that the present study was undertaken.

In spite of the simplicity of cyclonic separators, it is still not possible to predict from fundamental principles particle collection efficiencies for all geometries and operating conditions. A great deal of work has been done to develop equations and models to predict cyclone performance for certain standard geometries (Eg. Stairmand and Lappel designs) under conditions of low solids loading and low temperature. However, little work has been done to validate these equations and models for extreme conditions of temperature and particle loading. Also, little work has been done to verify the models

for cyclones of large industrial scale. Thus there is a need to establish scaling criteria to predict the operation of high temperature, high loading, large cyclones from the operation of lab scale models.

This thesis is divided into two parts. Part A deals with collection efficiency tests and considerations of scale-up. Part B considers measured combustion gas concentration profiles within a high temperature cyclone serving a pilot scale CFBC system and was intended to provide data for further research in the CFB field. The objectives of the two parts are as follows:

Part I. Collection efficiency and scale-up studies.

Firstly, to examine scale-up considerations by comparing the performance of a cold model cyclone to a large industrial high temperature cyclone. Secondly, to demonstrate the effect of solids loading on solids capture efficiency by means of laboratory experiments on a cold model cyclone. Thirdly to examine the effect of inlet modifications on capture efficiency. Lastly to perform visualization of particle flows within a cyclone.

Part II. Gas concentration profiles within a secondary cyclone of a CFBC.

To measure and report combustion gas concentration profiles within a secondary cyclone of a pilot scale CFBC facility.

For each of parts A and B, a discussion of previous related work and theory is followed by a brief description of the apparatus and experimental procedure. Experimental findings are then presented and discussed and conclusions are drawn.

PART I

COLLECTION EFFICIENCY TESTS

1.1 BACKGROUND AND THEORY

1.1.1 Introduction

Cyclones are examples of inertial separating devices. The particle collection efficiency, that is the mass ratio of particles caught to those fed within a given size range(6), is often expressed by a collection or grade efficiency curve. Ideally the designer can predict cyclone performance, and thus the collection efficiency curve for all sizes of particles from first principles, or lacking that, from accurate empirical relationships. Unfortunately this is not always possible, as the gas and particle behaviour is not well enough understood to predict particle trajectories under all circumstances. Nor is it always possible to rely on empirical relationships, as they are design-specific and offer good accuracy only when standard designs are considered. See reference 6 for a comparison of published data and empirical relationships. Thus there is a need for cold modeling and for valid scaling criteria (13). The work described in this thesis is of benefit for the consideration of large, high temperature and non-standard cyclones with tangential inlets.

1.1.2 DIMENSIONAL ANALYSIS AND PHYSICAL SIMILARITY.

Applying the principles of dimensional analysis to the problem of cyclone particle collection performance requires a complete list of the physical quantities controlling the fate of particles within a cyclone. These parameters can be divided into four groups: (i) those describing the cyclone itself, (ii) the operating parameters, (iii) properties of the particles being separated, and (iv) properties of the gas which carries the solids. Table 1.1 lists the most important variables.

Table 1.1 List of important parameters

Cyclone dimensions:

Body diameter	D
Inlet depth	a
Inlet width	b
Outlet diameter	D_o
Outlet length	L_o
Cylinder length	L_{cy}
Overall height	H_o
Bottom diameter	D_b

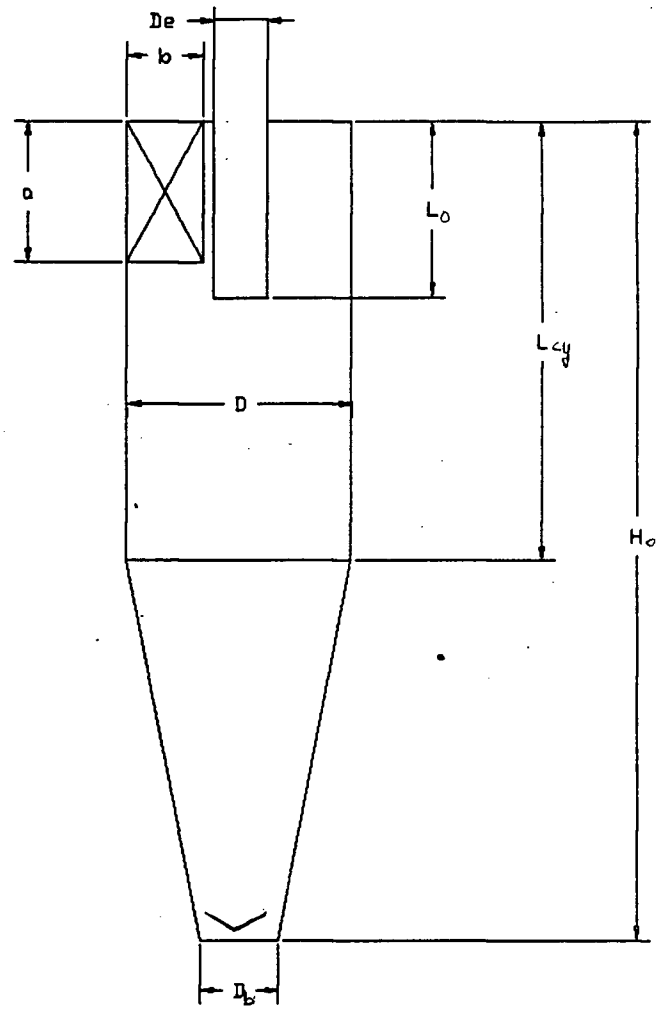

Operating parameters:

Inlet velocity	V_i
Gas split ratio	Q_c
Loading Ratio	L_p
Relative acceleration (centrifugal/gravitational)	A_c/A_g

Particulate characteristics:

Particle diameter	d_p
Particle density	ρ_p
Shape factor	(x)

Gas characteristics:

Gas density	ρ_g
Gas viscosity	μ_g

The seventeen variables listed above do not provide a complete list, as other variables may be important. For example surface roughness may play a role and the smooth polyacrylic surface of the scale model is not similar to the refractory lining of the high temperature Chatham cyclone. This is neglected. If, however, the dimensional analysis is limited to one geometric configuration or cyclone design, only one of the first eight need be considered since geometric similarity applies between the cold model and the Chatham cyclone being modeled. With ten individual variables and three fundamental dimensions (mass, length, time), there are seven independent dimensionless groups requiring separate consideration. The analysis can be simplified further if one assumes that the split ratio, i.e. the fraction of gas leaving by way of the underflow, is negligible and that there is similarity of shape factor for the solids systems considered. In addition if the relative acceleration is large in both cases (i.e. $A_c/A_g > 10$) this factor can be neglected as well. With these simplifications, four dimensionless groups are required.

The most common independent groupings of the remaining variables listed above are:

Flow Reynolds number $N_{REf} = p_g D V_i / u_g$ (1-1)

Density ratio $N_p = p_p / p_g$ (1-2)

Stokes number $N_{st} = d_p^2 V_i p_p / (D u_g)$ (1-3)

Loading ratio $L_p = \frac{\text{mass solids flow}}{\text{mass gas flow}}$ (1-4)

In addition to maintaining geometric similarity it is desirable to have kinematic and dynamic similarity. Kinematic similarity is similarity in motion, which implies that the paths that representative particles follow are geometrically similar and are travelled in a consistent, scaled period of time (20). Thus particle accelerations must also be similar (20). Dynamic similarity involves similarity of forces. In order that the two systems under comparison be dynamically similar, the magnitude of forces at each point must also be similar (20). It is commonly impossible to satisfy all requirements simultaneously. Thus ones of lesser importance are often sacrificed in order to assure similarity of others. In cyclones operating at high flow Reynolds numbers (i.e. high inlet velocities), centrifugal, as opposed to gravitational, are thought to dominate the motion of smaller particles. In situations where the viscous and inertial forces are most significant the flow Reynolds number may be used to compare experimental observations, provided the conditions of geometric similarity are met (20). However, it would be incorrect to assume that, after the onset of turbulent flow in cyclones, collection efficiency is independent of Reynolds number. In fact the contrary was found, i.e. collection efficiency is found to vary with the helical turbulent intensity (34). Thus the Stokes number, combined with geometric and Reynolds number similarity, may be used in the scaling process.

1.1.3 FLUID - PARTICLE SEPARATION CYCLONIC SEPARATORS

Before reviewing previous works on the subject of scale up of cyclone performance, it is useful to develop an equation describing particle capture, in order to demonstrate the relevance of the key parameters. This simplistic description makes some questionable assumptions and is only intended to introduce the effects of various parameters on collection efficiency.

Consider the fate of a particle of diameter d_{crit} that is caught with 50% efficiency in a cyclone of diameter D with an tangential entrance way having width b and height a. We make the following assumptions (5):

1. Particles move independently of one another.
2. The drag on the particle can be described by Stokes law regime expression.
3. Buoyancy and gravity effects are negligible.
4. The tangential velocity of the particle is constant and equal to the inlet velocity.
5. Secondary effects such as re-entrainment from the walls, eddy currents, etc. are negligible.
6. Laminar flow conditions.
7. Relaxation time is negligible.
8. Particles separate at constant velocity
9. Once at the wall particles have negligible chance of reentrainment.

10. Particles must reach the wall by moving across a gas stream, which retains its shape after entering the cyclone.

Upon entering a cyclone particles are acted on by a centrifugal force equal to $F_c = mV_i^2/R$ where:

m = particle mass

V_i = tangential particle velocity

R = radial coordinate of the particle.

$$F_c = \pi d_{crit}^3 \rho_p V_i^2/6R \qquad \text{centrifugal force} \quad (1\text{-}5)$$

This force accelerates the particle towards the wall. Opposing this motion is the drag force:

$$F_D = (C_D A_p \rho_g V_p^2)/2 \qquad (1\text{-}6)$$

where V_p is the particle's radial velocity component. The drag coefficient can be obtained by neglecting inertial terms in the Navier - Stokes equation for a rigid sphere in an unbounded fluid (5) i.e.

$$C_D = \text{drag coefficient} = 24/N_{Rep} = 24\mu_g/(\rho_g V_p d_{crit}) \quad (1\text{-}7)$$

In this simplified explanation, the particle must travel a radial distance b during a residence time defined by the time needed to travel a circular path of distance πDN in order to be

collected. If not it will enter a zone near the bottom of the cyclone where the radial gas velocity is much higher than in the separation zone (See Figure 2.3). The particle motion is thus:

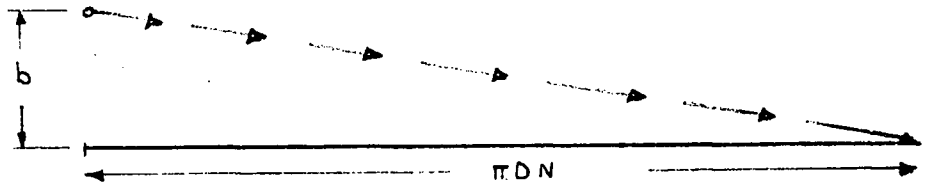

Substituting for C_D, $A_p = \pi d_{crit}^2 /4$, the drag force is seen to be:

$F_D = 3\mu_g d_{crit} V_i b/DN$ Stokes law resistance (1-8)

where:

b = entrance width

N = Number of revolutions

Equating expressions 1-5 and 1-8 allows prediction of particle cut diameter as follows:

$F_c = F_D$ (1-8a)

$\pi d_{crit}^3 \rho_p V_i^2 /6R = 3\mu_g d_{crit} V_i b/DN$ (1-8b)

$d_{crit}^2 = 18\mu_g bR/(\pi \rho_p DNV_i)$ (1-8c)

letting $R = D/2 - b/2$ such that $b = D - 2R$

$d_{crit}^2 = 18\mu_g R(D - 2R)/(\pi \rho_p DNV_i)$ (1-8d)

$d_{crit}^2 = 18\mu_g R(1 - 2R/D)/(\pi \rho_p NV_i)$ (1-8e)

or

$$d_{crit} = 3\left[\frac{2\mu_g R}{\pi \rho_p V_i N}(1 - 2R/D)\right]^{0.5} \quad (1\text{-}9)$$

This equation has generally the right form as cyclone experiments have shown (6) that collection efficiency improves with :

1. Increasing particle density.
2. Increasing cyclone vortex speed (i.e. V_i)
3. Decreasing cyclone diameter.

However as one would expect, such simplified descriptions have limitations and do not describe performance for all conditions. The effect that each parameter has been found to have on collection efficiency will now be considered. Particle loading is considered separately in section 1.1.4.

Inlet velocity

Collection efficiency has been found experimentally to increase with gas inlet velocity in several studies

(7,8,9). Increasing inlet velocity increases tangential velocity thereby improving separation. These improvements are not without limit, however, as secondary effects such as particle re-entrainment and eddy currents work to offset collection efficiency at higher V_i. The length of the gas vortex which exists below the vortex finder is a function of inlet velocity and cyclone geometry . The vortex end is experimentally defined as the position where the vortex core seeks the wall (16). Increasing V_i lengthens the vortex until the end interferes with the wall causing re-entrainment of the particles already caught, thus causing a reduction in collection efficiency. The observed peak in curves of efficiency vs V_i have been successfully delayed with the addition of an inverted cone, located axially above the solids exit (14, 15). The inverted cone is thought to anchor the vortex end and prevent it from reentraining particles at the wall. See drawing on Table 1.1 for an example of this cone.

Particle density

As stated above the centrifugal force is proportional to particle mass and hence to particle density. Theoretically collection efficiency is proportional to $\rho_p^{0.5}$. However, experimentally this is not confirmed (10).

Gas Viscosity and Density.

Particle motion is resisted by the viscous drag. For low particle Reynolds numbers, ($10^{-5} < \rho_g d_p V_p / \mu_g < 0.1$) (where V_p = particle velocity relative to the gas), viscous effects dominate and Stokes law can be used to predict individual particle behaviour in a gas. This is of particular importance in the discussion of scaling the performance of large cyclones at high temperature by small cold models. Particles separated in hot cyclones do so at lower particle Reynolds numbers (considering similar size, density and velocity) than those in cold models because of increased gas viscosity and reduced gas density.

1.1.4. PREVIOUS CYCLONE SCALING WORK

One of the first works on the subject of scaling cyclone performance was presented by Stairmand (2) in 1951. The following method for predicting performance of geometrically similar cyclones operating under varying conditions was proposed. To find the size of the dust caught with the same efficiency as the test dust, multiply the test dust size by:

$$\sqrt{\frac{\text{density of the test dust}}{\text{density of the new dust}}} \qquad (1\text{-}10)$$

$$\sqrt{\frac{\text{test flow}}{\text{new flow}}} \qquad (1\text{-}11)$$

$$\sqrt{\frac{\text{new viscosity}}{\text{test viscosity}}} \qquad (1\text{-}12)$$

$$\sqrt{\frac{\text{diameter of the new model}}{\text{diameter of the test model}}} \qquad (1\text{-}13)$$

These relations combined from the Stokes number N_{St} and imply that collection efficiency is a function of N_{St} only for a given geometry. Stairmand was careful to limit this scaling procedure to density differences within the ranges 1000 - 4000 kg/m^3. For cyclone diameter, the method is not recommended "without some experimental confirmation". Indeed mention is made of less than expected performance with cyclones of diameter greater than 1.22 m diameter.(2)

Other attempts have been made to correlate capture efficiency with dimensionless groups and thus provide a scaling basis. Parker et al. (11) performed experiments on a 50 mm diameter cyclone at a relatively low inlet velocities (5 m/s) at temperatures up to 700 °C, and pressures up to 25 atm. Data were plotted on a log log plot of d_{pa} vs $(N_{St})(N_{RE})^{0.5}$, the terms were defined as follows:

$$d_{pa} = d_p (C' p_p)^{0.5} \ (g/cm^3)^{0.5} \qquad (1\text{-}14)$$

$$N_{St} = C' d_{pg}^2 \ p_p \ V_i / (9 u_g D_H) \qquad (1\text{-}15)$$

$$N_{RE} = p_g \ D \ V_i / \ u_g \qquad (1\text{-}16)$$

where C' = Cunningham correction factor
p_p = particle density g/cm^3

$$D_H = 2ab/(a+b) \qquad (1\text{-}17)$$

Note that the particle diameter in the Stokes number d_{D50} refers to the mass median diameter of the feed aerosol used in his study and that D_H is the hydraulic diameter of the cyclone inlet . For the small cyclones under consideration the

resultant plot was nearly linear. See Figure 1.1a. Also noted in this study was a minimum collection efficiency phenomenon, occurring generally between 2 and 4 microns. This was attributed to the breaking up of agglomerated particles during sample preparation for particle analysis.

By examining the performance of two 1.2 m dia. "Stairmand high efficiency" cyclones used in series within a pressurized fluidized bed combustor, Wheeldon et al.(12) were able to plot grade efficiency curves for both the primary and secondary cyclones. The tests were done under conditions of high loading (50 g/m^3), temperatures of 640 to 910 °C and pressures of 6 and 12 bar. The authors compared their data, obtained in a relatively large cyclone, to the Stairmand data (2) obtained in small (31.5 mm dia.) cyclones. The comparison of Stokes numbers for particles caught with 50% efficiency is:

FBC primary $N_{Stk50} = 4 \text{ to } 10 \times 10^{-5}$

FBC secondary $N_{Stk50} = 8.6 \text{ to } 19.6 \times 10^{-5}$

Stairmand $N_{Stk50} = 9.4 \times 10^{-5}$

The author attributed the deviations to particle loading effects and concluded that standard expressions are sufficient to describe cyclone performance under elevated pressures and temperatures. Also observed in this study was a "fish hook" shaped collection efficiency curves which shows improved collection for smaller particles. (See Figure 1.1b). This effect was attributed to particle agglomeration within the cyclones of smaller particles on to much larger ones. Analysis

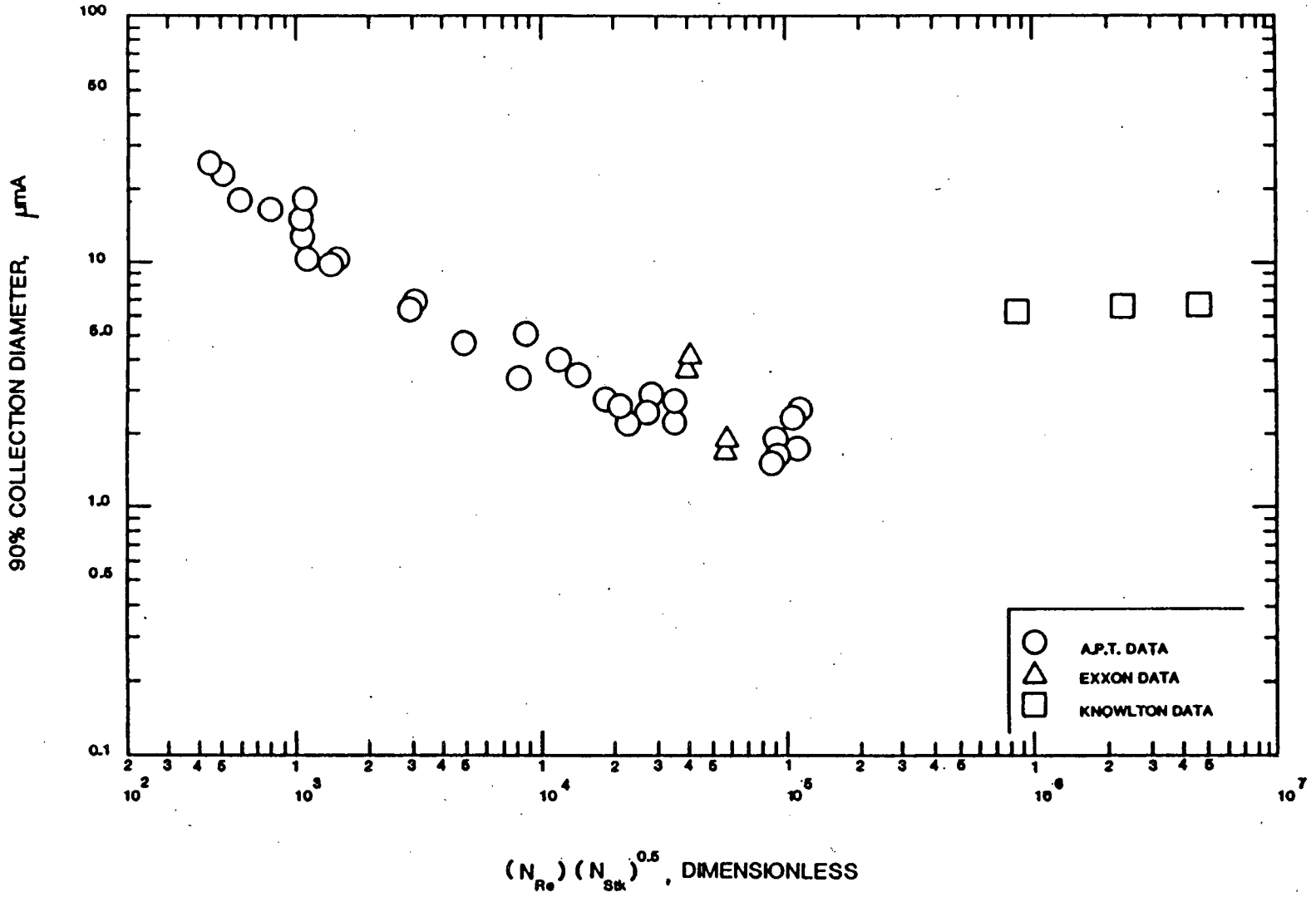

FIGURE 1.1a Collection Efficiency vs. $(N_{REP})(N_{ST})0.5$ (11). Conditions: D = 50 mm, temperatures between 20 and 693 °C, pressures between 140 and 2500 kPa, inlet velocities between 0.18 and 5.2 m/s, dust loadings between 0.04 and 9.56 g/m³.

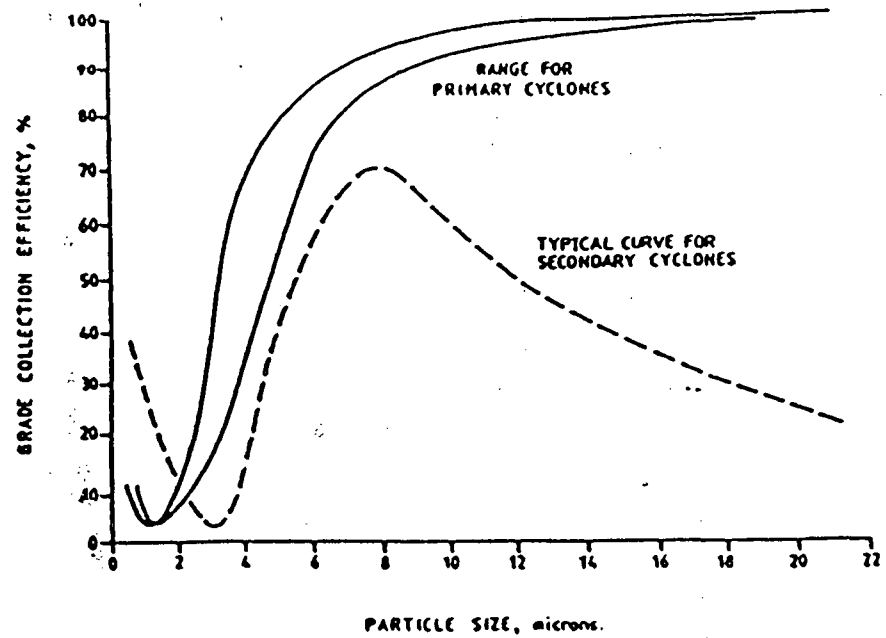

FIGURE 1.1b Collection efficiency curves with "fish hook" shape for primary and secondary cyclones(12). Conditions: D = 1.2 m, temperatures between 640 and 900°C, inlet velocities between 16.3 and 27.4 m/s, dust loadings between 1.5 and 140 g/m³.

procedures of the particles caused some disassociation and suggested higher collection efficiencies for the fines. This effect was also noted by Parker et al.

In an attempt to explain performance from a wide variety of cyclone designs operated under industrial conditions (160 < D < 1600 mm, 20 < temperature < 950 °C) Abrahamson and Allen (21) plotted capture efficiency vs a dimensionless particle diameter, $S^{0.5}$, defined as :

$$S^{0.5} = [V_{rp}/V_{rg}]^{0.5} \qquad (1\text{-}18)$$

where

V_{rp} = Radial particle velocity

V_{rg} = Radial gas velocity

These last two quantities are evaluated at a radial position R = $D_o/2$ just below the vortex finder. (See Figure 1.2a) V_{rg} is assumed to be constant over an imaginary cylinder, of radius R_x, extending from the lip of the vortex finder to a point on the cone having a diameter equal to that of the vortex finder. V_{rp} is calculated for the experimental data using the Abraham drag coefficient expression (16) which accounts for non - Stokesian fluid-particle behavior up to a particle Reynolds number of 6000 and gives V_{rp} without repetitive calculations.

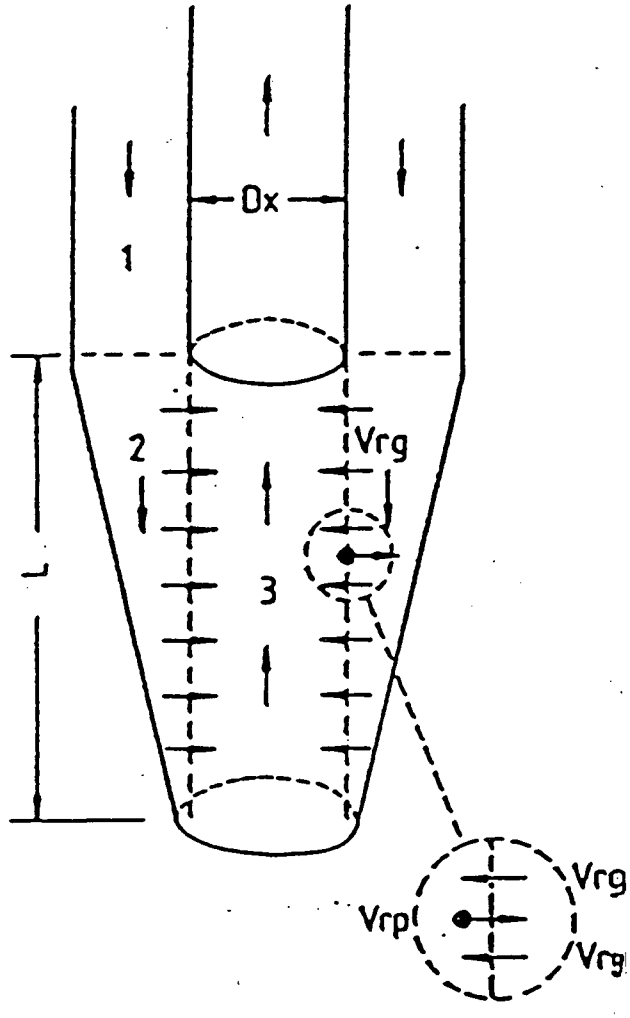

FIGURE 1.2 a. Gas and particle flow across imaginary cylinder, (21)

The procedure followed was:

1. Calculate G_a:

$$G_a = [\rho_g U_x^2 d_p^3 \rho_p]/(R_x \mu_g^2) \qquad (1\text{-}19)$$

where U_x = tangential gas velocity at R_x, assumed to be constant and equal to the inlet velocity.

2. Calculate N_{Rerp} (Reynolds number for radial particle motion):

$$N_{Rerp} = 20.5[(G_a^{0.5}/9.61 + 1)^{0.5} - 1]^2 \qquad (1\text{-}20)$$

3. Calculate V_{rg} from N_{RErp}.

Particles which have an equal chance of being caught or lost (i.e. d_{p50}) should on average move towards the gas exit as often as to the wall and thus the ratio V_{rp}/V_{rg} should have a value equal to one. The plot shows better agreement at the d_{p50} position than at other points along the grade efficiency curve (see Figure 1.2 b), a factor the authors attribute to differences in cyclone geometry which give different particle re-entrainment characteristics. The analysis is said to be limited to low concentrations of dust (less than 10 g/m^3), and to return flow designs with rectangular slot entries.

1.1.5 Loading effects on cyclone collection efficiency

Improved particle collection efficiency for cyclones operating at high dust loadings has been noted by several workers. (2,3,6,7,11,13,). Perhaps the most comprehensive description of this effect is detailed in an efficiency vs. loading plot published by the American Petroleum Institute

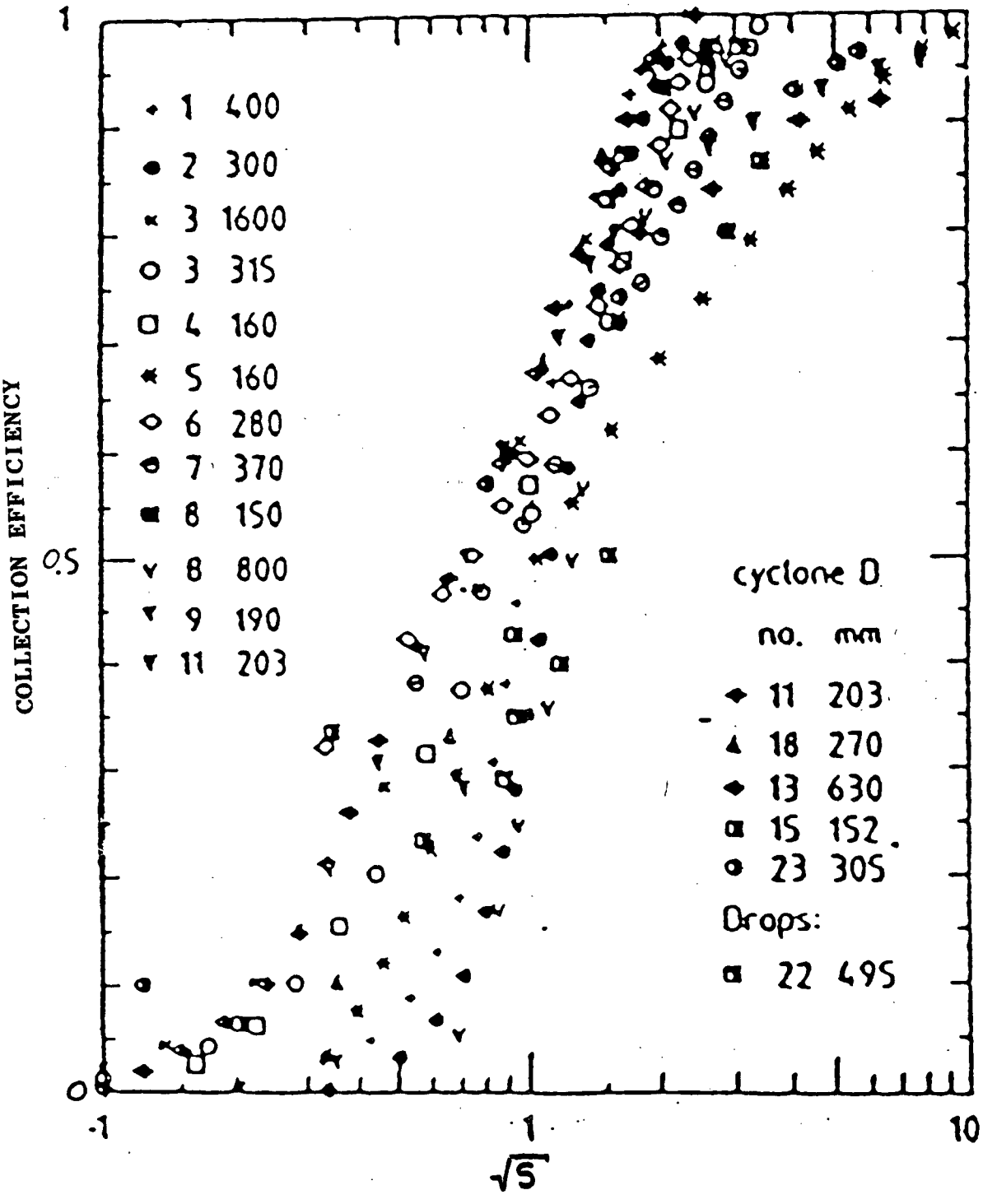

FIGURE 1.2 b. Experimental grade efficiency as a function of $(S)^{0.5}$ (dimensionless particle diameter) for industrial sized cyclones in air at room temperature (21).

(API)(17), reproduced in Figure 1.3 (13). A clear increase in capture efficiency with loading is noted. The influence of loading is seen to be greater for cyclones operated at lower " zero load E_o" efficiencies than for those with very efficient E_o. This effect is attributed to a scrubbing effect of large particles on finer particulate and has been accounted for in several ways. An excellent discussion of the mechanisms considered to be responsible is given by Mothes and Löffler (24). They point out that in spite of the observed reduction in particulate tangential velocity (and thus separating force) collection efficiency increases with increasing loading. They attribute the effect to agglomeration mechanisms. Figure 1.4 plots the expected collection efficiency for small particles (1 to 4 μm) as separated by larger particles (15 μm).

Briefly the "scrubbing effect" is a process whereby smaller particles are forced towards the wall because of the motion of larger particles which are separating out at a higher velocities. Either through direct impact with the larger particle (and the formation of a larger separating mass) or by entrainment in the flow field behind the larger particle, the smaller particle moves toward the cyclone wall with an increased velocity.

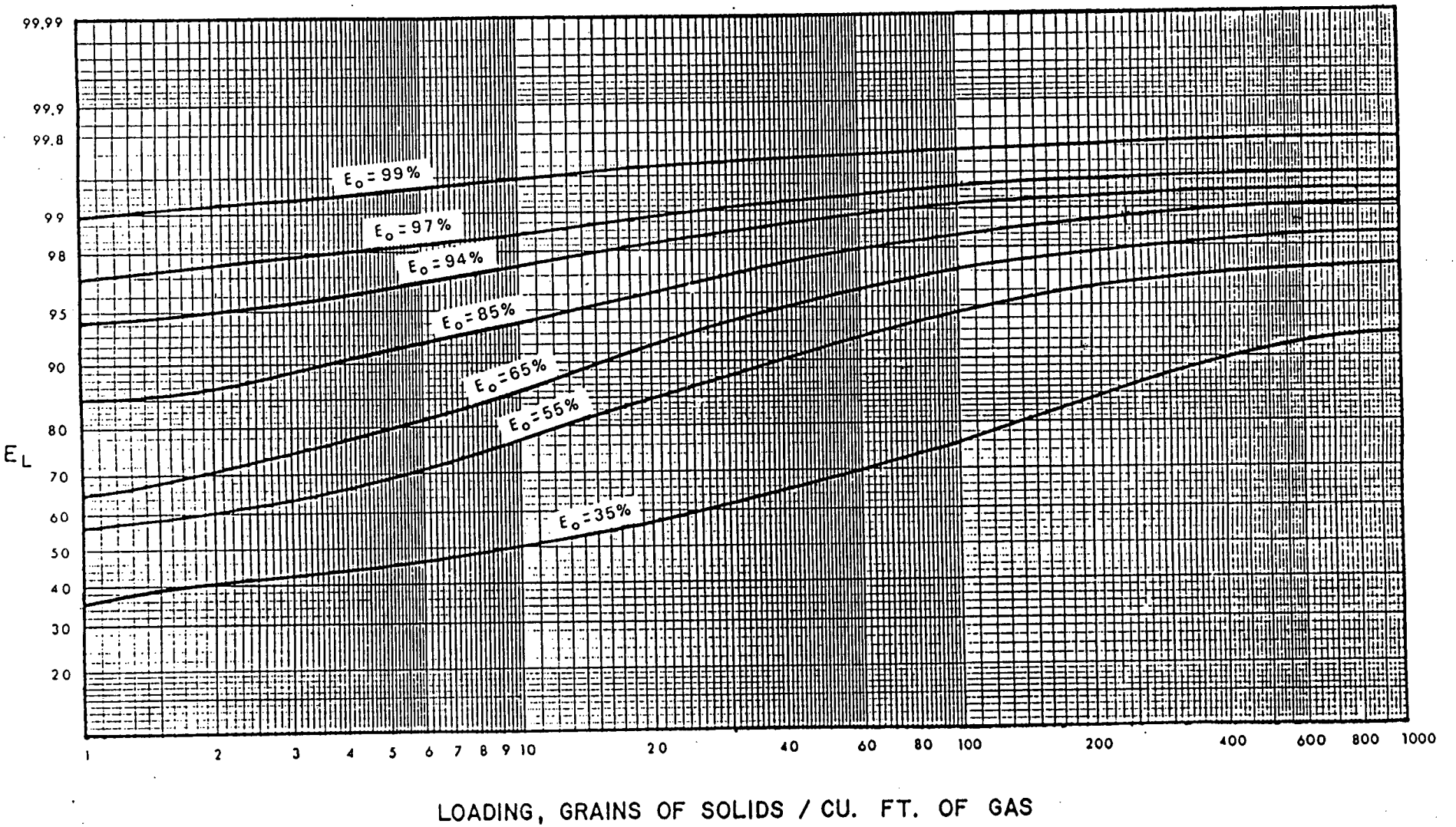

FIGURE 1.3 Loading effect on cyclone collection efficiency. Cyclone diameter up to 3.65 m diameter. E_o is zero load (less than 1 grain/ft^3) loading, E_L is higher loading efficiency. (18)

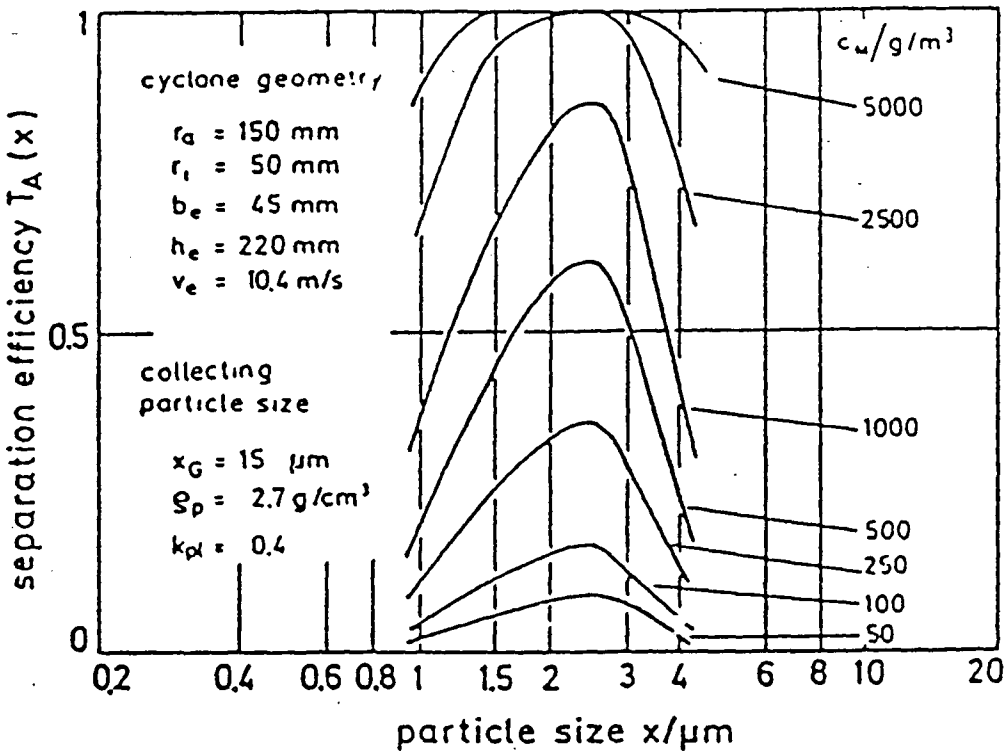

FIGURE 1.4 Predicted separation efficiency of fine particles swept out of the gas by large particles due to agglomeration (24).

$T_A(x)$ = predicted colection efficiency
r_a = cyclone radius,
k_{pl} = restitution coefficient.
r_i = vortex finder radius
b_e = inlet width
h_e = inlet depth
V_e = inlet velocity
x_G = mass median particle diameter
ρ_p = particle density

c_M = solids loading g/m³

An empirical expression proposed by Ogawa (22) for the effect of dust loading in conventional cyclones has the form (modified to give efficiency in %):

$$\text{efficiency}(\%) = 100 - b_1[\exp(-k_1 C_o)]100 \qquad (1\text{-}21)$$

where

b_1 = 0.032 dimensionless

k_1 = -.0157 dimensionless

C_o = dust loading (g/m^3)

for a 90 mm diameter cyclone operated with flyash with between 14 and 16 m/s. The negative value for k_1 accounts for a decrease in efficiency as C_o increases noted in experimental data of this author, contrary to the effect noted by other workers. For cyclones with an axial inlet geometry, collection efficiency was found to increase with loading.

Another empirical relationship was proposed by the API(17) in 1955 of the form:

$$\text{efficiency} = 100 - (100 - e_o)[c_o/c_a]^{0.2} \qquad (1\text{-}22)$$

Here the subscript 'o' refers to low loading conditions arbitrarily taken as 1 gr/ft^3 (2.3 g/m^3). Another correlation from the API (18) was of the form:

$$P(E) = P(E_o) + A \log L \qquad (1\text{-}23)$$

where A is the slope of the nearly linear curves relating P(e) and L and was empirically fitted by a polynomial as follows:

$$A = 0.67 - 2.11*E_o + 5.63*E_o^2 - 4.00*E_o^3 \qquad (1\text{-}24a)$$

and L the dust loading in expressed grains/ft^3. P(e) and P(E_o) are the probabilities associated with the collection efficiencies at high and low loading respectively, i.e. the fraction passing the cyclone at a given loading. These probabilities can be approximated by the log of [(1-x)/x] as:

$$\text{(Catch probability)} = [1 - \text{pass probability}]$$

$$= [1 - P(x)] \qquad (1\text{-}24b)$$

$$= [\ 1 - \log[(1-x)/x]\ ] \qquad (1\text{-}24c)$$

such that

$$[\ 1 - \log[(1-E)/E]\ ] =$$

$$[\ 1 - \log[(1-E_o)/E_o]\ ] + A\log(\ L\ ) \qquad (1\text{-}24d)$$

$$\log[(1-E)/E] = \log[(1-E_o)/E_o] - \log L^A \qquad (1\text{-}24e)$$

$$= \log[(1-E_o)/E_o L^A] \qquad (1\text{-}24f)$$

$$[(1-E)/E] = [(1-E_o)/E_o L^A] \qquad (1\text{-}24g)$$

$$[1/E - 1] = [(1-E_o)/E_o L^A] \qquad (1\text{-}24h)$$

$$E = E_o L^A/[E_o L^A + 1 - E_o] \qquad (1\text{-}24i)$$

such that

$$\ln(1-E) = \ln[(1-E_o)/(1 + E_o[L^A-1])] \qquad (1\text{-}25a)$$

Mansin and Koch(23) developed a correlation that accounted for the change in efficiency by modifying the effective viscosity of the gas as:

$$\mu_{g\,app} = \mu_g[1 + 0.09\log L + .02(\log L)^2]. \quad (1\text{-}25b)$$

(note log base 10 in equation 1-25b)

The model took the form:

$$\ln[(1-E)(1+E_o[L^A - 1])^{0.5}] =$$

$$-2.3\,SFACTOR[N_{ST}(n+1)A_i G/(LFAC2D_c^2)]^{(0.41/(n+1))} \quad (1\text{-}26)$$

where:

E = collection efficiency

E_o = low loading efficiency as determined by:

$$\ln(1 - E) = 2[[N_{ST}(n+1)/(A_i/2D_c^2)G]^{(0.5/(n+1))} \quad (1\text{-}27)$$

L = L loading gr/f^3

$SFACTOR = [(V_i/V_s)/2.5]^{0.41}$ for $V_i/V_s < 2.5$

$SFACTOR = [(V_i/V_s)/2.5]^{-0.31}$ otherwise

V_s = particle saltation velocity

N_{st} = Stokes number

A_i = Inlet area

G = cyclone configuration parameter.

$LFAC = 1 + 0.09\log_{10}L + .02(\log_{10})^2$

D_c = Cyclone diameter

n = Vortex exponent

This is actually the Leith and Licht (12) model with modifications for particle saltation and loading effects.

Figure 1.5 compares the Leith and Licht equation with and without these modifications.

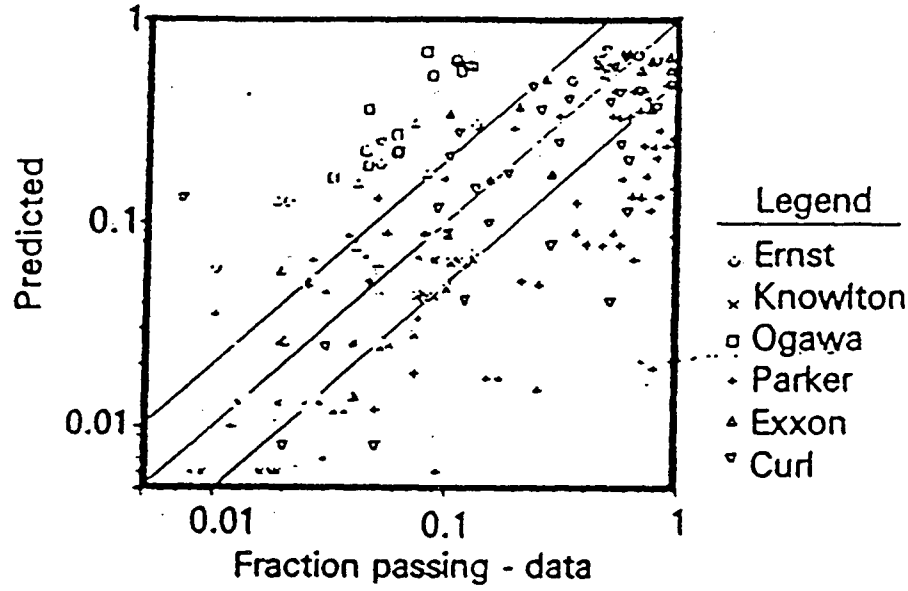

a.) Leith/Licht model without corrections.

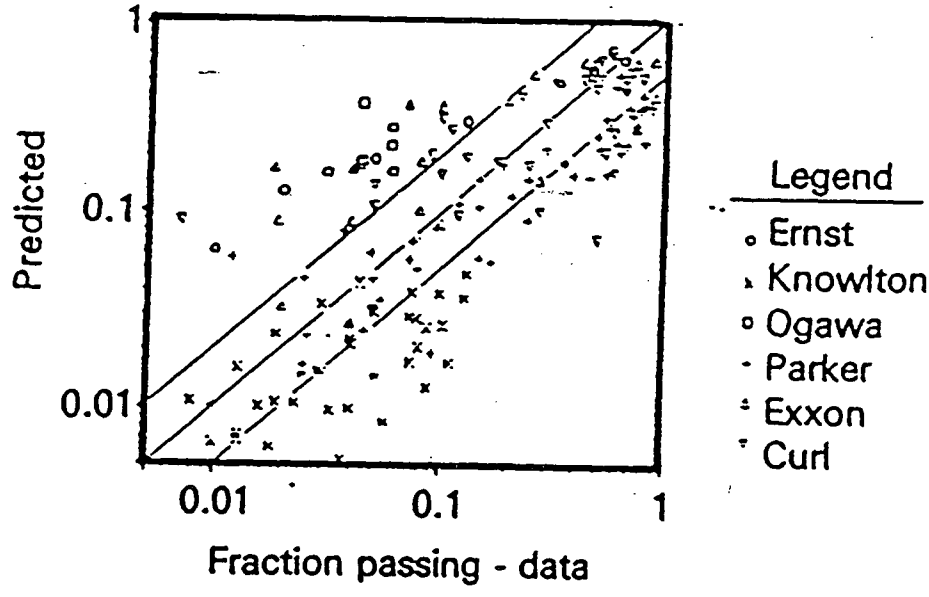

b.) Leith/Licht model with loading and saltation corrections.

Figure 1.5 Leith and Licht correlations with and without loading and saltation corrections. Conditions: D = 0.05 and 0.91 m, temperatures between 20 and 850 °C, inlet velocities between 1.8 and 46 m/s, dust loadings from 0.43 and 4450 g/m³. (25)

1.1.6. Summary

When describing fluid particle separation processes in cyclones it has been found necessary to include other parameters besides the Stokes number. Particle loading and secondary effects such as particle re-entrainment play an important role and should be taken into consideration. An increase in collection efficiency with increased particle loading has been reported by several workers.

1.2 Apparatus and Experimental Procedure

1.2.1 Introduction

Several experimental arrangements were tested in the course of the experimental program before the set-up was finalized. Results from these preliminary "shake down" experiments are not reported in the body of this thesis but do appear in Figure A1 of the appendix and are discussed in section 1.3.1. What follows is a description of the equipment, particulate solids used, and the procedure for data acquisition and analysis.

1.2.2 Model Cyclone Apparatus

Figure 1.6 shows a schematic of the apparatus used for the majority of tests performed in Part I of this thesis project. The apparatus was comprised of four separate systems:

1. Blower, piping, orifice flow metering system
2. Solids feed system
3. Polyacrylic cyclone
4. Filter system.

Each is described below.

For all experiments, compressed air was provided by a positive displacement Roots type blower, powered by a 37 kW (50 hp) diesel engine. The air flow could be varied over a wide range (0 - 1100 scfm or 0 - 0.52 m^3/s) by controlling the

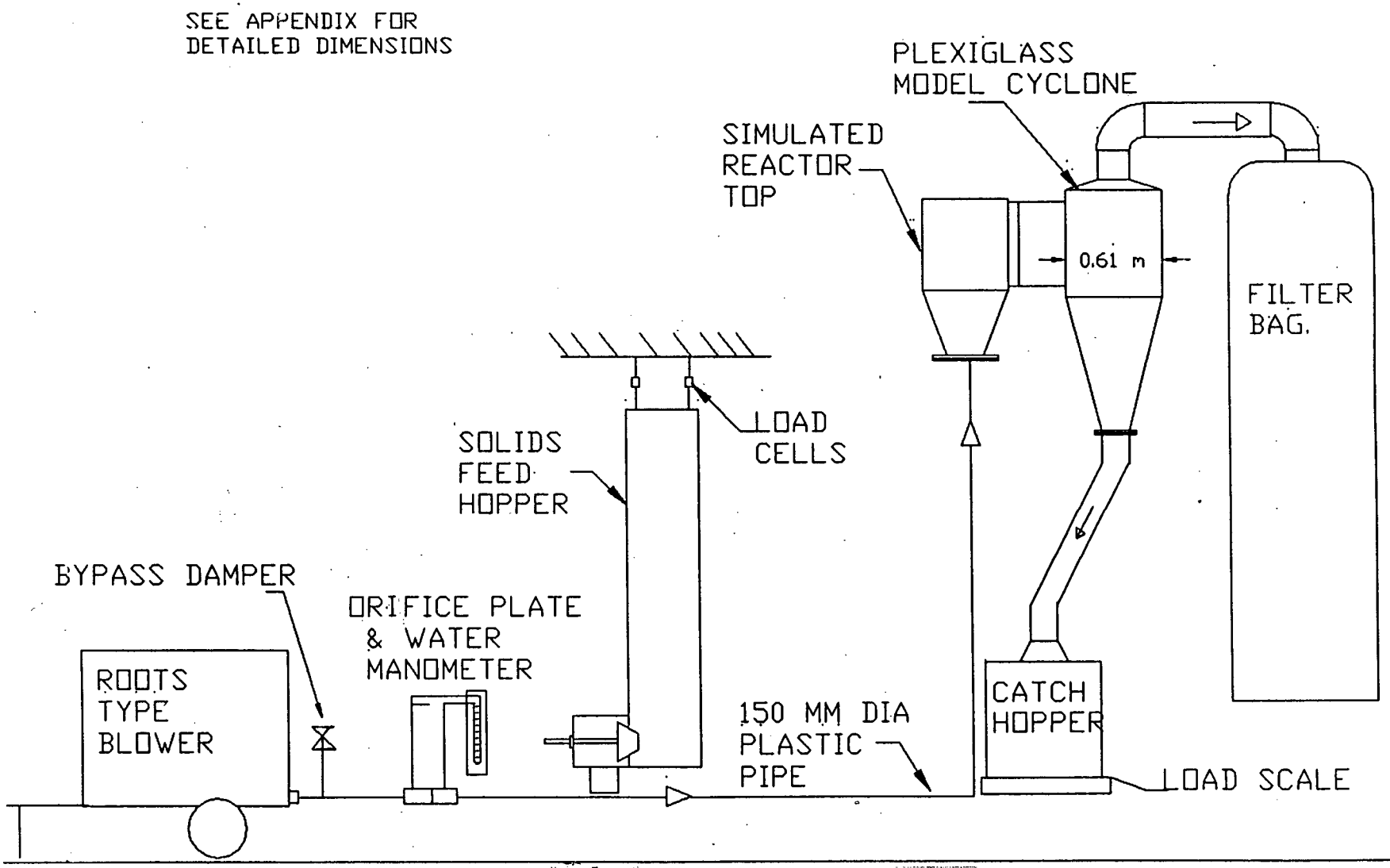

FIGURE 1.6 UBC apparatus schematic used in runs B1 through B38.

engine speed and a bypass damper. The bypass damper was shut for all experiments to ensure constant flow. The flow vs. blower speed curves are shown in Figure 1.7.

A 150 mm (nominal) dia. plastic pipe connected the blower to the feed hopper while in between, located after more than 4 m of straight pipe run, was the flow measurement orifice plate. This brass plate, designed and installed according to ASME standards (28), had a 101.5 mm (4 in.) i.d. orifice. The orifice pressure drop was measured by means of a water manometer, and because the reading was usually unstable, due to fluctuations in pressure in the simulated reactor top, the best accuracy attainable was +\- 5 mm. The absolute pressure at the orifice plate was observed to fluctuate with solids loading and was in the neighborhood of 30 to 60 cm (12 to 24 inches) water column pressure. The flow vs. orifice plate pressure drop curve appears in Appendix I (Figure A2).

Solids to be fed to the system were contained in a 3.05 m tall by 0.36 m square hopper equipped with a manually operated 0.254 m dia. (aperture opening) cone valve (see Figure 1.8.). Located at the bottom of the hopper was a 0.36 m square windbox, constructed with a 30% free area distributor plate and lined with a 3 mm thick layer of commercial grade bleached kraft paper (softwood) to ensure even distribution of air. Additional fluidization air was provided by a 6 mm diameter pipe entering opposite to the solids valve. Fluidization air flow rates were measured by means of a rotameter. During the runs the hopper was pressurized, (by means of a 32 mm dia.

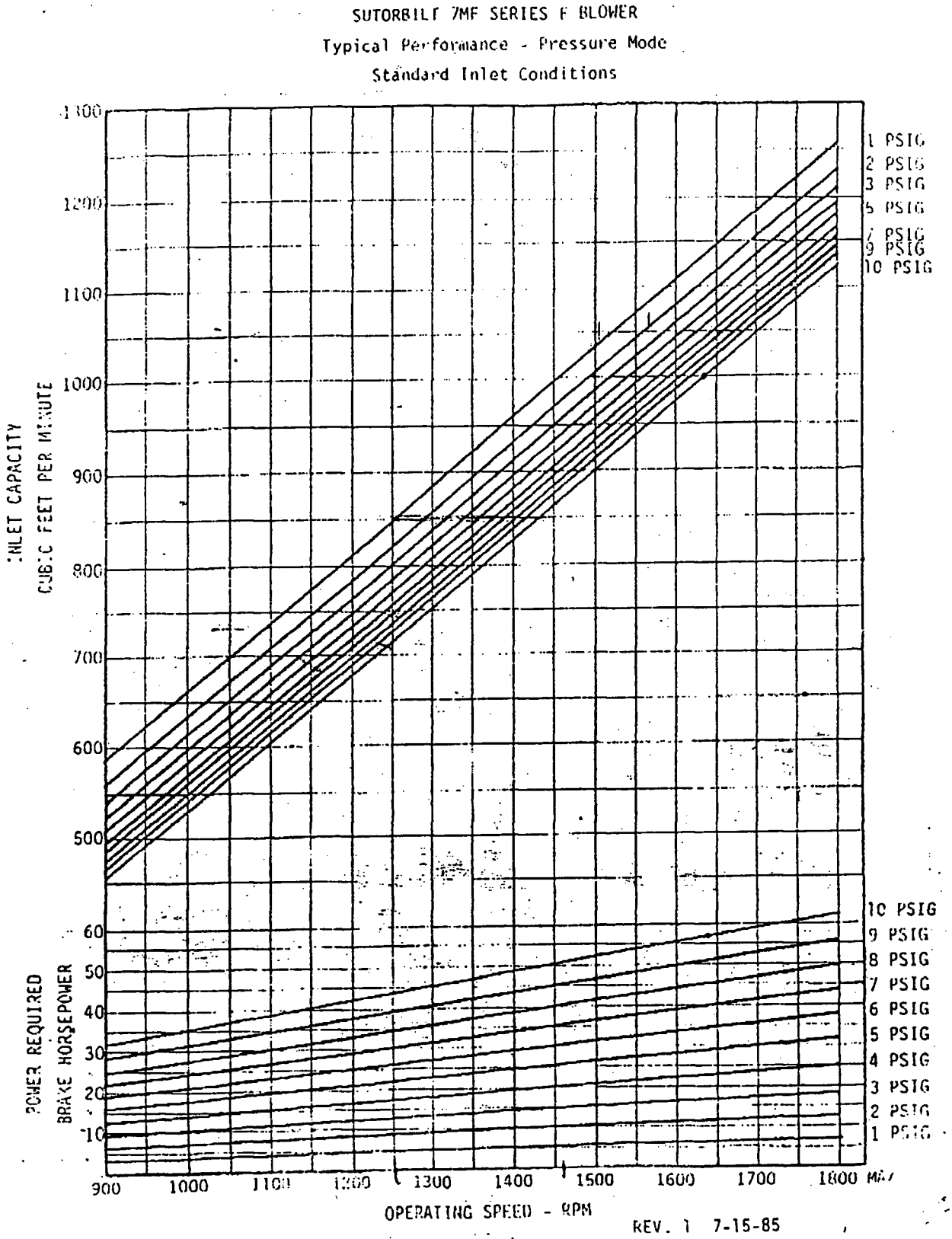

Fig **Figure 1.7 Plot of blower speed vs flow/pressure drop. (Pumps and Power Inc.)**

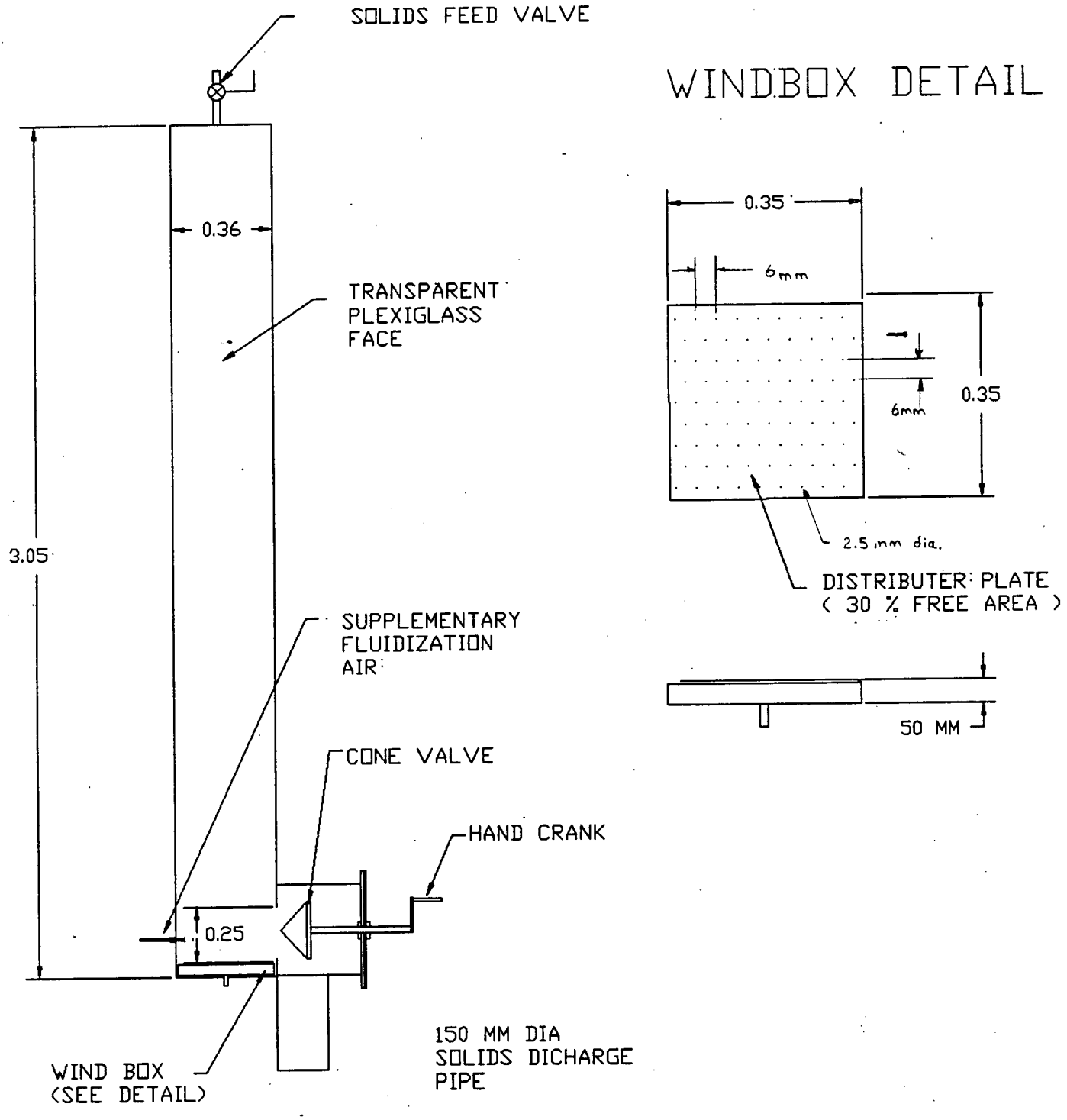

Figure 1.8 Diagram of UBC solids hopper used in runs B1 through B35.

pipe connected upstream of the orifice plate), to a pressure slightly above that of the transport air to allow steadier and more rapid solids feeding. The hopper was supported by three load cells (1000 kg capacity each, 9 mV output at rated capacity) which allowed mass flow rate to be determined for the duration of the experimental runs. Hopper mass information was logged on an XT computer at 1 s intervals. Error is estimated to be +/- 1 kg, largely due to friction between the hopper and the pneumatic transport pipe. A flexible connection was used at this junction to minimize this friction. The air transport pipe turned twice between the solids input point and the cyclone, once through 45°, then again through 90°.

In order to model the Chatham cyclone more effectively the polyacrylic cyclone was preceded by a polyacrylic entrance section, and a steel enclosure geometrically similar to the top of a circulating fluidized bed riser section. This included a slanting riser ceiling piece, inclined at 10° towards the cyclone as shown in Figure 1.9. A 50 mm wide rubber strip sealed this reactor top to the cyclone entrance way and was installed taut, thereby minimizing flow interference.

The polyacrylic entrance-section was built as a scale model of the original configuration of the entrance-way. It was 445 mm high by 140 mm wide at the entrance point to the cyclone. Within the entrance-way were installed wooden inserts, designed to model proposed geometric changes being considered for the Chatham cyclone. Details of the entrance geometries studied are given in Figure 1.10.

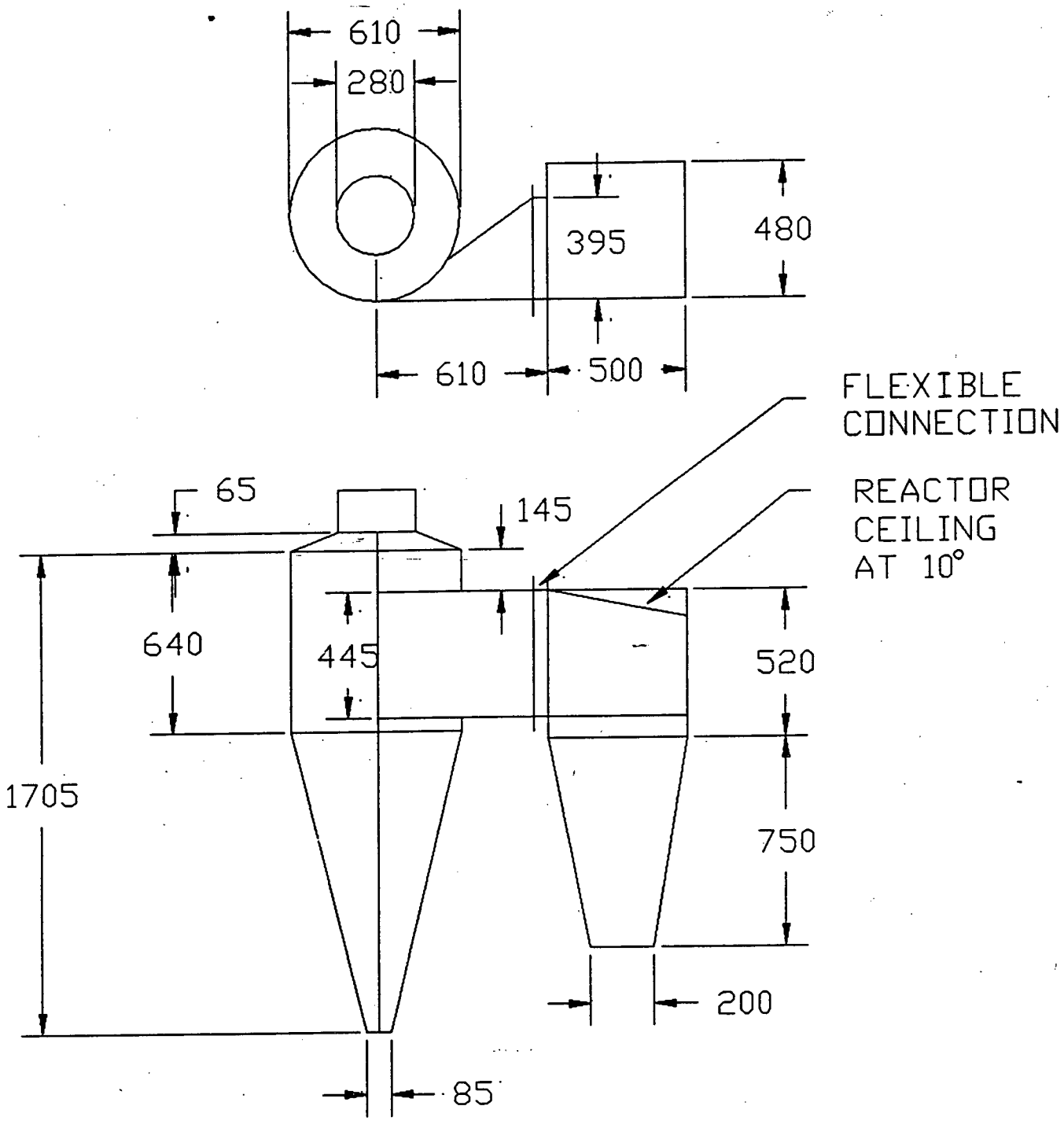

FIGURE 1.9 DIAGRAM OF MODEL REACTOR TOP AND MODEL CYCLONE

(ALL DIMENSIONS IN MM)

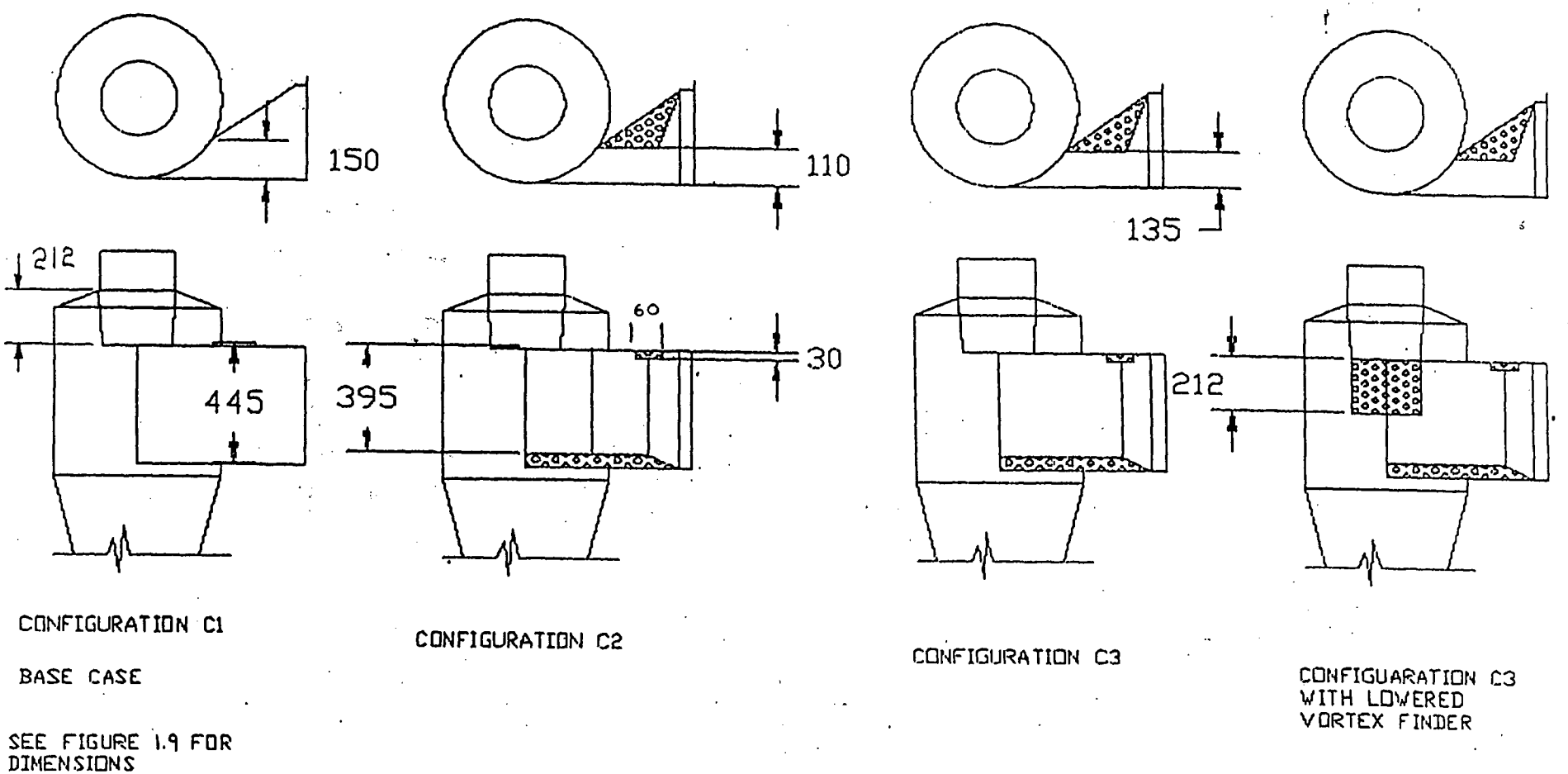

Figure 1.10 Entrance geometry configurations for inlet modification tests. Shaded areas show inserts. All dimensions in mm. See section 1.3.3 for details.

The model cyclone itself was a one-ninth (0.11) scale replica of the Chatham CFBC cyclone existing at Chatham New Brunswick. The model cyclone was constructed from 6 mm thick clear polyacrylic and dimensions were held to a tolerance of +/- 3mm. The scale was decided upon by assuming that the cyclone Stokes number was roughly similar i.e.

$$N_{ST\ UBC} = N_{ST\ CHATHAM}$$

Operating conditions are presented in the results section, in Table 1.4.

It can be immediately noticed that the Chatham cyclone design chosen is non-standard. Compared to standard designs it is squat, having a height/diameter ratio of $H_o/D = 2.8$, while standard designs have $H_o/D = 3.7$ to 4.0. In addition the vortex finder or gas exit duct does not extend below the floor of the entrance way, which raises the possibility of gas short circuiting the separation zone. Extending the vortex finder below the entrance floor by D/10 is not uncommon in standard designs (5). Also peculiar to this design is the inclusion of an annular zone, concentric with the cyclone itself but positioned above the entrance ceiling but below the cyclone ceiling. It is believed that this squat design was chosen to meet dimensional requirements, but it unclear why the concentric annular region near the top was included.

The model provided for two types of vortex finders, the first being made of steel with provision for an additional section, while the second made of polyacrylic, could be retracted from the cyclone body, thereby simulating other

configurations. Gas exited the cyclone to a short 300 mm dia. steel duct which then turned 90°, traversed approximately 600 mm and finally turned down 90° to a bag filter.

For runs B1 to B10, performed under high loading conditions it was necessary to use a large sock shaped bag filter to handle the higher solids flows. This bag filter had the dimensions of 0.78 m dia. by 4 m long and was made of 100% cotton, 452 g/m^2 weight. The bag filter was securely attached to the exit duct, thus preventing solids losses. For subsequent runs, performed under low loading runs, a high efficiency (99 % collection efficiency for 5 micron diameter particles, 4 m^2 cloth area) ventilation bag filter was used because it offered higher collection efficiency and could handle the lower solids loadings.

A 1.7 m long, 100 mm dia. flexible hose connected the solids exit of the cyclone to a storage hopper. The hopper was located below and to the side of the cyclone, thus reducing the possibility of solids re-entrainment from the hopper back to the cyclone, a problem experienced by Stairmand (2). The solids hopper itself rested on a load scale, allowing for measurement of the solids caught. The scale was calibrated to +/- 10 grams, and values were logged on an XT computer at 1 s intervals. The data logging program appears in Figure A3 of the Appendix.

In an effort to simulate the high loading conditions in the cyclone at Chatham a solids recycle system was designed and built. Figure A4 in the appendix shows a schematic of the

system. Briefly the setup envisioned recycling separately, in two similar systems, the solids caught and those passing the polyacrylic model cyclone. Not only were the systems to recycle the solids, they were also intended to measure the solids flow to provide loading and collection efficiency data. Each solids recycle system included a fluidized seal equipped with dual distributor plates, and a solid flow measurement vessel equipped with a porous measurement swing plate, cone valve for solids flow control, and a distributor plate to distribute fluidization air.

The solids measurement vessel was intended to measure solids flow by means of a porous swing plate positioned within the measurement vessel (first proposed by Turner(40)). This porous paper lined, 30 % free area punched hole plate could be manually rotated to block solids falling within the measurement vessel. Once the plate was rotated closed, the falling solids were to collect on the lined plate and be measured. Measurement was to be performed by observing the pressure differential across the plate and deposited solids and thus infer a solids flow rate. The pressure differential was to arise due to the upward flow of fluidizing air originating from the distributor plate located at the bottom of the measurement vessel, below the solids exit.

While the larger solids recycle system was to receive solids directly from the polyacrylic cyclone model, the second smaller recycle system was to handle fines that passed the model. These fines were to be caught with a multiclone,

containing 120 small plastic cyclones, each 50 mm in diameter. These high efficiency Stairmand type cyclones were to separate the fines from gas stream, and deposit them in a steel hopper with sides inclined at 45°. From there the fines were to have fallen into the fluid seal, continued into the fines measurement vessel and finally recycled back into the feed stream. The cleaned gas stream continued on to a bag filter, positioned just downstream of the multiclone. Fines flow measurement was to occur in a similar fashion as in the large recycle system.

Upon commissioning it was found that this system did not work for two reasons. Firstly the multiclone was unable to capture all of the fines and let an unacceptable amount of solids pass, overloading the filter. Attempts to increase the multiclone efficiency by increasing the inlet velocity to each small cyclone were unsuccessful. Secondly it was found that the solids caught by the multiclone were so cohesive that they remained in the multiclone hopper. Other elements of the system such as the fluidized seals and the porous measurement swing plates remain untested.

While it was considered possible to rectify these problems with another multiclone design and different solids system, it was not considered to be a practical means to achieve the objectives of this study, given the resources (i.e. time constraint) at hand.

1.2.3 Particulate solids

Fluid cracking catalyst fines, obtained from tertiary cyclones serving a fluid catalytic cracking unit at the Chevron Canada Ltd. oil refinery were used in the experiments reported in this thesis. The equivalent volume sphere diameter, as determined using an Elzone particle analysis instrument, was approximately 22 μm. The size distribution of the feed material appears in Figure 1.11. A photograph of the test dust appears in Figure 1.12. The bulk density was determined with the solids in a loose form and was found to be 770 kg/m^3. Assuming a voidage of 0.5 the particle density was estimated to be 1540 kg/m^3.

1.2.4 Data acquisition and analysis

Each test of the cold model cyclone was performed according to the following procedure:

1. As an initialization procedure, the system was cleaned out by rapping each component part while scouring the system with air. The mass of the feed hopper, catch hopper(with lid connection off), and filter bag were next recorded. The wet and dry bulb temperature were then noted. (See Appendix Figure A8 for temperatures) The plastic cyclone was wrapped with aluminum foil to reduce electrostatic effects, and the feed hopper pressurization line was then connected.

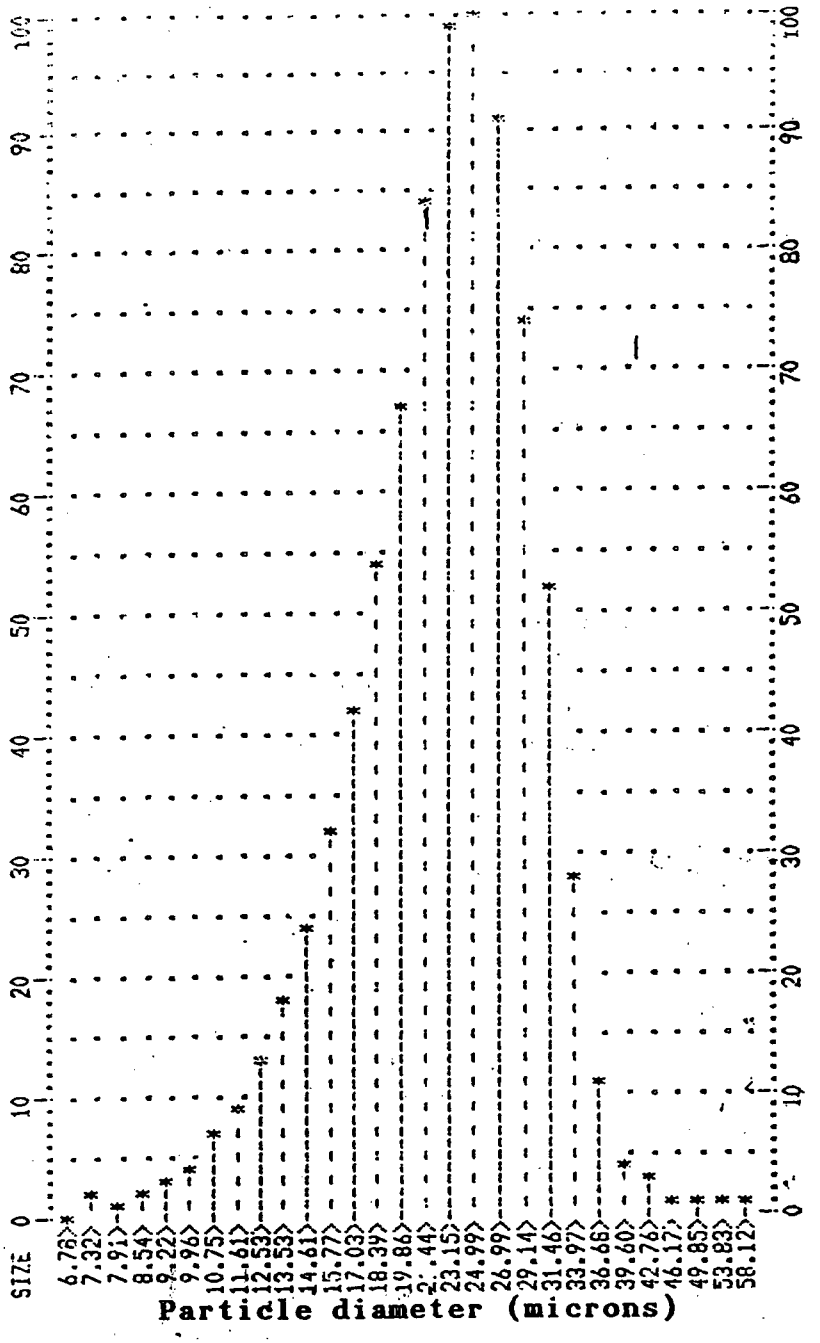

Figure 1.11 Size distribution of feed solids.
(22 um mean size)

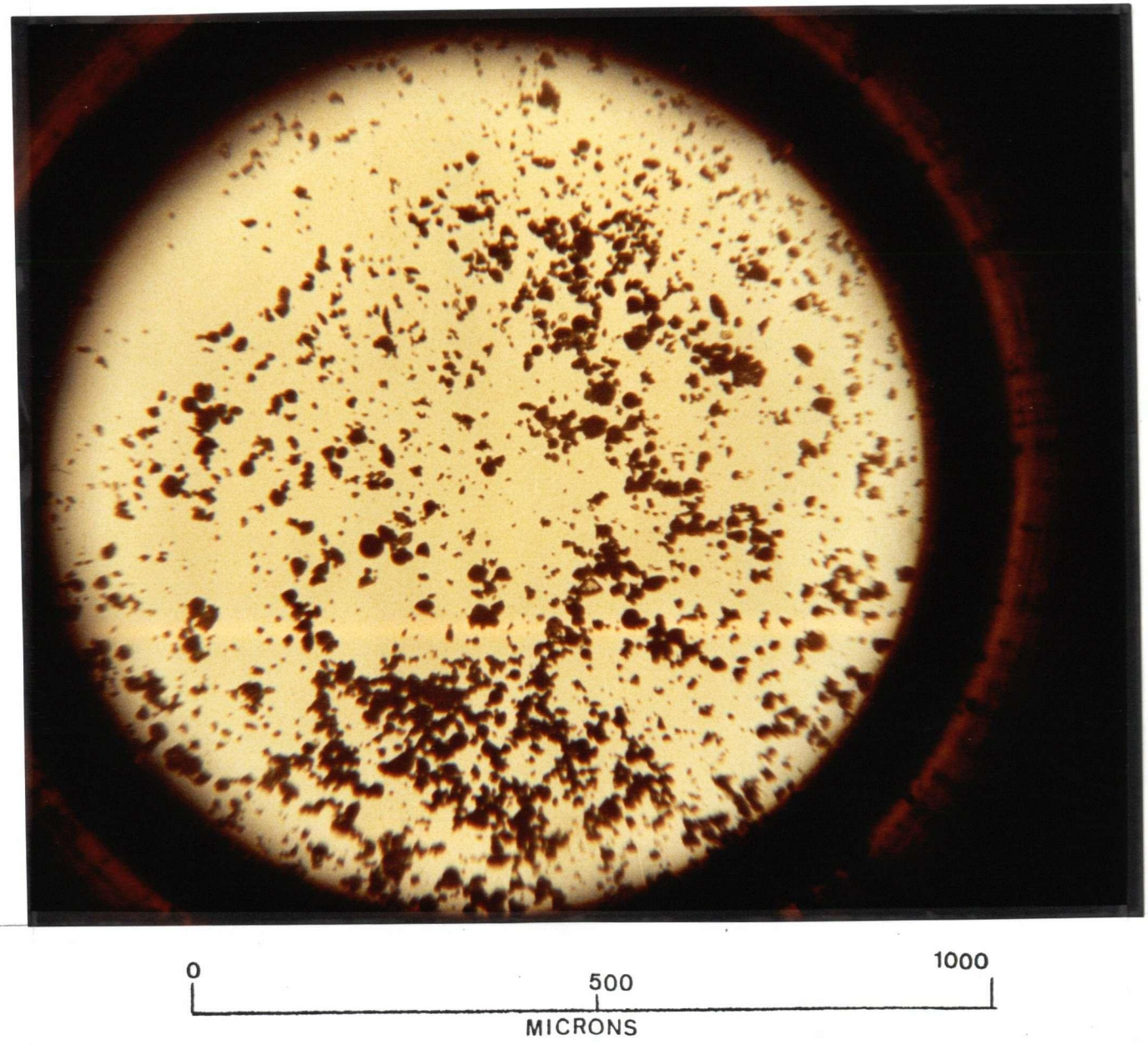

Figure 1.12 Photograph of FCC test solids (22 um mean size)

2. With the fluidization air turned on to the wind box, the feed hopper was charged by scooping solids from a barrel and feeding, by means of a funnel, through the 50 mm dia. feed port at the top of the hopper.

3. The receiving storage hopper was sealed.

4. The blower was connected and started. Then the air flow was adjusted via. engine speed.

5. The data logging program was started on the XT computer.

6. The fluidization air was increased until solids were seen to be bubbling and circulating within the hopper. (fluidizing air flow was approximately 100 lpm)

7. The solids feed valve was rapidly opened and the hopper rapped as solids were rapidly fed. Figure 1.8 shows the valve arrangement.

8. The solids valve was quickly shut after the desired amount of solids had been fed.

9. With the blower still running, the system (pipes, model cyclone, exit pipes) was violently rapped to dislodge solids adhering to inner surfaces.

10. The blower was stopped, and the filter bag mass, receiving hopper mass, and feed hopper mass were recorded. Solids samples were taken from the filter bag and receiving hopper for analysis of their particle size distributions.

Deviations or unusual occurrences from the above procedure are reported in Table 1.3.

In order to derive the collection efficiency curves needed for this study, both the particle size distribution and masses of the feed, catch and loss particles needed to be obtained. As previously mentioned, the total catch and feed masses were determined from the load cells and load scale. The mass of particulate passing to the model cyclone was measured by determining the difference in the filter mass before and after each run.

An Elzone particle analysis instrument (model 286XY), interfaced with an AT computer, was used to characterize the particle size distribution. The instrument was calibrated prior to analysis with particles of mean diameter of 5 μm and 20 μm, to correspond approximately to the expected mean sizes of the cyclone loss and catch respectively. ASTM standard C690 -71 T for particle size distribution analysis by electronic counting

was followed. A Leitz Tas Plus Image Analysis System was used to confirm the particle size distributions.

The particle collection efficiency curve for each run was obtained by comparing the mass caught to that fed for each channel (i.e. for each size interval) as follows:

$$E_i = (C\ c_i)/(C + L)f_i \qquad (1\text{-}28)$$

where E_i = collection efficiency for channel i.

C = total mass caught

L = total mass lost (via. filter bag measurement)

c_i = fraction by mass for channel i of catch.

f_i = fraction by mass by channel of feed

1.2.5 Error Sensitivity

As in any experimental program, the error expected in measurements must be significantly less than the observed quantities in order for the results to be meaningful. The experiments described in this thesis were set up with this in mind. For example, in order that there be sufficient resolution between experiments, the solids chosen had to be fine enough to allow a significant amount to pass the cyclone.

As well, the manner in which the efficiency was calculated was important. Given the feed, catch, and passing masses from a particular test, there are four ways to calculate the primary dependent variable collection efficiency. They are:

a.) $$E = \frac{\text{(catch mass)}}{\text{(feed mass)}} \qquad (1\text{-}29)$$

b.) $$E = \frac{\text{(catch mass)}}{\text{(catch mass + loss mass)}} \qquad (1\text{-}30)$$

c.) $$E = \frac{\text{(feed mass - loss mass)}}{\text{(feed mass)}} \qquad (1\text{-}31)$$

d.) $$E = \frac{\text{(feed mass - loss mass)}}{\text{(catch mass + loss mass)}} \qquad (1\text{-}32)$$

In Figure 1.13 a comparison is made of the collection efficiency errors resulting from hypothetical experimental errors for equations 1-29 to 1-32. The graphs were prepared while considering the case with a gross collection efficiency of 95%. From these graphs it can be seen that equations 1-30 and 1-31 are less susceptible to experimental error than 1-29 or 1-32.

The error in each variable depends on solids caught up in the system, attrition or agglomeration (if any) and measurement error. The efficiency of the bag filter influences

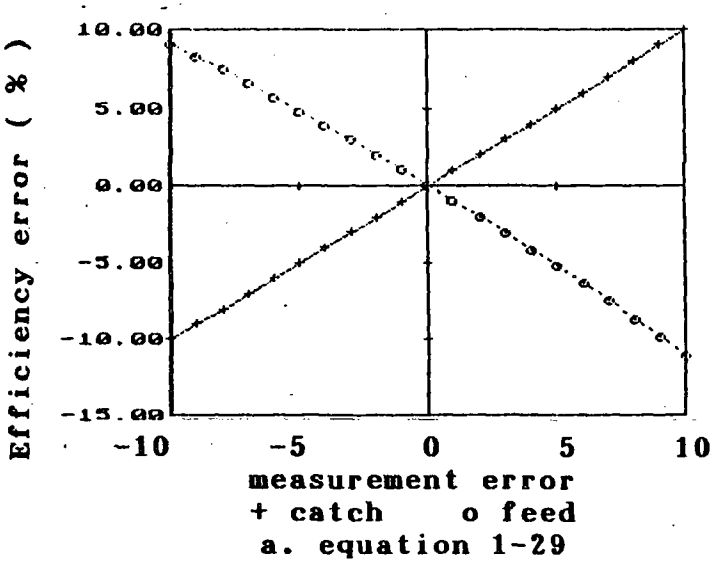

a. equation 1-29

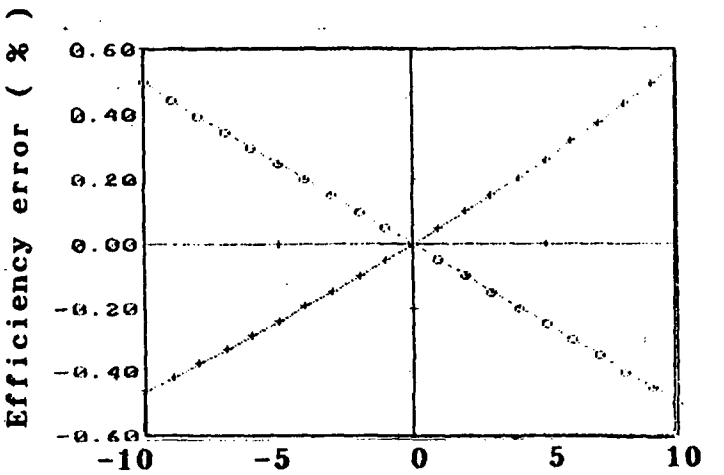

b. equation 1-30

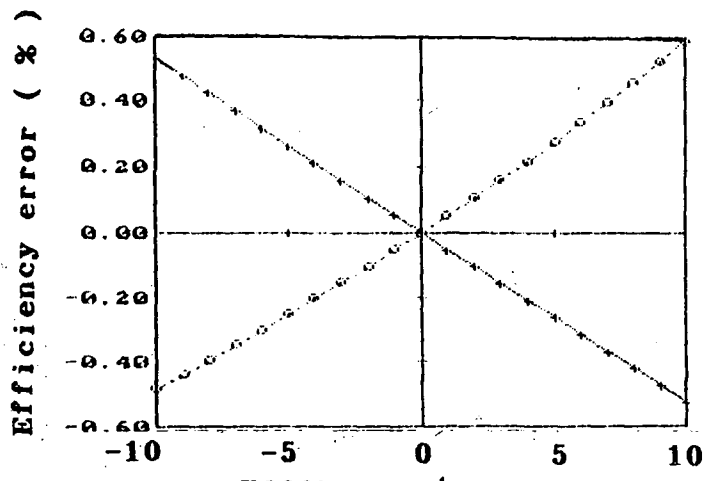

c. equation 1-31

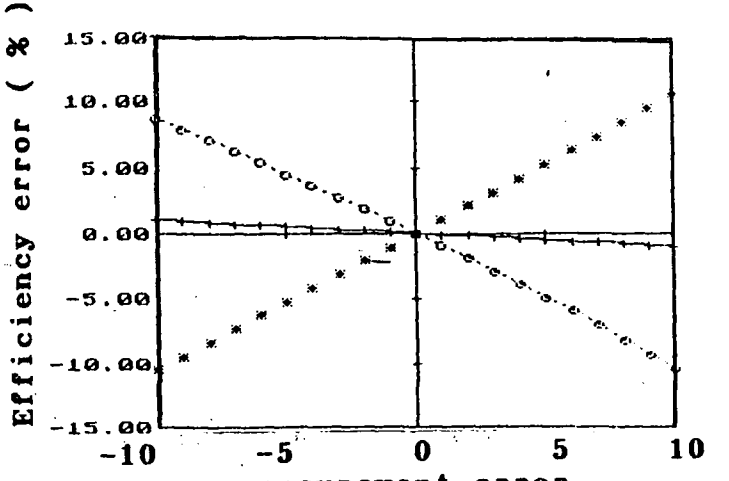

d. equation 1-32

FIGURE 1.13 Collection efficiency error estimates for equations 1-29, 1-30, 1-31, and 1-32.

loss measurement error. As previously stated the scale accuracies were:

feed scale	+/- 1 kg
catch scale	+/- 0.01 kg
loss scale	+/- 0.001 kg

The measurements suffered from the problem of solids lodging in the system. The feed measurement was particularly susceptible to error. This is because the solids fed to the system had more opportunity to be caught up in the piping and entrance way, thus reducing the actual amount reaching the cyclone chamber itself. The catch mass measurement fared much better as the passage to the storage hopper could be easily cleared of any material that was retained. Measurement of solids not captured by the cyclone was hindered not so much by the scale accuracy, but rather by the inevitable loss of particles due to filter inefficiency. This rendered the loss particle size distribution inaccurate and unreliable. A mass balance, performed on a per channel basis failed to close for particle smaller than 15 μm dia as is shown in Figure A7 Thus collection efficiency calculations were based on the catch and feed particle size distributions as per equation 1-28.

1.2.6 Chatham cyclone data

Figure 1.14 shows a schematic of the Chatham CFB Boiler, a complete description of the installation can be found in

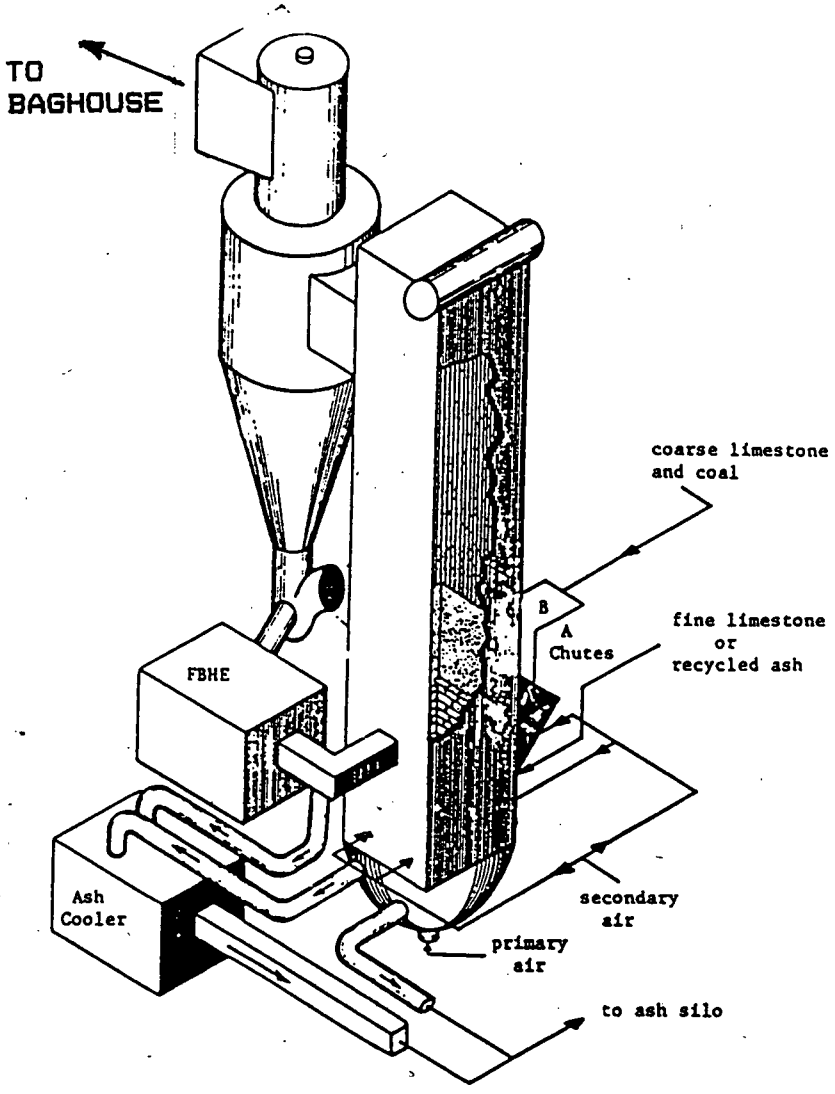

Figure 1.14 Schematic of Chatham CFB Boiler(32)

reference 1. Briefly the Chatham CFB boiler consists of a 23.8 m high fluidized bed furnace which discharges solids and combustion gases to a 5.6 m diameter cyclone. Solids are separated from the combustion gases in the cyclone and are returned to the bottom of the furnace. A portion of these solids pass through the Fluid Bed Heat Exchanger (FBHE).

The catch sample analyzed in this thesis was taken from the FBHE. A photograph of the Chatham cyclone fines appears in Figure 1.15. The loss particle size distribution was established by analyzing particulate samples from the bag house with the Elzone particle analyzer. The catch sample was sieved (ASTM Standard Test Method for Sieve or Screen Analysis of Fine and Coarse Aggregates: C-136-76) to give a rough particle size distribution. The fines (i.e. material passing a #70 mesh screen) were analyzed further with the Elzone particle analyzer. Equation 1-30 was used to calculate gross collection efficiency data.

Solids flux in the reactor was measured at several levels (32) and found to be of the order of 20 kg/m^2s. This is said to be similar to values, as yet unpublished, found by isokinetic sampling trials performed by others in the cyclone inlet (35). The solids loading, calculated assuming 1600 m^3/s gas flow at STP, and a reactor riser area of 16 m^2 was estimated to be 10 kg solids/ kg gas.

The runs typically lasted for weeks. Thus it is assumed that steady state conditions prevailed. It is assumed that the

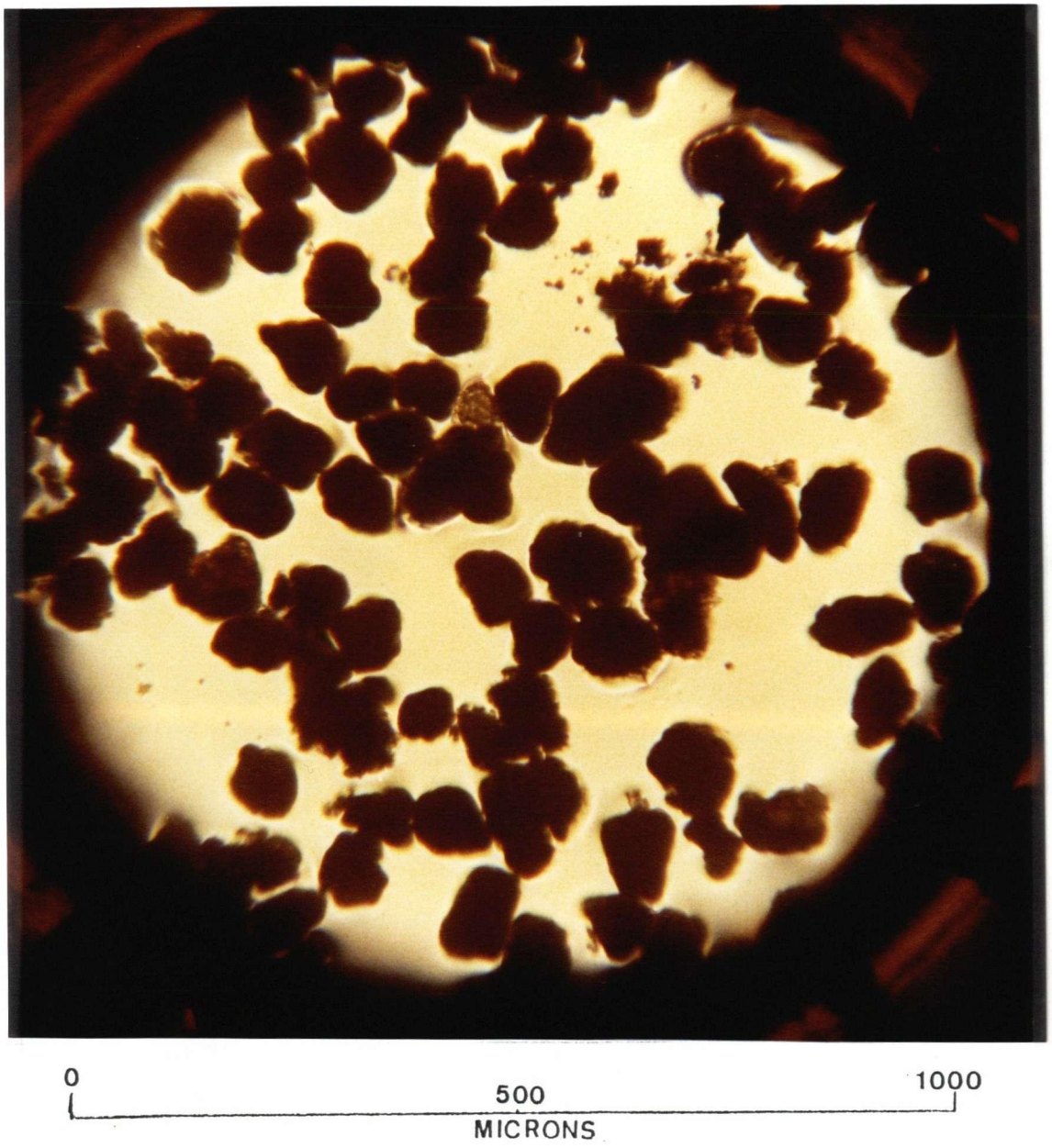

Figure 1.15 Photograph of fines from Chatham fluid bed heat exchanger, sampled on April 17, 1990.

size distributions did not significantly change during transport from the cyclone to the point of sampling or during transport from New Brunswick to Vancouver. This assumption could not be verified because at the time of writing it was not possible to obtain samples directly from the base of the cyclone itself. Data concerning the operation conditions or other entrance configurations will be available pending completion of work at the University of New Brunswick (35). All samples were taken on April 17, 1990, during which time the cyclone had entrance configuration C3 (see Figure 1.10). The operating conditions are summarized in Table 1.2.

TABLE 1.2

CHATHAM OPERATING CONDITIONS FOR APRIL 17, 1990

		COMMENTS	REFERENCE
TEMPERATURE	850 C	TOP OF FURNACE	(32)
GAS FLOW	1600 m^3/min.	STP	(32)
GAS VISCOSITY	0.000018 kg/ms		(36)
GAS PRESSURE	37.5 cm H_2O	@ CYCLONE ENTRANCE	(32)
PRESSURE DROP	12.25 cm H_2O		(32)
SOLIDS FLUX	20 kg/m^2s	(see note above)	(32)
GROSS COLLECTION EFFICIENCY	99.2 %		(1)

While the method for the cyclone efficiency calculation is not stated, it is believed that the catch mass flow is calculated from an energy balance across the fluid bed heat exchanger and thus is not very accurate.

The bulk particle density for Chatham solids was measured to be 1600 kg/m^3 and assuming a voidage of 0.4 the particle density was calculated to be 2650 kg/m^3.

1.3. RESULTS INTRODUCTION

Part I of this study examines the collection efficiencies of two geometrically similar cyclones operating at different temperatures, with different solids, and with different inlet velocities. It also examines the performance of the smaller cyclone under different inlet velocities and with various inlet geometries. This variation in inlet geometries was performed in order to provide some initial guidance on similar proposed changes in the Chatham cyclone. Significant attempts were made to match the loading conditions of the Chatham unit but this was not completely possible. Problems associated with feeding solids, collection of the fines not captured by the cyclone, and solids analysis limited the accuracy of the results.

The polyacrylic cyclone was sized so as to not exceed the capacity of the mobile blower while maintaining a cyclone inlet velocity between 5 and 10 m/s, and yet be as large as possible. Less consideration was paid to the required solids loading which proved to be very difficult to meet. Initial efforts focused on a system capable of recycling all the solids (both those caught by the cyclone and those lost, see Figure A4 in the appendix). These attempts were thwarted by the inability of a 'homebuilt' multiclone, consisting of 120 cyclones, each of 50 mm diameter, to capture all the fines. The particles caught by the multiclones was so cohesive that it failed to fall out of the multiclone catch hopper, adhering instead to the hopper walls, which were inclined at 45°, without aggressive rapping. The failure to achieve complete recycle

meant that the solids could only be fed through once, as a short batch operation. Typically each run involved feeding for a period of only a few minutes. Figure 1.16 plots catch hopper mass vs time for run B4, giving an indication of the variation in the feed rate. Typically there was little variation in the feed rate.

The particles were chosen as a compromise under a set of conflicting requirements. It had to be fine enough to allow significant losses (and thus experimental resolution between different conditions) and yet not so fine that the fraction passing could not be handled. The first three runs were performed with FCC solids with a mean diameter of 60 microns and resulted in 99% and 98.3% capture efficiencies respectively, too high for the resolution required. Subsequent runs used FCC solids with a mean diameter of 22 microns and resulted in acceptable lower efficiencies. Unfortunately, these fines were more cohesive, and proved to be more difficult to feed and analyze.

Experimental results are summarized in Table 1.3. Experiments B1 to B3 were shakedown runs using the larger solids (60 micron mean). Runs B4 to B11 attempted to achieve high solids loading rates, while the remaining experiments focused on solids loading effects and the influence of inlet modifications on collection efficiency.

Preliminary "shakedown" tests, performed before run B1, used solids with mean particle diameters of 11 μm and 50 μm, at inlet velocities between 3.6 and 5.6 m/s. Inlet geometry

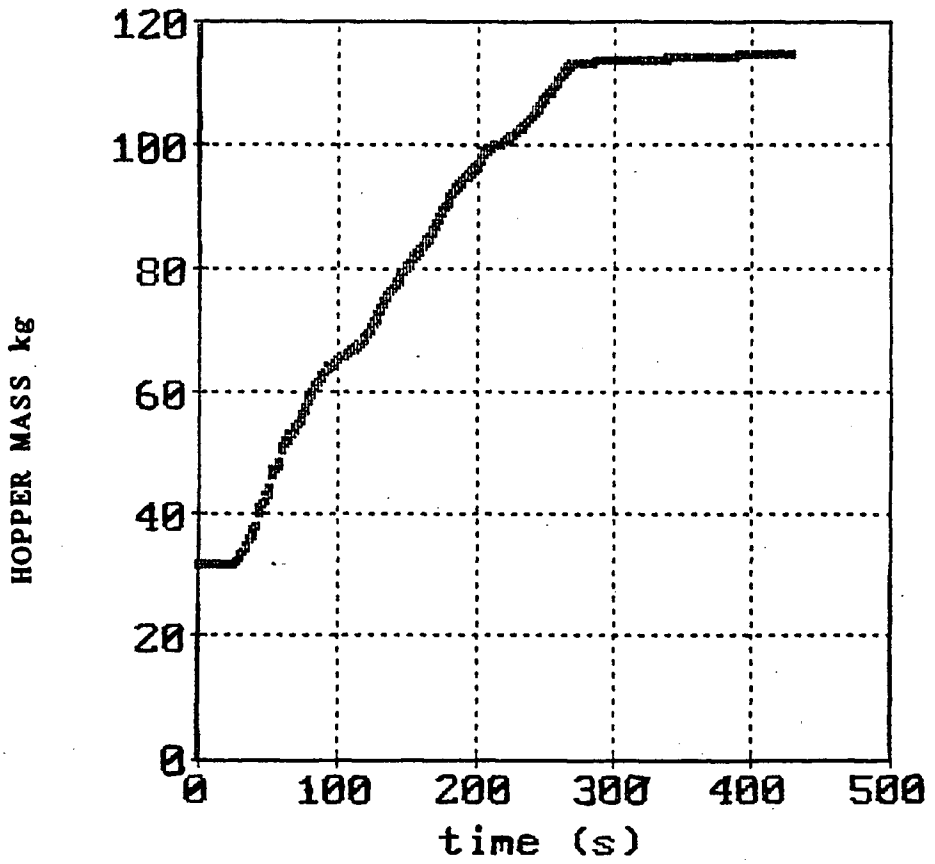

Figure 1.16 Catch hopper mass vs time indicating steady state solids feed rate. Run B4.

RUN #	DATE	PURPOSE	CONFIGURATION (see Figure 1.10)	SOLIDS AVERAGE DIAMETER	LOADING (MASS SOLIDS) (MASS AIR)	FLOW m3/s	INLET VELOCITY m/s	MASSES kg CAUGHT	MASSES kg LOSS	EFF. %	COMMENTS
B1	15/5/90	SHAKE DOWN	C3, HIGH V.F.	60 UM FCC	2.60	0.19	3.67	n/a	n/a	n/a	FEED PROBLEMS
B2	22/5/90	SHAKE DOWN	C3, HIGH V.F.	60 UM FCC	0.63	0.19	3.67	79.6	0.80	99	BAD MASS BALANCE
B3	23/5/90	SHAKE DOWN	C3, HIGH V.F.	60 UM FCC	3.14	0.19	3.67	50	0.84	98	feed mass caught in pipes
B4	24/5/90	scaling	C3, HIGH V.F.	22 UM FCC	1.25	0.19	3.67	83	1.96	98	mass balance closes to 2.7%
B5	24/5/90	scaling	C3, HIGH V.F.	22 UM FCC	n/a	0.19	3.67	n/a	n/a	n/a	feed problems
B6	20/6/90	scaling	C3, HIGH V.F.	22 UM FCC	1.96	0.26	5.04	85.15	3.69	96	GOOD RUN
B7	20/5/90	scaling	C3, HIGH V.F.	22 UM FCC	n/a	0.26	5.04	n/a	n/a	n/a	feed problems
B8	02/7/90	scaling	C3, HIGH V.F.	22 UM FCC	7.17	0.28	5.50	101.78	1.13	99	GOOD RUN
B9	10/7/90	scaling	C3, HIGH V.F.	22 UM FCC	7.49	0.26	5.04	91.50	1.44	98	GOOD RUN
B10	10/7/90	scaling	C3, HIGH V.F.	22 UM FCC	5.38	0.19	3.67	126.99	0.61	995	solids valve stuck open
B11	12/7/90	scaling	C3, HIGH V.F.	22 UM FCC	n/a	0.26	5.04	n/a	n/a	n/a	feed problems
B12	18/7/90	LOADING	C3, HIGH V.F.	22 UM FCC	0.23	0.26	5.04	3.9481	0.3697	91	GOOD RUN
B13	18/7/90	LOADING	C3, HIGH V.F.	22 UM FCC	0.12	0.26	5.04	1.9692	0.2972	87	GOOD RUN
B14	18/7/90	LOADING	C3, HIGH V.F.	22 UM FCC	0.13	0.26	5.04	4.3351	0.4936	90	GOOD RUN
B15	18/7/90	LOADING	C3, HIGH V.F.	22 UM FCC	0.15	0.26	5.04	2.6652	0.345	89	GOOD RUN
B16	18/7/90	LOADING	C3, HIGH V.F.	22 UM FCC	0.44	0.26	5.04	3.636	0.4035	90	GOOD RUN
B17	18/7/90	LOADING	C3, HIGH V.F.	22 UM FCC	0.38	0.26	5.04	4.8347	0.4975	91	GOOD RUN
B18	18/7/90	LOADING	C3, HIGH V.F.	22 UM FCC	1.30	0.26	5.04	9.513	0.4339	96	GOOD RUN
B19	18/7/90	LOADING	C3, HIGH V.F.	22 UM FCC	0.048	0.26	5.04	2.7358	0.5217	84	GOOD RUN
B20	18/7/90	LOADING	C3, HIGH V.F.	22 UM FCC	0.66	0.26	5.04	2.8295	0.2171	93	GOOD RUN
B21	4/8/90	GEOM. CHNG.	C2, HIGH V.F.	22 UM FCC	0.36	0.24	4.58	14.5138	0.7697	95	GOOD RUN
B22	4/8/90	GEOM. CHNG.	C2, HIGH V.F.	22 UM FCC	0.26	0.24	4.58	8.6637	0.7046	92	GOOD RUN
B23	4/8/90	GEOM. CHNG.	C2, HIGH V.F.	22 UM FCC	0.15	0.24	4.58	7.4569	0.6722	92	GOOD RUN
B24	4/8/90	GEOM. CHNG.	C3, HIGH V.F.	22 UM FCC	0.23	0.24	4.58	7.1836	0.4793	94	GOOD RUN
B25	4/8/90	GEOM. CHNG.	C3, HIGH V.F.	22 UM FCC	0.23	0.24	4.58	7.5607	0.603	93	GOOD RUN
B26	4/8/90	GEOM. CHNG.	C1, HIGH V.F.	22 UM FCC	0.20	0.24	5.41	6.8837	0.35	95	GOOD RUN
B27	4/8/90	GEOM. CHNG.	C1, HIGH V.F.	22 UM FCC	0.20	0.24	5.41	5.5855	0.294	95	GOOD RUN
B28	4/8/90	GEOM. CHNG.	C1, HIGH V.F.	22 UM FCC	0.24	0.24	5.41	4.3072	0.2865	94	GOOD RUN
B29	4/8/90	GEOM. CHNG.	C3, LOW V.F.	22 UM FCC	0.36	0.24	4.58	6.0028	0.2812	96	GOOD RUN
B30	4/8/90	GEOM. CHNG.	C3, LOW V.F.	22 UM FCC	0.34	0.24	4.58	5.6125	0.304	95	GOOD RUN
B31	4/8/90	GEOM. CHNG.	C3, LOW V.F.	22 UM FCC	0.11	0.24	4.58	2.8368	0.229	93	GOOD RUN
B32	29/08/90	GEOM. CHNG.	C3, LOW V.F.	22 UM FCC	0.17	0.24	4.58	6.2787	0.3067	95	GOOD RUN
B33	29/08/90	GEOM. CHNG.	C1, HIGH V.F.	22 UM FCC	0.17	0.24	3.81	4.3102	0.3403	93	GOOD RUN
B34	29/08/90	GEOM. CHNG.	C1, HIGH V.F.	22 UM FCC	0.096	0.24	3.81	4.2827	0.3315	93	GOOD RUN
B35	29/08/90	GEOM. CHNG.	C3, HIGH V.F.	22 UM FCC	0.097	0.24	4.58	3.9135	0.5507	88	GOOD RUN

TABLE 1.3 EXPERIMENTAL RESULTS

configurations C1 and C3 were used with vortex finder length as a variable. Particle loading rates were below 0.05 kg solids/kg air. Collection efficiencies were found to vary between 41 and 96 %. A summary of this test appears in Figure A1 of the Appendix.

Runs B4 and B10 were chosen for comparison in the scaling study because of particle analysis and data logging problems (i.e. program failed to record data) in the other runs. Specifically it was found that the particle catch distribution was greater than the particle feed distribution for particle diameters less than 15 microns. It is thought that the feed sample, which was taken before run B4, was finer than that actually fed in subsequent runs. This is attributed to the practice of recycling spent solids from one run to the subsequent run. This was necessary as all the available solids had to be fed in each run in order to achieve the desired loading levels. Unfortunately feed samples were not taken for each run as it was assumed that collection efficiency could be calculated from the catch and loss distributions alone. Note that fresh, unrecycled feed solids were used in runs B4 and B10.

1.3.1 Scaling Considerations

Catch particle size distributions for runs B4 and B10 appear in Figure 1.17a and Figure 1.17b respectively. Figure 1.17c shows the collection efficiency curve for run B4 as determined from particle size distributions obtained with the Elzone particle analysis instrument(model 286 XY) and the collection efficiency curve for run B10 as determined by the Tas Plus Image analyzer (model LSI -11). The first method reports the equivalent volume sphere diameter, while the second leads to an equivalent projected-area circle diameter (37). Figure A5 of the appendix details the particle size information.

Note that in Figure 1.17c the mass of particles greater than 20 μm in diameter have been combined into one channel with mean diameter of 31 μm. A similar adjustment was made to the run B10 collection efficiency curve with particles larger than 15 μm diameter being combined into one channel of 31 μm mean diameter. This grouping of the higher end channels was performed because of the erratic nature of the collection efficiency curve above 20 microns. It can be seen from Figure 1.17c that the cyclone was 50% efficient for particles of 10 μm diameter. A similar performance is noted in the efficiency curve for run B10 which shows a d_{p50} of 10 μm. This is surprisingly efficient performance for a 0.61 m diameter, non-standard design cyclone operating with an inlet velocity of only 3.6 m/s.

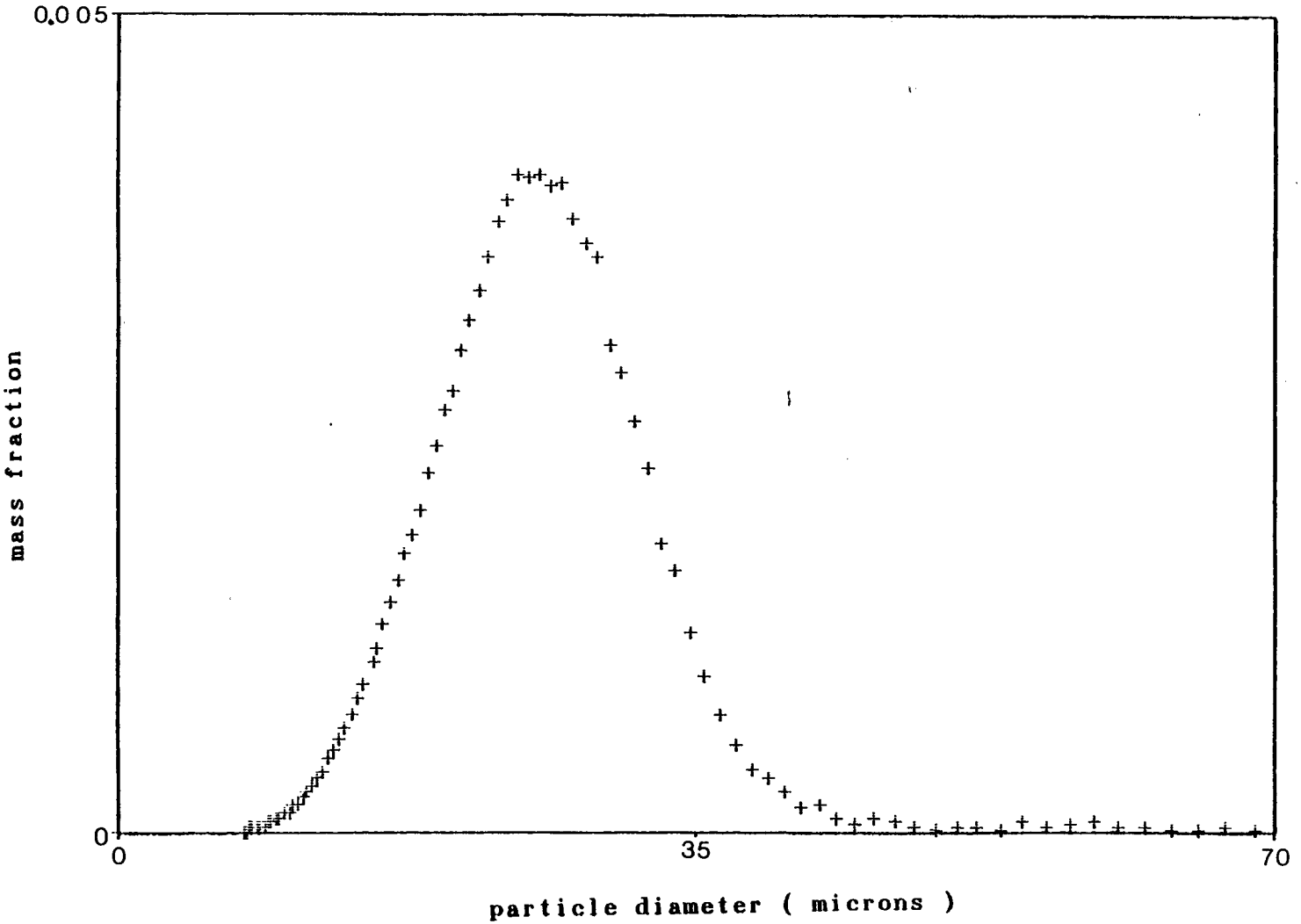

Figure 1.17a Catch particle size distribution for run B4
Particle size analysis by Elzone analysis machine.

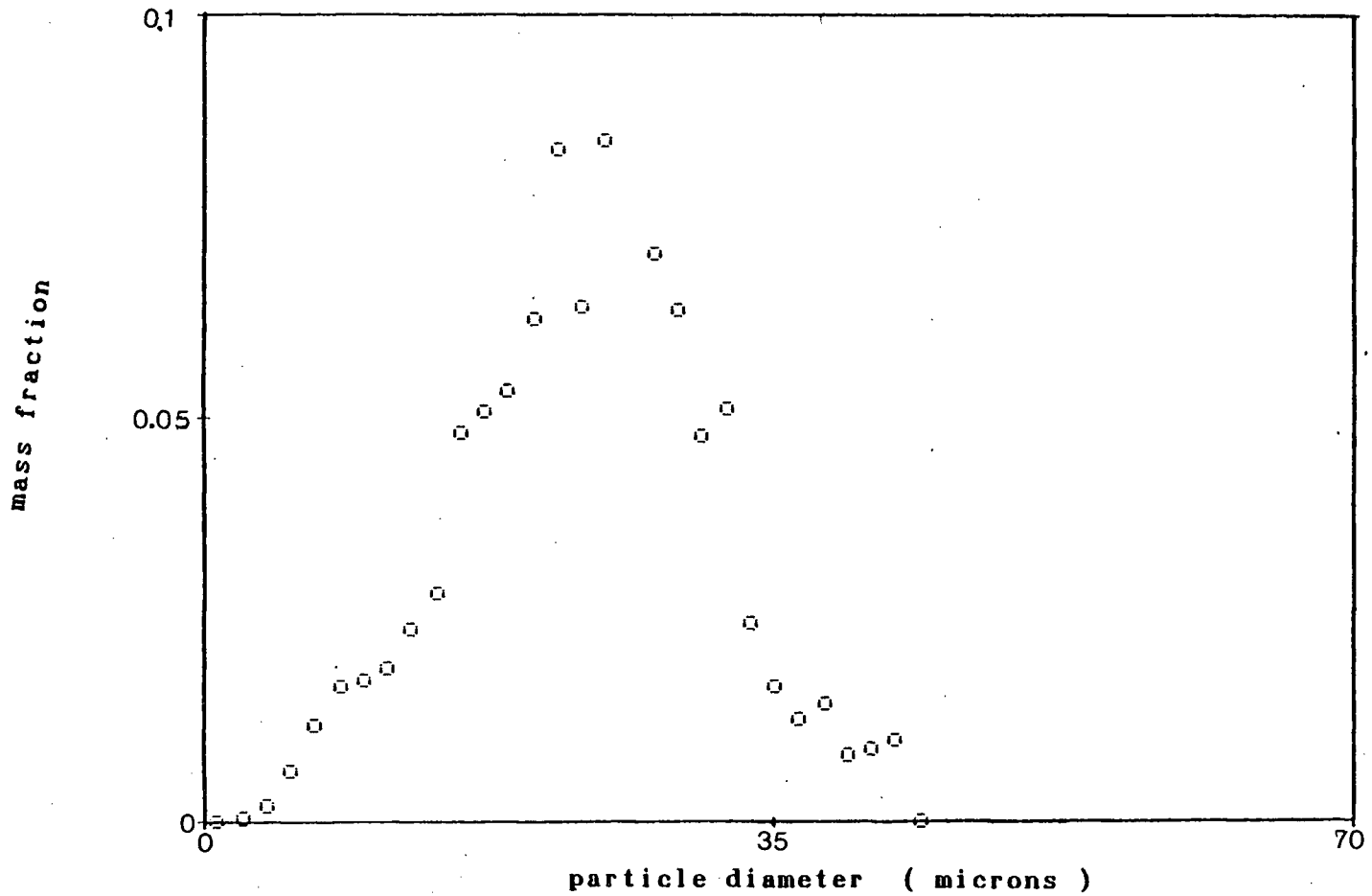

Figure 1.17b Catch particle size distribution for run B10
Particle size analysis by image analyzer.

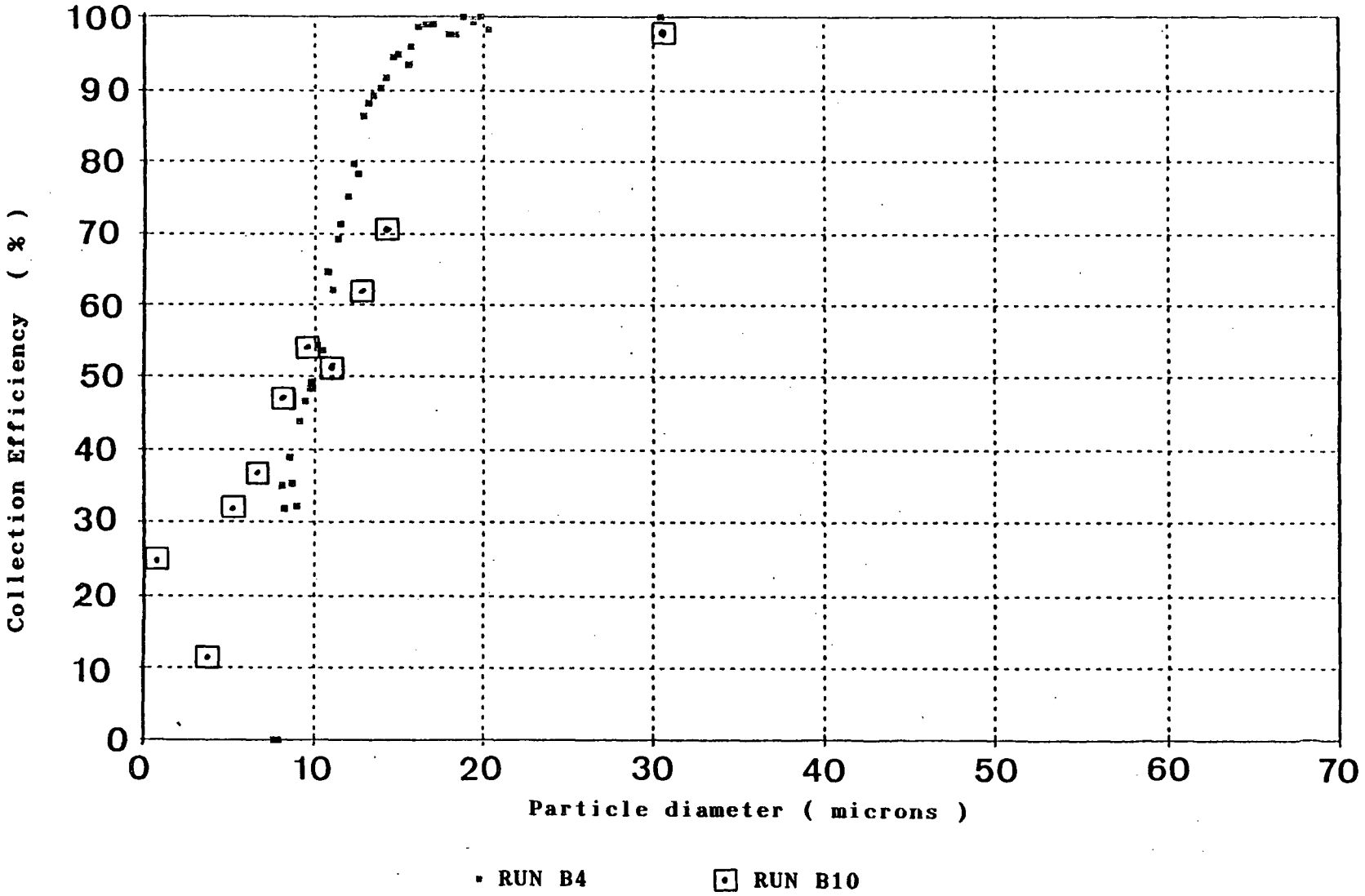

Figure 1.17c Collection efficiency curves for runs B4 and B10. Run B4 particle size distributions determined by Elzone particle analysis instrument. Run B10 particle size distribution by image analysis methods. Conditions as stated in Table 1.3.

There is a minimum in the collection efficiency at about 2.5 μm diameter in the run B10 efficiency curve, with a small increase in efficiency for smaller particles. There are three probable reasons for this. The first is that because of the cohesive nature of the solids, significant amounts of fines may have adhered to larger particles in the catch. During analysis these fines agglomerated with larger particles may have broke free and been counted as individual particles. This would have increased the mass fraction of fines reported in the catch.

The second possible reason arises from the problems of dispersing the dust in the feed gas stream. Particles fed to the cyclone came from the solids feed hopper and were maintained in a bubbling fluidized bed. It is possible that the smaller particles started out in an agglomerated state, were fed into the gas stream in this state and finally separated as large agglomerates. It may be necessary to provide a means of dispearsing the particulate while in the feed stream in order that the fines could be truly dispersed.

The third possible reason for the surprisingly high measured fines collection efficiency is that the fines may have been swept out of the gas stream by other larger particles. This effect has been reported by others (12, 24).

Mothes and Löffler (24) discuss in detail the phenomenon of improved collection efficiency for small particles separated in cyclones with high particle concentrations. They state that particle separation mechanisms other than separation in the vortex must have a major effect on particle separation and

develop a model to describe this effect. Briefly the calculation of fine particle collection due to agglomeration involves three steps:

1. The initial deposition efficiency of fine particles on larger particles settling towards the wall is calculated.

2. The gas volume cleaned by the larger particles traveling towards the wall is determined.

3. The decrease in fine particle concentration caused by the cleaning effects of the larger particles is estimated.

The model predicted that the separation efficiency of small particles in cyclones is a function of scrubbing particle size, small particle size, dust concentration, flow conditions and material properties. As an example they considered the case of 15 μm diameter particles scrubbing out particles sized below 6 μm diameter. The results are presented in Figure 1.4 and show a peak in the collection efficiency curves for particles sized between 2 to 3 μm diameter. A similar effect is noted in Figure 1.17c and occurs in the same range of particle diameters.

Considering the Chatham cyclone size distribution in Figure 1.18(a) the loss distribution was clearly separated from the catch particle size distribution with little overlap.

Comparison of the two distributions resulted in a typical collection efficiency curve with a dp_{50} value of 41 microns as can be seen in Figure 1.18(b). This is in the range reported in reference 1, that being 30 to 45 microns.

Performance comparison

The collection efficiency curves for run B4 and the Chatham cyclone are plotted in Figure 1.19.

In order to verify Stokes scaling, as interpreted by Stairmand, the performance of the Chatham cyclone was shifted to see if the performance would be close to the performance of the UBC cyclone. That is:

$$N_{st} \text{ of shifted } dp_{50} = N_{st} \text{ of Chatham } dp_{50}$$

$$\frac{dp_{50new}^2 \rho_{pUBC} V_{iUBC}}{D_{UBC}\ \mu_{UBC}} = \frac{dp_{50old}^2 \rho_{pCHATHAM} V_{iCHATHAM}}{D_{CHATHAM}\ \mu_{CHATHAM}}$$

$$dp_{50new}^2 = \frac{dp_{50old}^2 \rho_{pCHATHAM} V_{iCHATHAM} D_{UBC}\ \mu_{UBC}}{\rho_{pUBC} V_{iUBC} D_{CHATHAM}\ \mu_{CHATHAM}}$$

Table 1.4 states the assumed scaling conditions. While the curves are brought closer together, a significant discrepancy is still seen. It is clear that the cold model with Stokes law scaling predicts too optimistically the performance of the Chatham cyclone.

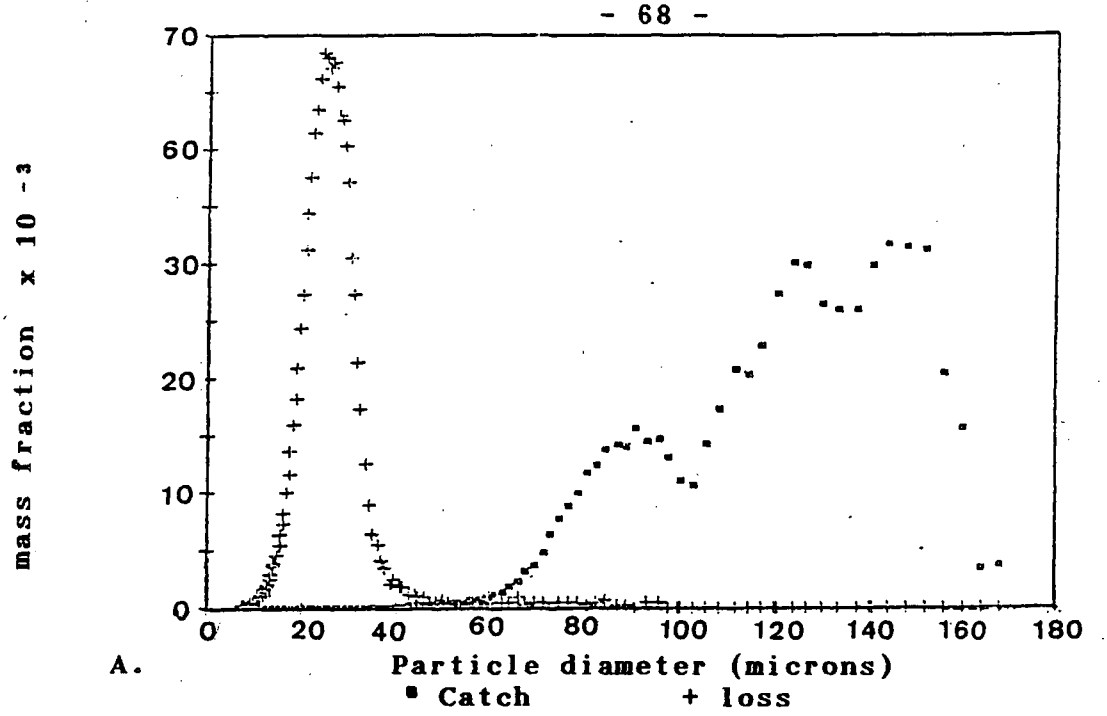

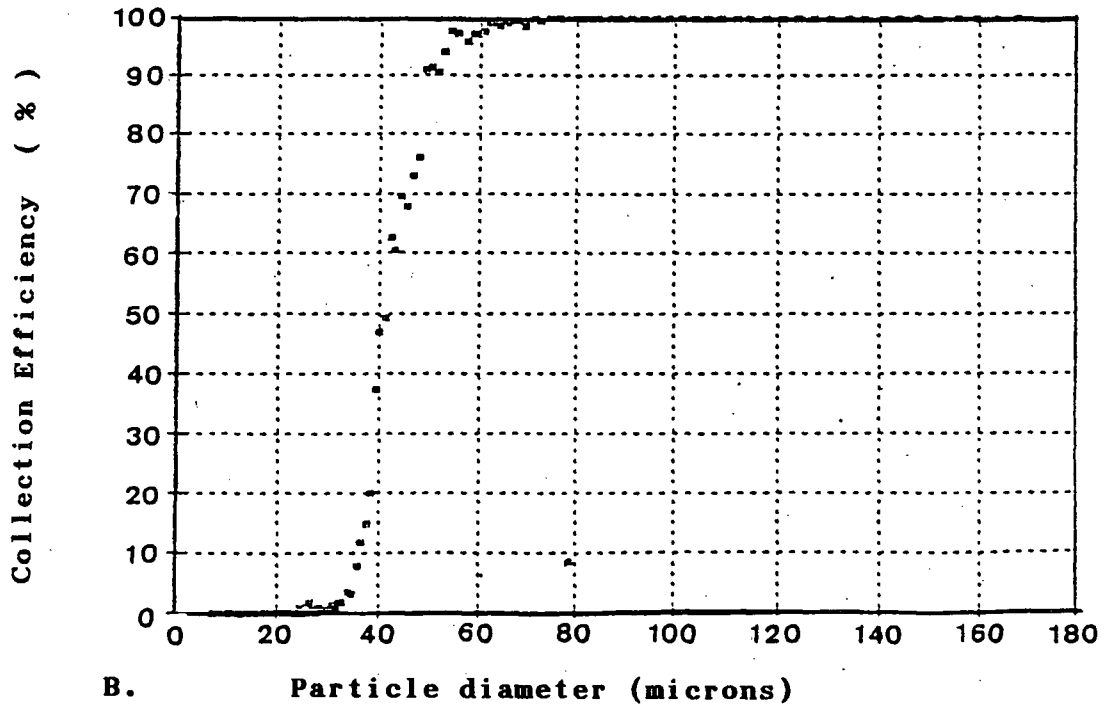

Figure 1.18 a.) Particle size distributions from Chatham fluid bed heat exchangers sampled April 17, 1990.
b.) Collection efficiency curve derived from particle size distributions. $E = (Cl_i/(Cl_i + Ll_i))$

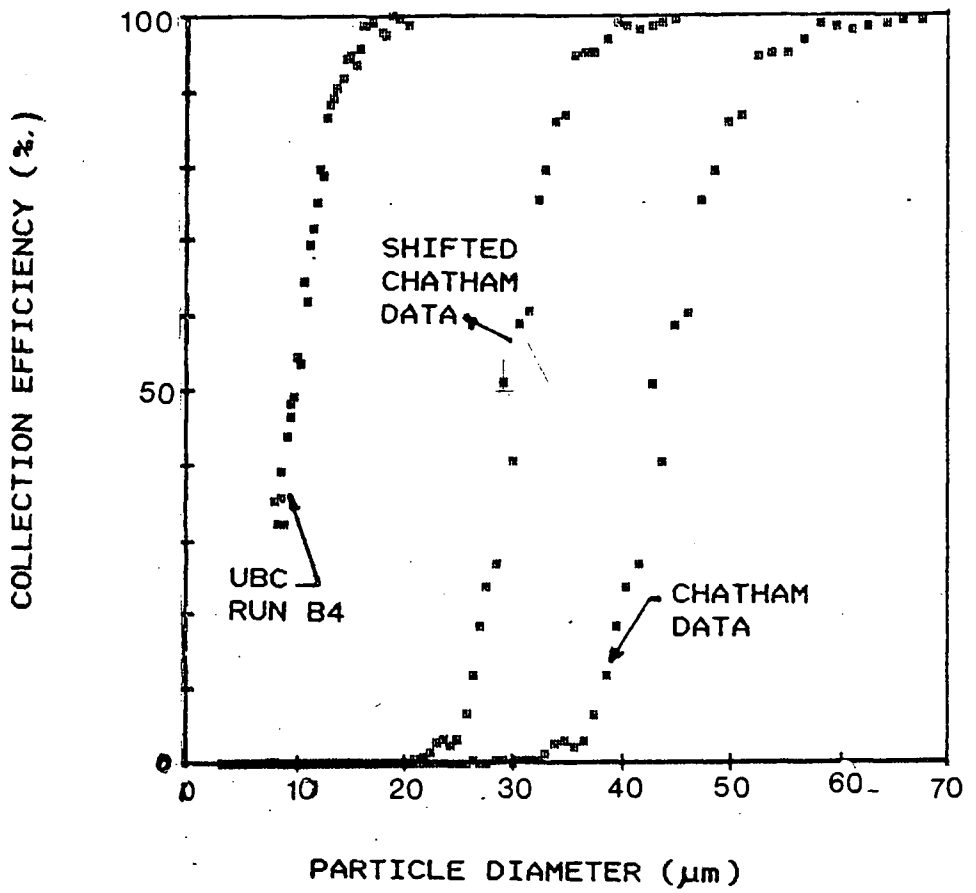

Figure 1.19 Collection efficiency curves for run B4, the Chatham cyclone and the Chatham cyclone shifted according to Stokes Law scaling. Scaling conditions as per Table 1.4.

TABLE 1.4. CYCLONE OPERATING CONDITIONS

	Chatham	UBC (Run B4)	
CYCLONE DIAMETER	5.6	0.61	m
TEMPERATURE	850	21	°C
GAS DENSITY	0.326	1.20	kg/m^3
GAS VISCOSITY	0.000045	0.000018	kg/m/s
PARTICLE DENSITY	2650.	1540.	kg/m^3
AIR FLOW (@STP)	1600	11.2	$m^3/min.$
INLET VELOCITY	20.4	3.66	m/s
STOKES NUMBER	0.020	0.0029	-
REYNOLDS NUMBER	830 000	149 000	-
LOADING RATIO	8.8	1.4	kg/kg

Note that the Stokes Number is defined as:

$$N_{ST50} = dp_{50}^2 \rho_p V_i / (18\ \mu\ D)$$

and the Flow Reynolds number is defined as:

$$N_{Re} = \rho_g V_i D / \mu$$

In Figure 1.20 experimental data are plotted against the particle size dependent dimensionless number $S^{0.5}$ proposed by Abrahamson and Allen (21) to correlate efficiency data from large, high temperature cyclones to those operating at room temperature. This approach was first discussed in section 1.1.4. Data from the Chatham cyclone appears to closely follow the trend shown in Figure 1.2b with the d_{p50} value falling close to 1. However data from Run B4 are less comparable, indicating a much greater collection efficiency than would be expected.

The Parker et al... study compared small cyclones operating at extreme temperatures and found that the efficiency data could be plotted against $(N_{RE})(N_{ST})^{0.5}$. A plot of the UBC

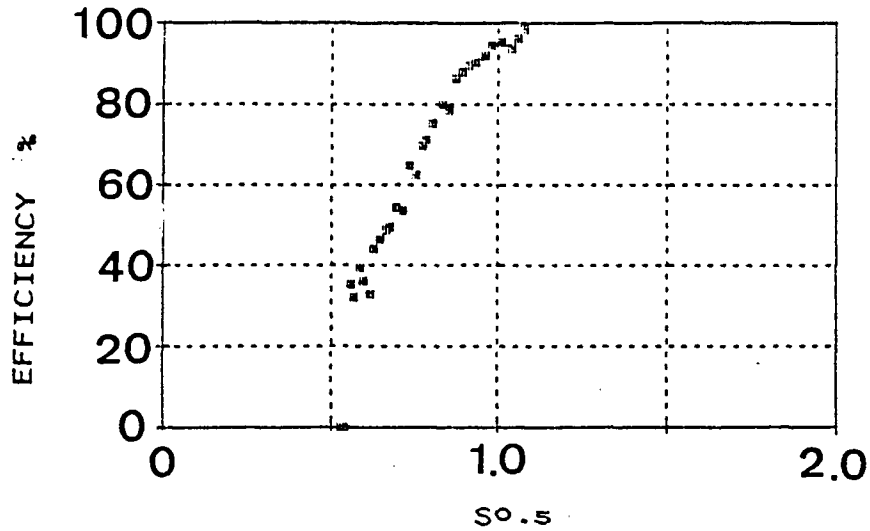

A.

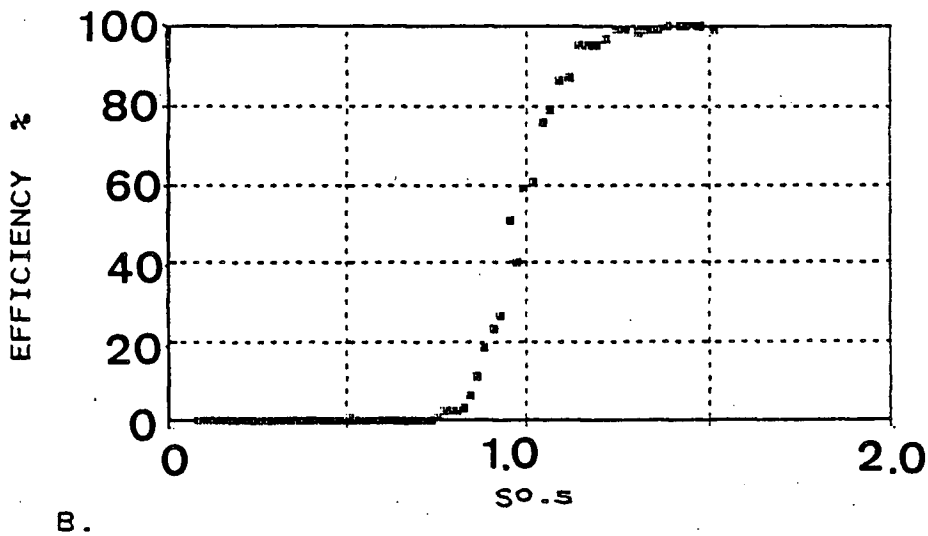

B.

Figure 1.20 UBC and Chatham data plotted according to Abrahamson and Allen correlations.
a.) UBC data (run B4 conditions).
b.) Chatham data.
See Table 1.4 for operating conditions.

and Chatham data on the same graph appears in Figure 1.21. Both the UBC and Chatham data fall above the small cyclone Parker et al. data. This was also found to be the case for other larger cyclones compared in their study. The authors suggest that cyclone diameter must play an important role (11).

The major discrepancy between the UBC and Chatham collection efficiency curves, and the fact that the model's performance was much superior to other cold models compared in the Abrahamson study leads one to suspect the experimental data. It is suspected that,in the UBC tests, particles separated in an agglomerated form, separating as large masses rather than independent entities. Sample preparation, which required sonicating the sample in a liquid media, may well have resulted in disassociation of particles which were then counted individually. Indeed a certain degree of agglomeration is evident in the photographs of the test dust.

A means of determining the level of agglomeration within the cyclone would be needed to confirm this. Particle agglomeration may have been influenced by two factors.

1. Electrostatic forces, induced by the motion of the particles in the polyacrylic cyclone, may have caused particles to agglomerate. Repeating the experiments in a steel cyclone or with the addition of an anti-static compound may reduce these effects.
2. Poor dispersion of particles being fed to the cyclone may have resulted in the particles entering the cyclone in an agglomerated state. Changing the experimental apparatus to

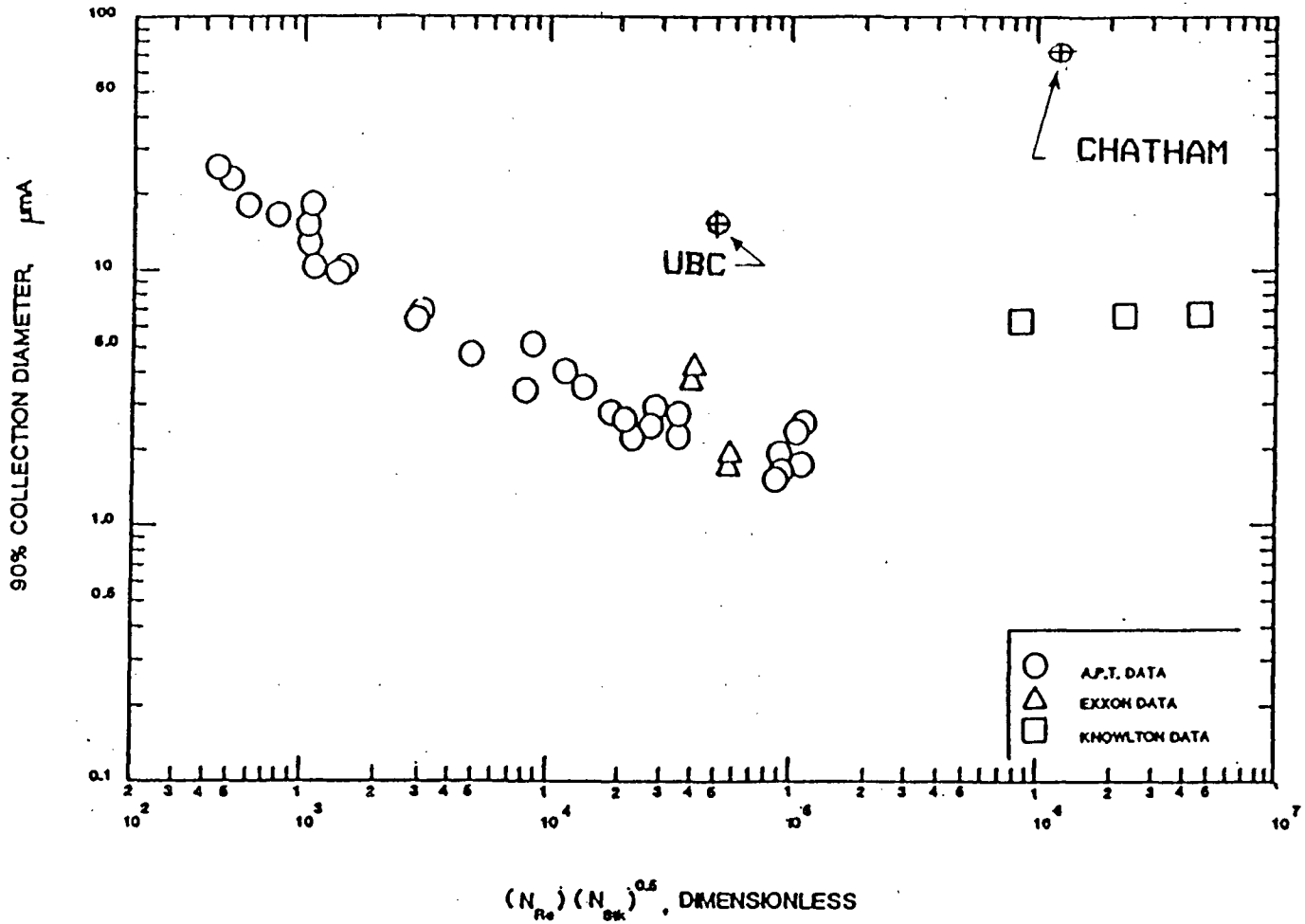

Figure 1.21 UBC Run B4 and Chatham data compared with Parker et al. data. Conditions as stated in Table 1.4

include a section where particles are smashed against a baffle or disassociated by sonic action may resolve this problem.

1.3.2 Loading effect

Runs B9 and B12 through B20 were performed for the particle loading study and the results are plotted in Figure 1.22 and the data is presented in Tabel 1.5. A clear increase in collection efficiency is noted as particle loading is increased.

Table 1.5 Particle Loading Data

run #	loading $\frac{\text{MASS SOLIDS}}{\text{MASS AIR}}$	collection effficiency %
B12	0.235	91
B13	0.124	87
B14	0.134	90
B15	0.147	89
B16	0.437	90
B17	0.376	91
B18	1.303	96
B19	0.049	84
B20	0.658	93
B9	7.49	98

These reults are consistant with that reported in other works (18) in two ways in that efficiency increases with loading and no limit or maximum is found. Attempts to increase the loading to levels greater than 7.5 kg solids/ kg air were not successful due to solids feeding limitations.

The loading effect is commonly attributed to the action of particle-particle collisions and agglomeration mechanisms which allow the solids to settle out in large clusters and strands rather than individual particles (23,24). Confirmation of this

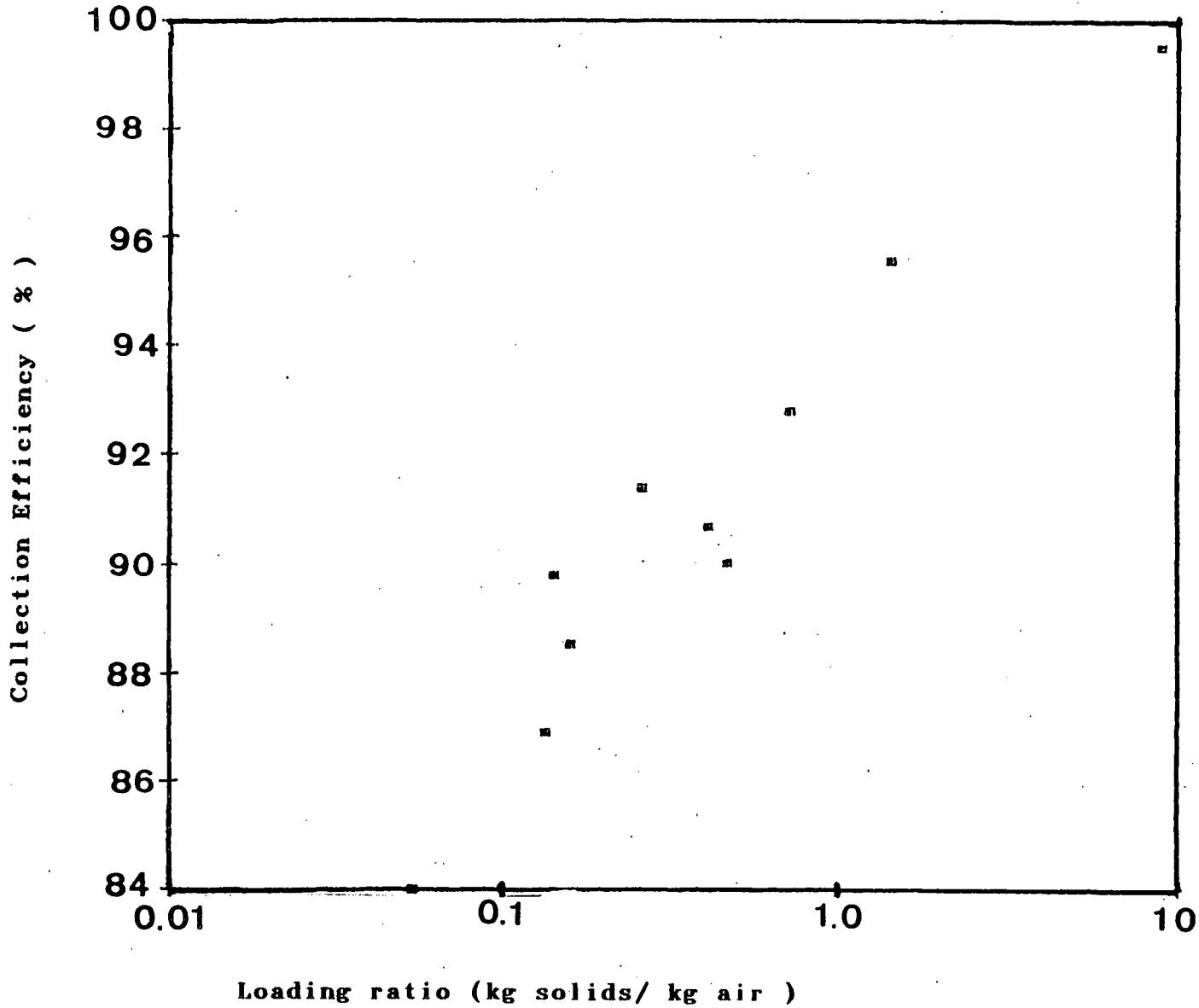

Figure 1.22 Loading effect on collection efficiency (UBC data). V_i = 5.0 m/s, T = 21 °C, P = 1 atm..

theory is not possible from this experimental work, but it may be possible to verify this if a method of measuring agglomeration levels in the separation zone as a function of inlet loading can be found.

Unfortunately it was not possible to achieve the very low loadings (1 gr/ft^3, 2.3 g/m^3) reported in the API study (see Figure 1.3) because of problems with the large solids feeding cone valve. An improved experiment would include a means of feeding solids on the 1 to 10 gr/ft^3 (2.3 to 23 g/m^3) range. A smaller cone valve, one tenth the size of the 0.25 m diameter valve would likely suffice.

1.3.3 Inlet Modifications

Table 1.6 summarizes the experiments devoted to inlet modifications. In order to compare the collection efficiencies for the different inlet configurations the efficiencies listed here have been modified to account for loading effects. The modification procedure was as follows:

> All runs are compared on a basis of the loading found in run B24 i.e. 0.232 (mass solids/ mass air). This run was chosen because its loading value fell in the middle of all the other loadings encountered in the inlet modification tests.
>
> A best fit line was drawn through the loading data found in section 1.3.2 and the equation of this line established as:
>
> $E(L) = (0.0301)\ln(L) + 0.9097$
>
> where
>
> $E(L)$ = collection efficiency at loading L
>
> L = Loading (mass solids/mass air)
>
> Taking the derivative one obtains:
>
> $$\frac{dE(L)}{dL} = \frac{0.0301}{L}$$

Corrected efficiency values ($E_{corr.}$) were obtained by according to:

$$E_{corr.} = E_{exper.} + 0.0301(L_{exper.} - L_{B24})/L_{exper.}$$

where

$E_{exper.}$ = efficiency determined at other loading

$L_{exper.}$ = loading in test

During the run the inlet geometry and vortex finder length were altered, resulting in different inlet velocities and particle paths within the cyclone. The runs have been placed in order of increasing inlet velocity, with the final three runs differing from the rest in that the vortex finder was elongated 212 mm in this situation. The data is plotted in Figure 1.25.

Inlet geometry details are shown in Figure 1.10 and briefly described below.

Configuration C1. The base case situation with no inlet inserts or vortex finder changes have been made. See Figure 1.9 for dimensions.

Configuration C2. The inlet floor has been raised 50 mm above the original floor and the ceiling lowered 30 mm for a short section near the reactor. The rear wall has been straightened out reducing the inlet width to 110 mm from 150mm.

Configuration C3. As per configuration C2 but with the inlet width enlarged to 135 mm.

Configuration C4. As per configuration C3 but with the vortex finder lowered 212 mm.

TABLE 1.6 Inlet Modification Tests

RUN	CONFIGURATION	COLLECTION EFFICIENCY
B26	c1	96
B27	c1	96
B28	c1	94
B33	c1	94
B34	c1	97
B24	c3	94
B25	c3	93
B35	c3	92
B21	c2	94
B22	c2	92
B23	c2	93
B29	c3 & low vortex finder	94
B30	c3 & low vortex finder	94
B31	c3 & low vortex finder	96
B32	c3 & low vortex finder	96

It would be expected that collection efficiency would increase as the entrance inlet area was decreased, that is as the configuration was changed from C1 to C3 to C2. However, this was not evident in the data and the base case with the lowest inlet velocity performed better than either C2 or C3. Configuration C3 coupled with a lower vortex finder offered better collection efficiency than C2 or C3, alone but still not significantly different than the base case.

For the same geometric configuration it was not possible to reproduce the same collection efficiency as is seen in Figure 1.25. Only in runs B26, B27, B28 and B33, for configuration C1, were similar collection efficiencies noted. This variation is attributed to differences in the experimental

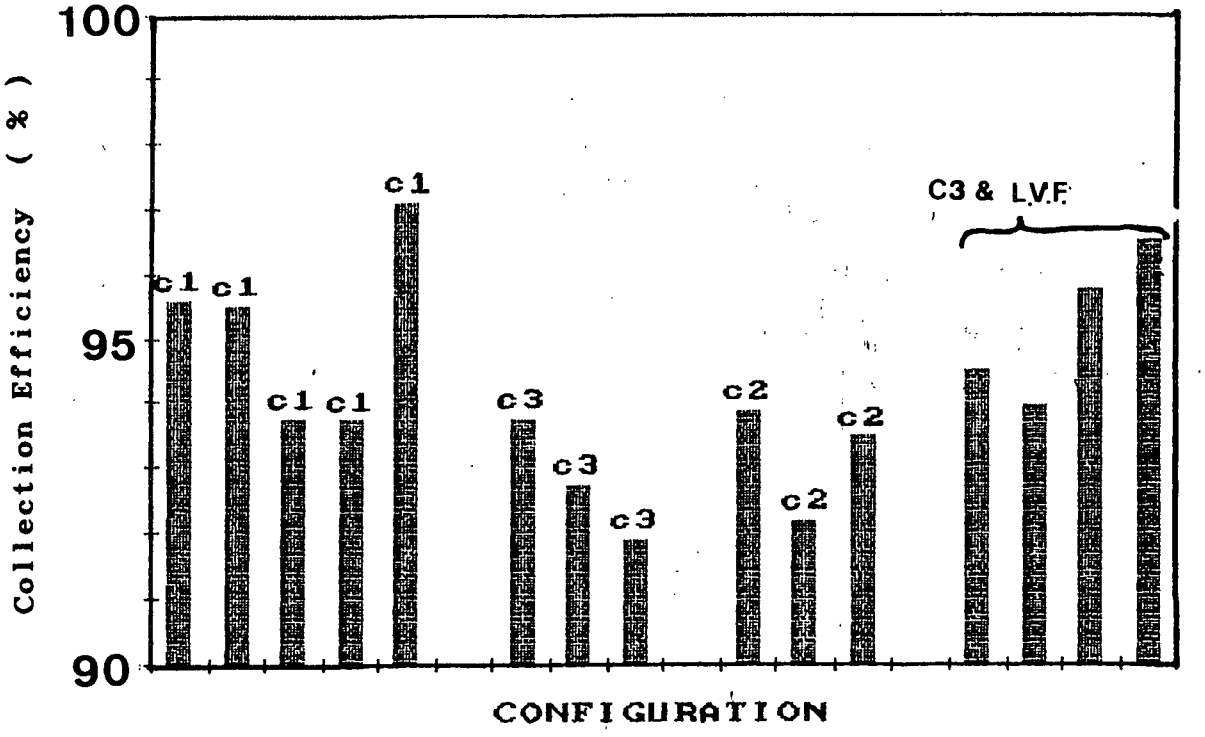

Figure 1.23 Comparison of collection efficiencies for different inlet configurations. See Table 1.3 for conditions. (solids loading corrected).

conditions between these runs, specifically the variations in the loading rate.

While it seems clear that collection efficiency is greater than 90% for all runs, it is not possible, based on the data collected to date, to declare a "winner" among those tried. These puzzling results suggest that a different experimental approach is necessary. An improved experimental program would result in a steadier feed rate, perhaps by way of a mechanical feeder as it was difficult to repeat loading levels with the present solids valve feeding arrangement. As well, a solids system less prone to agglomeration would allow efficiency curves, which span a full range of efficiencies, to be determined. Examination of these improved efficiency curves may offer better answers.

1.3.4 Flow visualization

Separate runs of the cyclone apparatus were performed for the purpose of flow visualization. Collection efficiency was not evaluated during these runs. These runs were performed at low loading in order that flows in the interior could be observed.

During the trials the following observations were made for all geometries:

Recirculation zone below roof: It could be seen that a distinct annular region exists, concentric with the cyclone itself but situated above the roof of the entrance and below the roof of the cyclone. Suspended solids either enter this zone or fall from it to the separation region below. Any solids that found their way into this zone are eventually reentrained in the incoming flow, but spend considerable time in the region.

Reentrainment into incoming flow: Solids that manage to reach the outer wall must drop below the bottom of the entrance if they are not to be reentrained again by the incoming flow. The Stokes number scaling

approach is unlikely to apply to particle-particle and particle-wall interactions. Their effect may cause performance to be somewhat unrepresentative of performance in the full scale cyclone. It can be argued that those particles whose misfortune it was to reentrained must then be separated once again with particles in the incoming flow, and thus may be representative of matters at Chatham.

For the base case, where no inlet inserts were used, a recirculation zone could be seen positioned in the entrance way near the top of the model combustor. This recirculation was not evident with the inserts in place as in Configuration C2 or C3. There was no great visible difference in the particle paths for the existing and modified vortex finder configuration. This may be due to the difficulty in seeing flow patterns in the dilute region close to the vortex finder. More advanced techniques for flow visualization (e.g.. laser Doppler techniques) would be required to study this in detail. The video tape sent to Energy, Mines, and Resources shows the observations discussed above.

1.4 Conclusions and Recommendations.

The main features of part I of this study are as follows:

1. A one-ninth scale polyacrylic model of the non-standard design industrial cyclone operated at the 22 MWe CFBC facility at Chatham, New Brunswick has been constructed and operated at room temperature. Particle collection performance has been tested under various solids loadings and inlet geometries.
2. A solids recycle system, utilizing a multiclone to capture fines and a recycle system to provide continuous operation was built, but did not work well because of solids capture problems and the cohesive nature of the fine solids. As a result, all of the results presented are for a batch system.
3. At inlet velocities varied between 3.7 and 5.5 m/s, solids loadings between 0.05 and 7.5 (kg solids/kg air), for FCC solids having a mean diameter of 22 μm, cyclone collection efficiencies remained above 90%.
4. There was disappointing agreement between the results from the Chatham unit, scaled according to Stokes Number scaling, and the findings obtained from the cold model unit.
5. The grade efficiency curve showed a minimum efficiency for fine particles, 2.5 to 3.0 μm in diameter. This is likely due to agglomeration effects as a mass balance performed on a per channel (i.e.

size interval) basis did not close for particles smaller than 15 um diameter.

6. Increasing particle loading led to an increase in collection efficiency.
7. Inconclusive results were found when the inlet configuration was changed while using 22 um mean particle diameter FCC solids.
8. Flow visualization trials were performed with the polyacrylic cyclone. Reentrainment into the incoming flow of captured solids skipping along the wall was observed. A videotape of these observation was prepared and sent to Energy, Mines and Resources in Ottawa.

It is recommended that, in order to verify the scale-up criteria, the experiments be repeated with a different solids system less prone to agglomeration. Successful collection efficiency studies have been performed using flyash at lower loadings (11, 12) suggesting that flyash might be a suitable material.

PART II

HOT CYCLONE TESTS

2.1 INTRODUCTION

Circulating Fluidized Bed Combustors (CFBC) rely on inertial separation devices to separate combustion gases from entrained solid particles and to return those solids to the reactor. Cyclones are usually chosen to perform this high temperature, high loading and sometimes high pressure separation because they offer reasonably good particle collection efficiency and are easy to design, operate and maintain. When used in such circumstances, some combustion inevitably occurs within the cyclone.

In order to better understand the combustion processes within the cyclone, radial combustion gas concentration profiles were measured within a secondary cyclone serving a pilot scale CFBC system operated at the University of British Columbia. The profiles presented in this thesis were all obtained with Highvale coal, a low sulphur coal from Alberta as a fuel. For details of properties of the coal see See Figure A6 of the appendix. In this section a brief review of gas and solids flows within a cyclone is given, followed by a description of the apparatus and a presentation of the measured combustion gas combustion profiles. The profiles are then discussed and conclusions presented.

2.2 Theory

Combustion processes occurring within cyclones are dependent on the nature of the solids, the composition of

the gas as well as the operation mode of the combustion system. Gas and solids flow patterns within cyclones are functions of several variables including cyclone dimensions and geometry, gas flow rates, and particle loading. When used in a CFBC system, the solids are a combination of unreacted fuel particles, inert solids (Eg. sand and ash) and sorbent material (if a sorbent is used). The combustion gas composition depends on fuel type, combustor configuration, mode of operation, operating temperature and other parameters. In order to understand the gas concentration profiles, it is first necessary to briefly describe the gas and solids flow patterns within a reverse return cyclone and to present the overall combustion equations which characterize CFBC systems.

Flow patterns

Gas and solids flow patterns within a cyclone are intimately related. Solids flow patterns have been observed in a cold model by the author (see section 1.3.4) and documented by several other workers (2, 25). The radial, tangential, and axial components of the solids velocity vary with position and solids loading (15). Predictions of low loading particle mean trajectories appear in Figure 2.1 (25) and show the predicted axial and radial position of particles of various sizes.

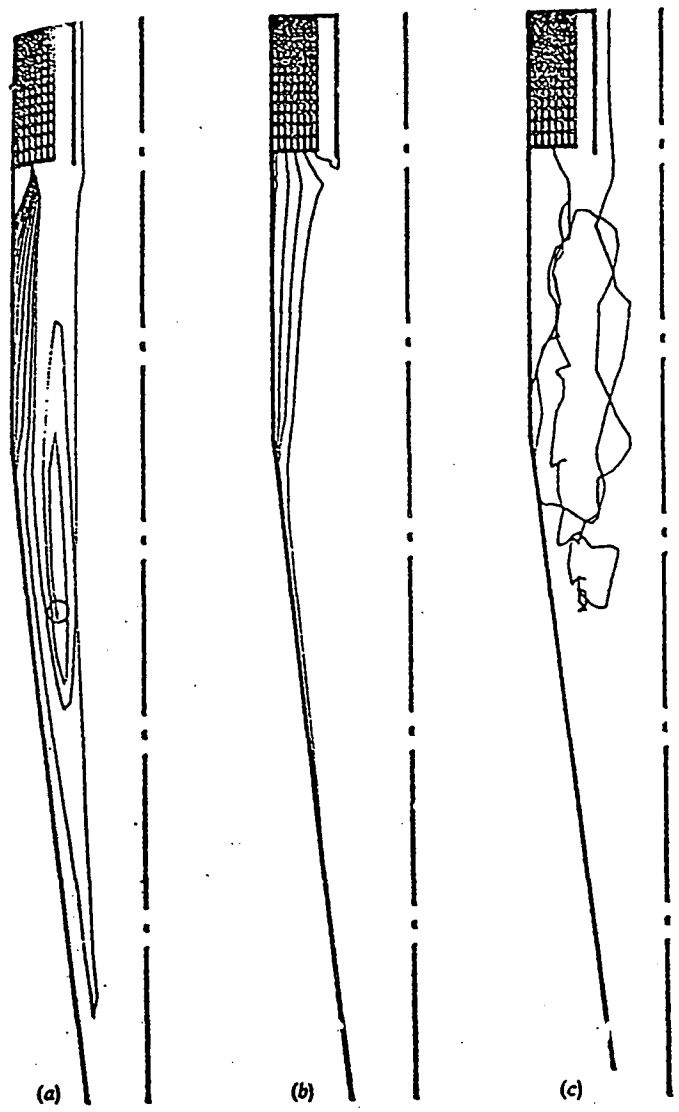

Figure 2.1 Predicted particle trajectories in a vertical plane within a Stairmand type cyclone. Low loading conditions. (25)

a. Mean particle trajectories for particles of diameter 1 to 10 microns.
b. Mean particle trajectories, 3 micron.
c. Random particle trajectory of 2 microns particle in turbulent flow.

In Figure 2.2 the axial gas velocity is seen to be a function of radius, with downward motion occurring in the outer regions, while within the core the flow reverses and travels up with increased velocity towards the vortex finder. The tangential velocity has been found to increase with decreasing radius, reaching a maximum in the central core region below the vortex finder. Increased particulate loading has been found to reduce the tangential component of gas velocity (24). Figure 2.3 shows the combined radial and axial velocity vector field.

Particle trajectories

Particle motion within these complex flow patterns depends on gas and particle characteristics, and on solids loading (15). As solids loading increases, particle-particle collisions become more frequent, forming larger clusters and strands which assist particle collection. Once the particles have reached the wall they may be re-entrained should some disturbance occur, forcing the solids back into the gas flow. Disturbances such as large bouncing particles, interior wall surface imperfections and interference of the gas vortex with the cyclone wall have been discussed by various authors (2,24). At the wall a dense layer of solids forms, with particles travelling around and down the cyclone body, eventually concentrating into a distinctive dense strand which "snakes" its way down to the solids exit at the base.

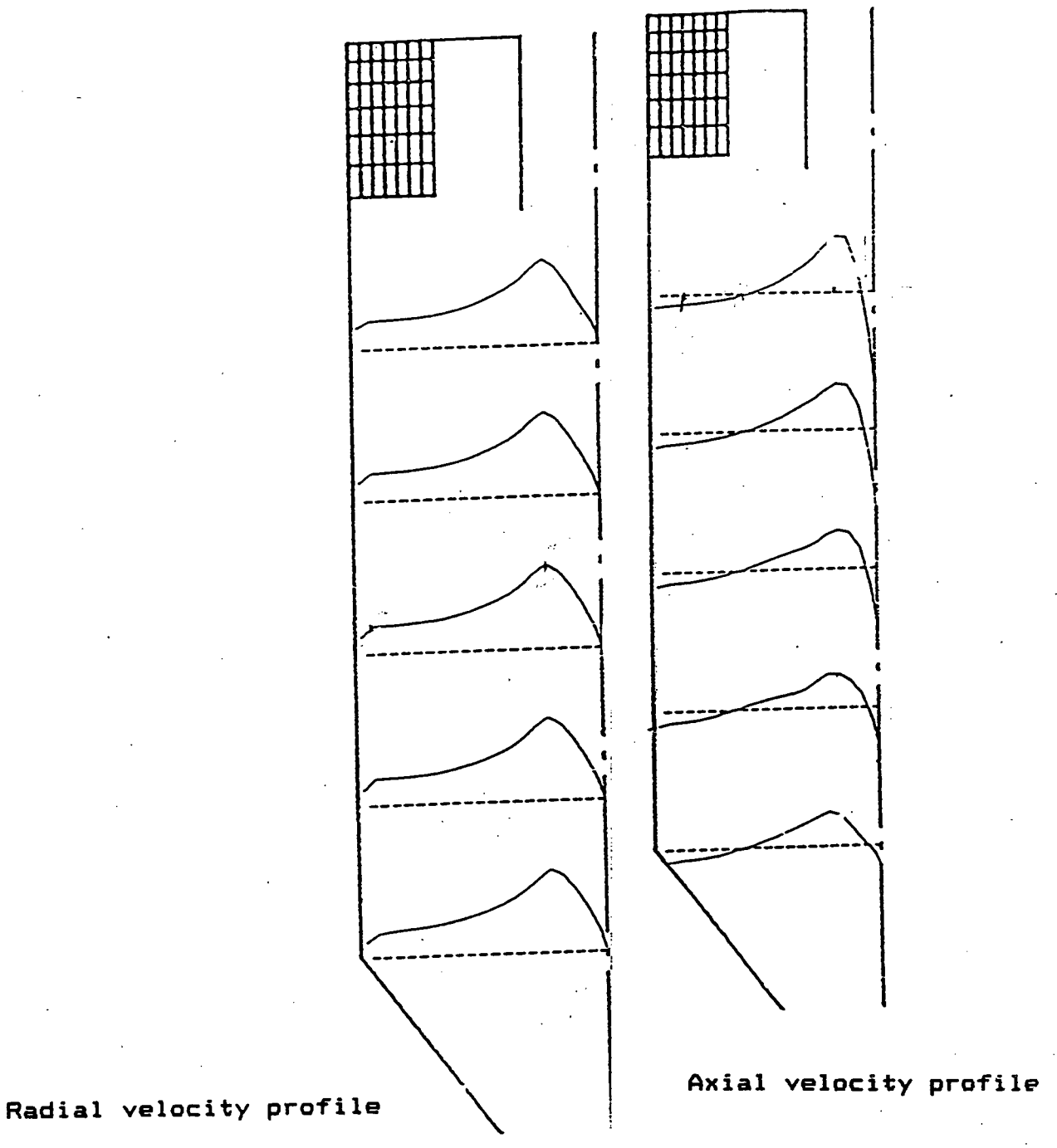

Figure 2.2 Predicted radial and axial gas flow patterns in a Stairmand type cyclone. Low loading conditions (25).

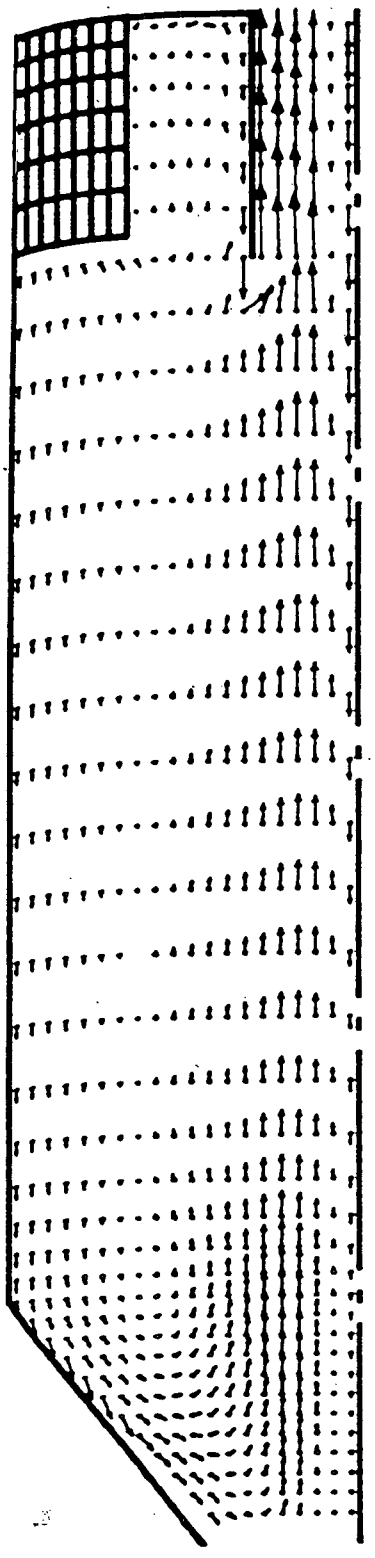

Figure 2.3 Predicted combined axial and radial velocity vector diagram in a Stairmand type cyclone. Low loading conditions(25)

Summary of combustion equations.

While it is not within the scope or intent of this thesis to discuss heterogeneous combustion mechanisms for coal combustion within a CFBC, it is useful to describe the primary reactions affecting the gases measured within the cyclone. The gases CO_2, CO, CH_4, SO_2, and NO_x are all formed during coal combustion. CO_2 is primarily formed by the two reactions (26):

$$C^* + O_2 \rightarrow CO_2$$

$$CO + 1/2\ O_2 \rightarrow CO_2 \ .$$

CO can be formed as follows:

$$C^* + CO_2 \rightarrow 2CO$$

$$C + H_2O \rightarrow CO + H_2$$

$$CO_2 \rightarrow CO + 1/2\ O_2$$

C^* represents the burning char.

CH_4 can be formed from:

$$C^* + 2\ H_2 \rightarrow CH_4 ,$$

or released as volatiles are evolved.

SO_2 can be considered to form via:

$$S + O_2 \rightarrow SO_2 \ .$$

while NO_x is formed by reactions of the type

$$1/2\ N_2 + x/2\ O_2 \rightarrow NO_x \ .$$

At temperatures of interest in FBC processes, it is fuel nitrogen, rather than nitrogen present in the air, which is predominantly responsible for NO_x formation (38).

Because most combustion within the CFBC system occurs before the secondary cyclone, much of each gas measured originates before the cyclone. A lesser amount is formed within the cyclone contributing to the measured values.

2.3 Apparatus and Data Acquisition

The apparatus used in this high temperature study is the pilot scale fluidized bed combustor at the University of British Columbia in its modified configuration (30). A schematic is shown in Figure 2.4. In brief, the set-up includes a refractory lined reactor (152mm square in cross-section by 7.3m tall), a primary and secondary cyclone with provision for solids recirculation via an L-valve and jet educator respectively, hoppers for feeding the fuel and sorbent, and primary and secondary air injection. The system is well instrumented. Comprehensive descriptions can be found elsewhere (27, 29). The secondary cyclone was chosen over the primary cyclone for these experiments because of the probe plugging problems associated with gas sampling in regions of high solids density (e.g.. at the cyclone wall). The insulated stainless steel secondary cyclone is situated after the primary cyclone and thus receives the reactor flue gases and particles not captured in the primary cyclone. A scale drawing of the secondary cyclone appears in Figure 2.5. This 0.2 m i.d. cyclone was modified to allow the insertion of a gas sampling probe through the wall at several levels. The probe itself was connected via cooling

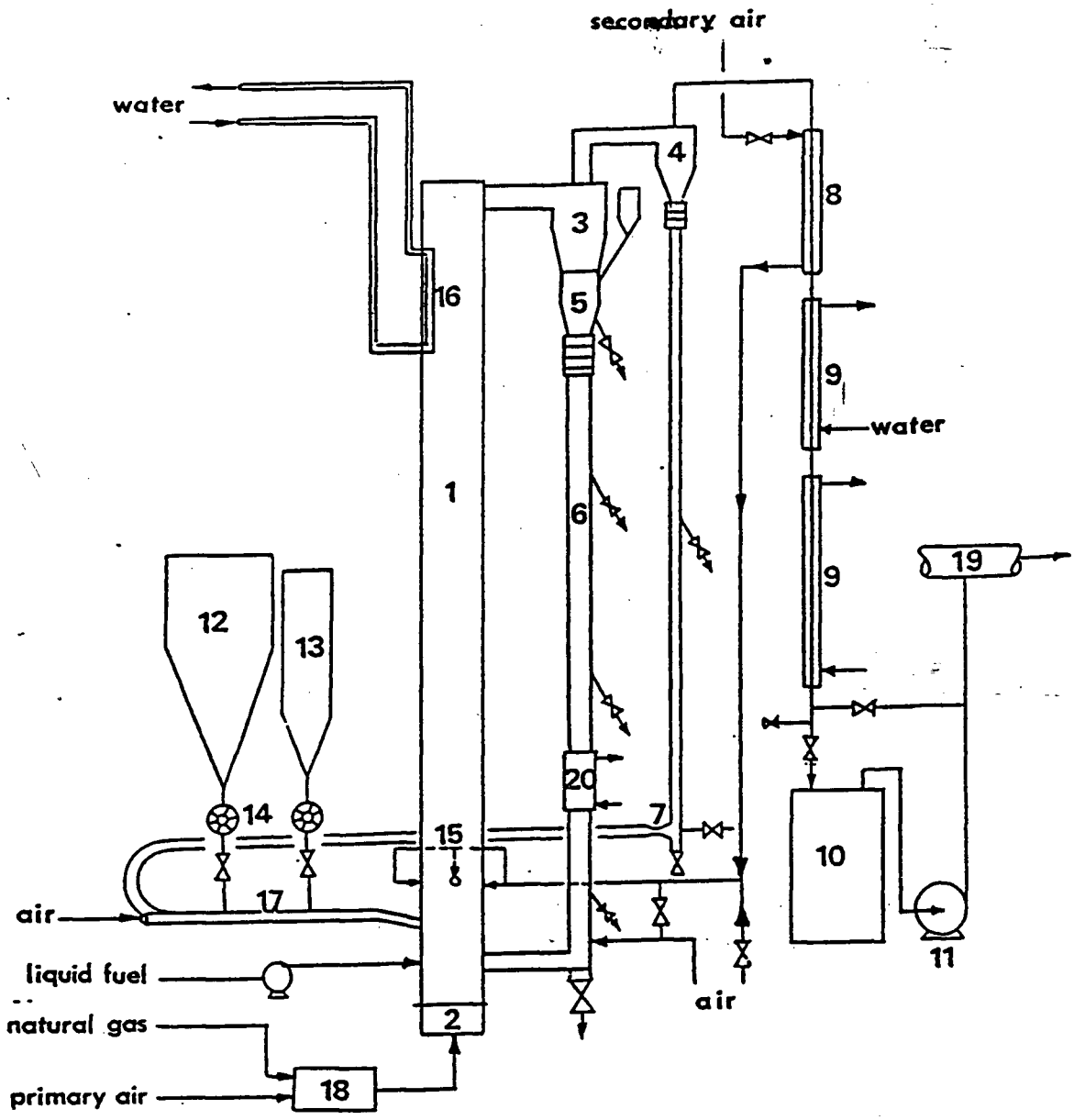

Simplified schematic diagram of circulating fluidized bed combustion facility

1. Reactor; 2. Windox; 3. Primary cyclone; 4. Secondary cyclone; 5. Recycle hopper; 6. Standpipe; 7. Eductor; 8. Secondary air preheater; 9. Flue gas coolers; 10. Baghouse; 11. Induced draught fan; 12. Fuel hopper; 13. Sorbent hopper; 14. Rotary values; 15. Secondary air ports; 16. Membrane wall; 17. Pneumatic feed line; 18. External burner; 19. Ventilation; 20. Calorimetric section

FIGURE 2.4 CFBC Schematic (27)

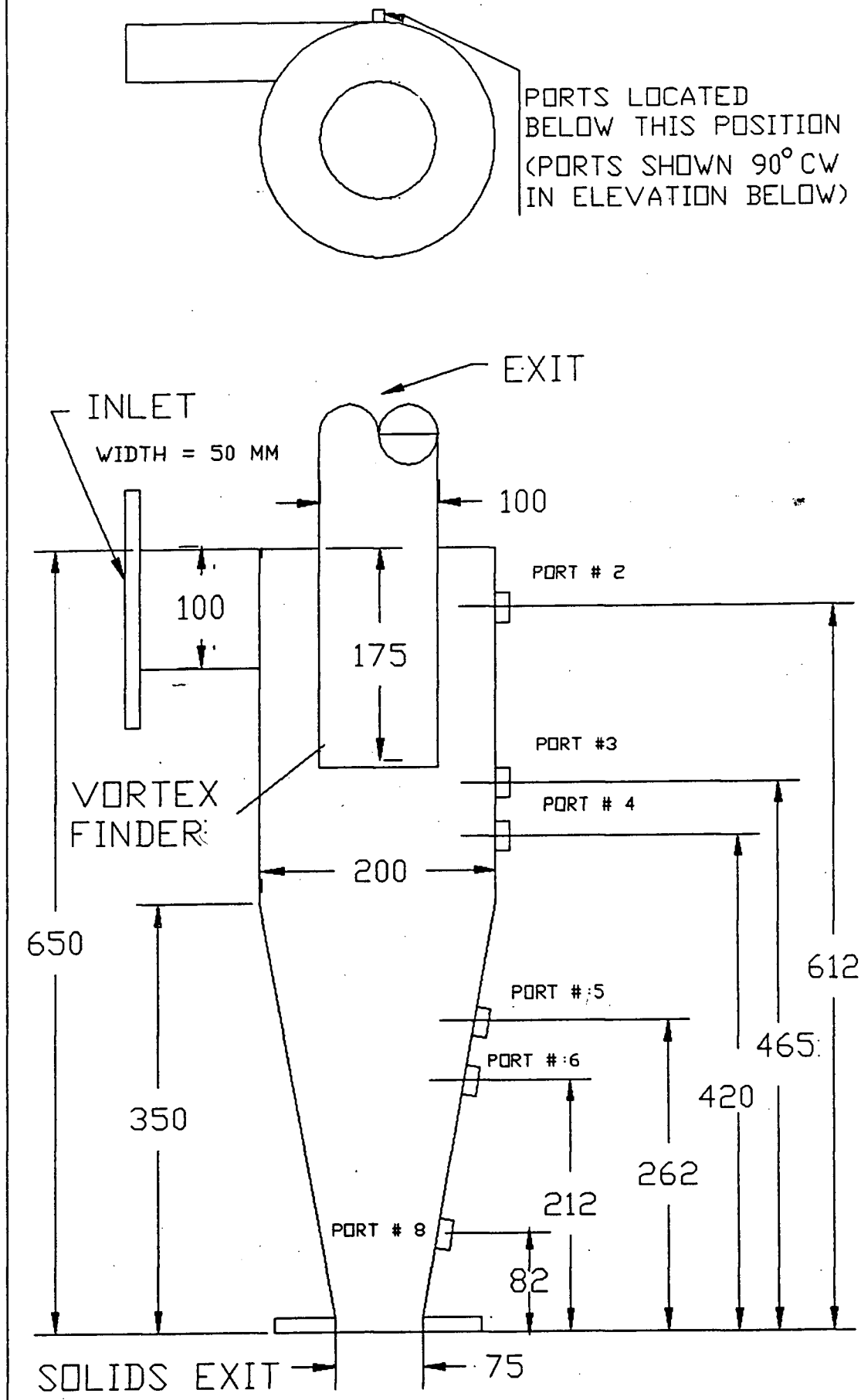

FIGURE 2.5 Scale drawing of secondary cyclone of UBC CFBC system.

and filtration stages to a gas sampling train. Figure 2.6 shows a schematic of this apparatus.

The gas sampling train leads to five analyzers for the measurement of CO_2, CO, CH_4, SO_2, NO_x, and O_2 gases. A brief summary of key features of these instruments is presented in Table 2.1. A more detailed review is found in reference 34.

TABLE 2.1: DESCRIPTION OF ANALYTICAL INSTRUMENTS

GAS	MAKE/ MODEL	RANGE (ACCURACY) (% full scale)	OPERATION PRINCIPAL	RESPONSE time
O2	HORIBA PMA 200 OXYGEN ANALYZER	0 - 25 % (1%)	PARAMAGNETIC TYPE	20s
C02	FUJI 732	0 - 20 % (1 %)	NDIR	5 s
C0	FUJI 732	0 - 1000 PPM (1 %)	NDIR	5 s
CH4	FUJI 730	0-0.5 % (1 %)	NDIR	5 s
S02	HORIBA PIR 2000	0-1000 PPM (1 %)	NDIR	5 s
NOX	MONITOR LABS INC. MODEL 8840	0-500 PPM (1 %)	CHEMILUMINESCENCE	3 min

Each of these instruments was calibrated using standard gases prior to each run.

The procedure followed to obtain data was as follows:

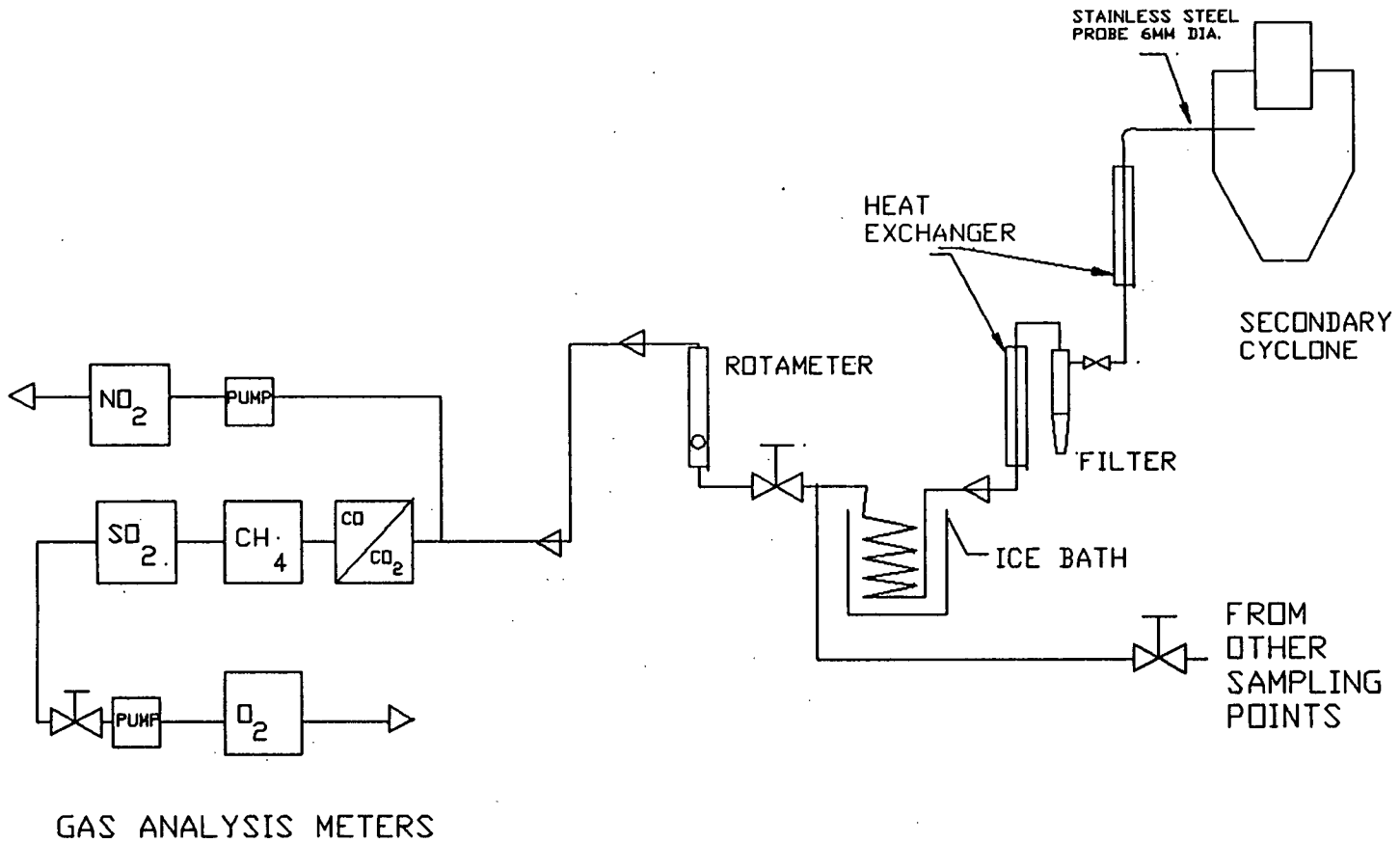

FIGURE 2.6 Gas sampling system serving UBC CFBC system.

1. With the pilot plant operating as nearly as possible under steady state conditions and gas analyzers prepared according to manufacturers' instructions, calibrated, the sample probe was inserted to the desired radial position and gas sampling commenced.

2. After a period of 4 minutes the gas transport lines were assumed to be purged and the gas analyzers reading steady state values.

3. Gas concentration values were recorded.

4. A flue gas [O_2] measurement was obtained from a separate gas meter operating on a separate sampling line connected downstream of the cyclone. The sampled gas stream was filtered and cooled.

5. The sample probe and filter were purged with compressed air, then moved to the next radial position. A random order was followed in probe positioning in order to avoid systematic variations.

2.4 Results and Discussion

The CFBC operating conditions under which the gas concentration profiles were obtained are outlined in Table 2.2 for each of the five runs where data were obtained.

Table 2.2 UBC CFBC operating conditions

RUN #	RUN TEMPERATURE (C)	AIR RATIO 2nd/prim.	RUN SUPERFICIAL VELOCITY IN RISER (M/S)
17	870	1	6
18	870	1	6
5	886	2	6
6	870	2	6
10	870	0.5	7

The secondary air ports, as shown in Figure 2.4, supplied between 50 to 100 % of the primary flow and were located 0.9 m above the primary air distributor. The riser velocity is

the superficial velocity in the upper part of the column above the secondary air ports.

The gas concentration profiles for runs 17, 18, 5, 6, and 10 appear in Figures 2.7, 2.8, 2.9, 2.10, and 2.11, respectively. For each gas the actual measured concentration is plotted against the non-dimensional radius r/R, where R refers to the cylinder or core radius at that level.

For all of the measurements it was possible to maintain sufficient sample gas flow to allow easy measurement, with the exception of readings taken right at the wall. For these measurements gas flow was possible for 10 minutes at most before blockage occurred, necessitating probe and filter purging. This is understandable since a denser region of solids exists at the wall than in the interior of the cyclone. While it was possible to obtain measurements in the vicinity of the wall the values may be affected by excessive solids in the probe and filter portions of the sampling system itself. Char caught in the probe could continue to burn, thereby increasing the CO and CO_2 values while, reducing the measured O_2 values. This effect is assumed to be negligible, however, as the gases and particulate were quickly cooled after extraction in the cooling section of the probe and thus were much less reactive. Typically the solids caught by the secondary cyclone had a mean diameter between 40 to 58 μm (29). Trends for the various components measured were as follows:

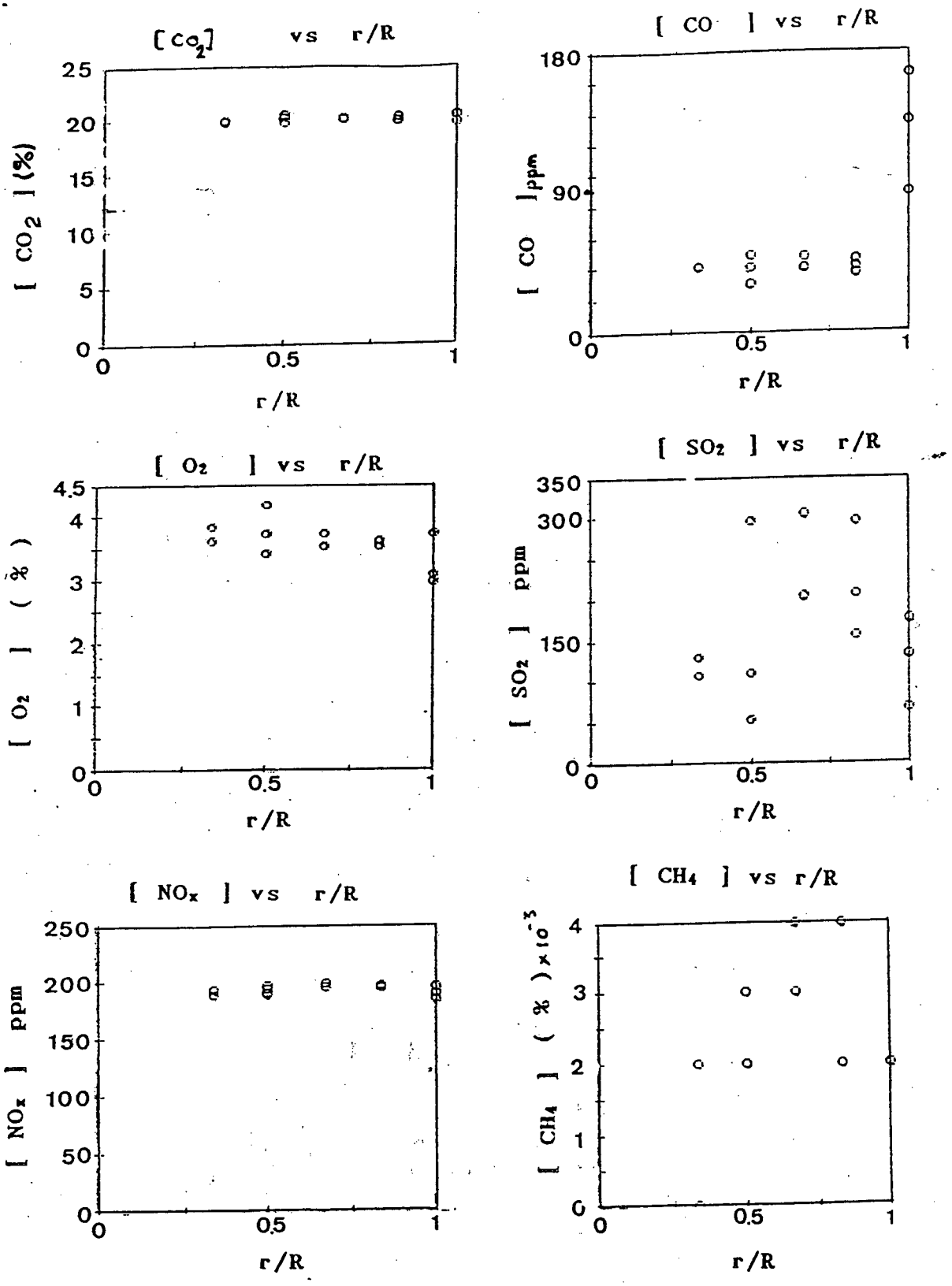

FIGURE 2.7 Gas Concentration Profiles for run 17.
port # 4

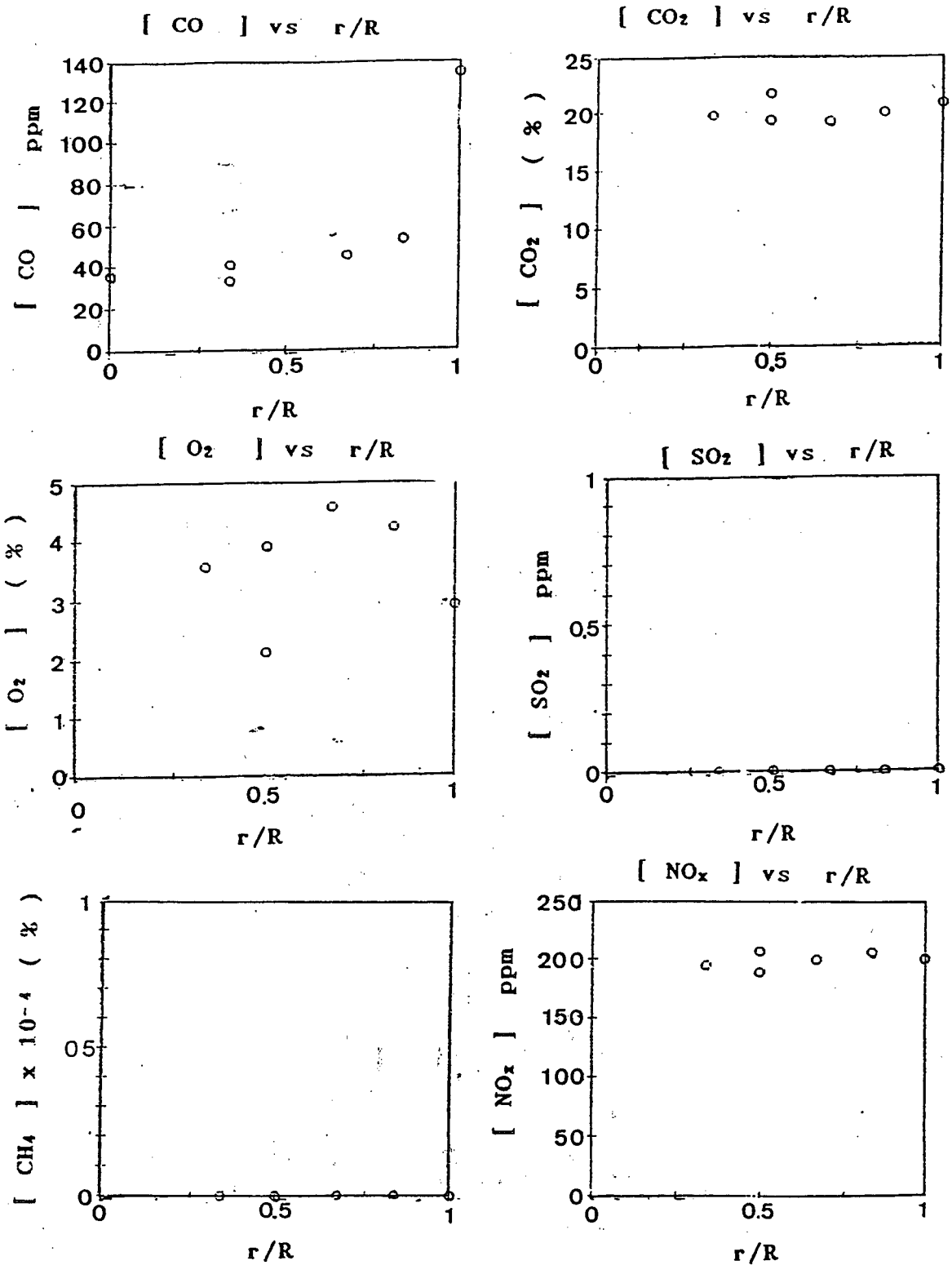

FIGURE 2.8 Gas Concentration Profiles for run 18.

port # 4

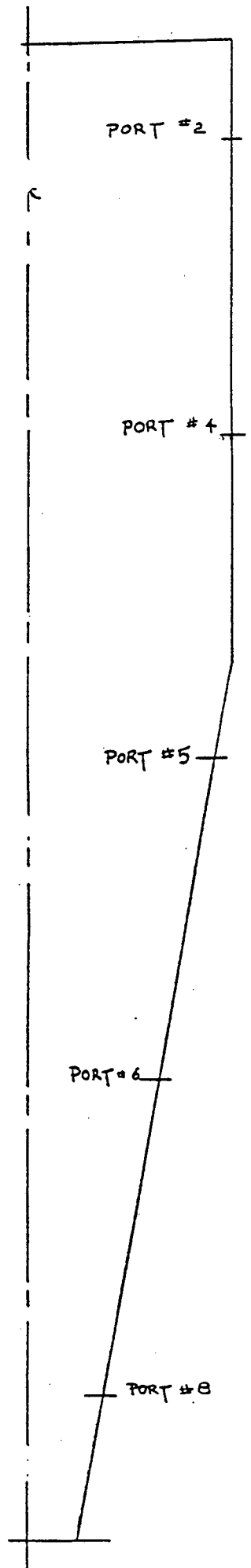
PORT #2
PORT #4
PORT #5
PORT #6
PORT #8

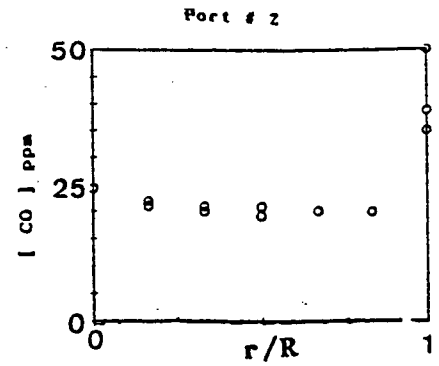
Port # 2
[CO] ppm
50
25
0
0
r/R
1

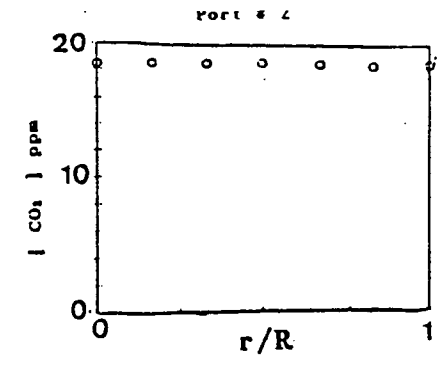
Port # 2
[CO2] ppm
20
10
0
0
r/R
1

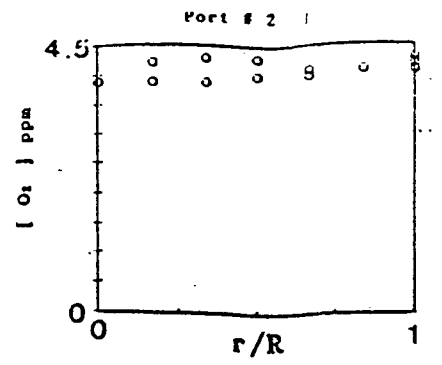
Port # 2
[O2] ppm
4.5
0
0
r/R
1

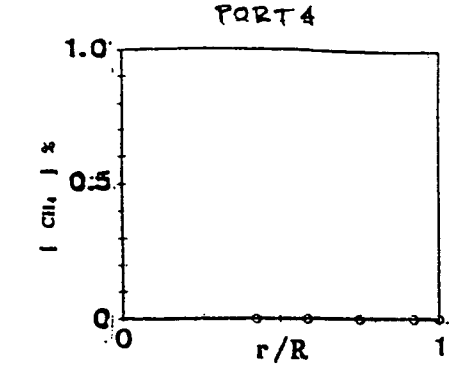
PORT 4
[CH4] %
1.0
0.5
0
0
r/R
1

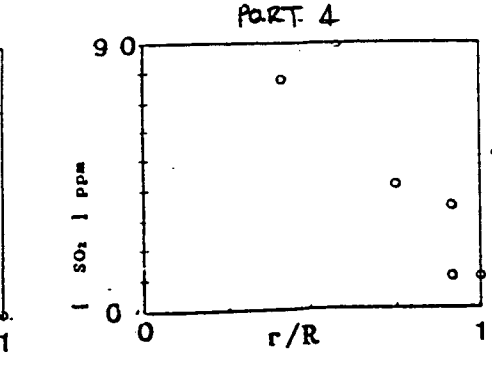
PORT 4
[SO2] ppm
90
0
0
r/R
1

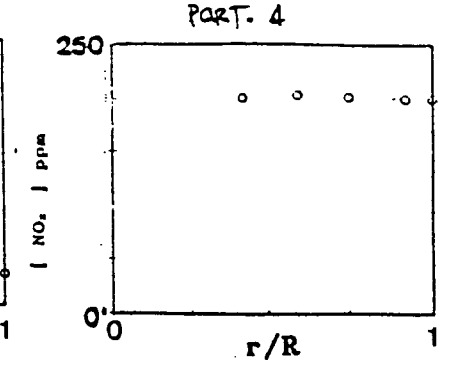
PORT 4
[NO2] ppm
250
0
0
r/R
1

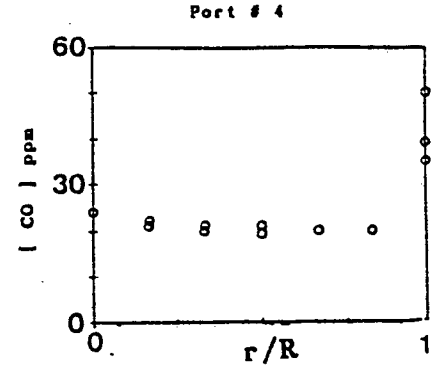
Port # 4
[CO] ppm
60
30
0
0
r/R
1

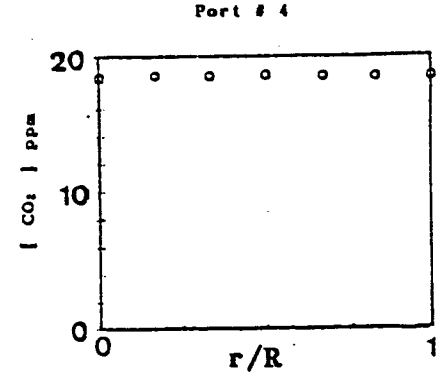
Port # 4
[CO2] ppm
20
10
0
0
r/R
1

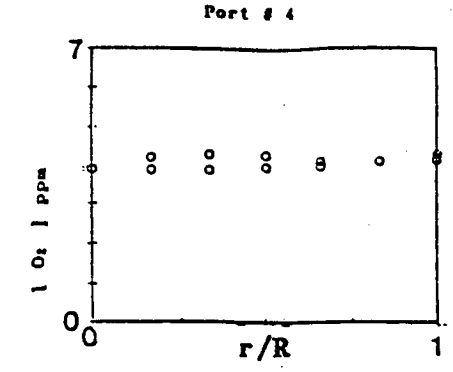
Port # 4
[O2] ppm
7
0
0
r/R
1

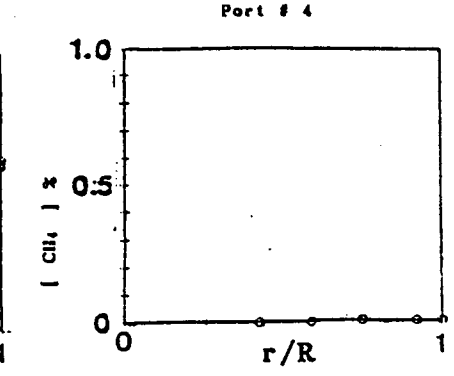
Port # 4
[CH4] %
1.0
0.5
0
0
r/R
1

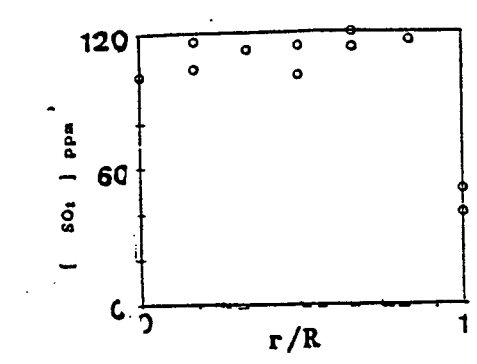
Port # 4
[SO2] ppm
120
60
0
0
r/R
1

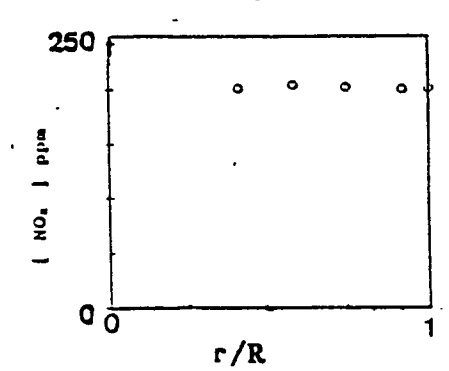
Port # 4
[NO2] ppm
250
0
0
r/R
1

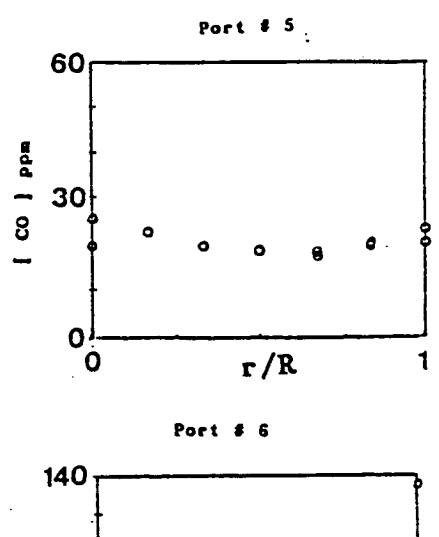
Port # 5
[CO] ppm
60
30
0
0
r/R
1

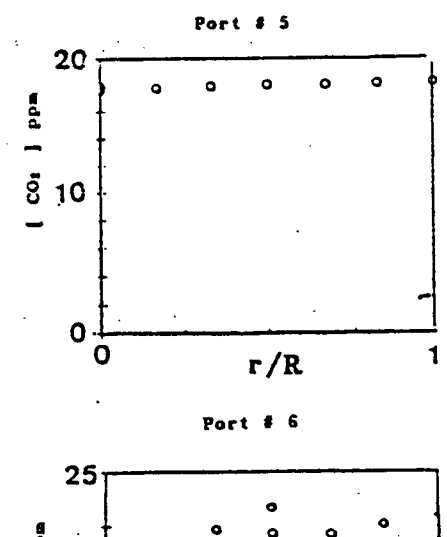
Port # 5
[CO2] ppm
20
10
0
0
r/R
1

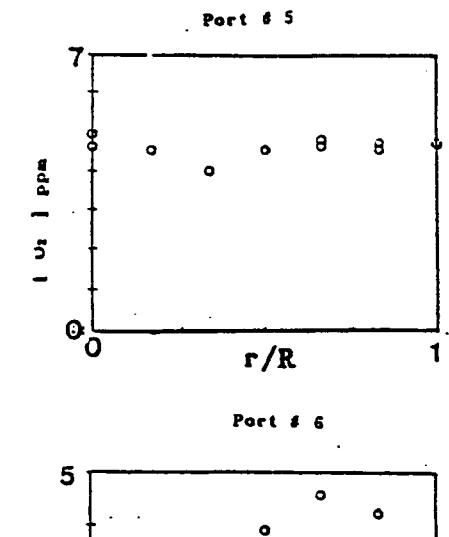
Port # 5
[O2] ppm
7
0
0
r/R
1

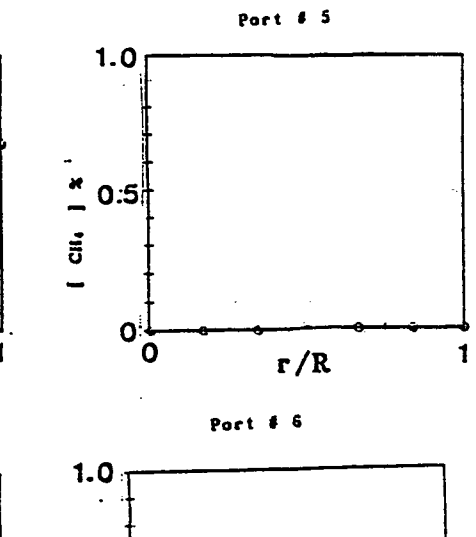
Port # 5
[CH4] %
1.0
0.5
0
0
r/R
1

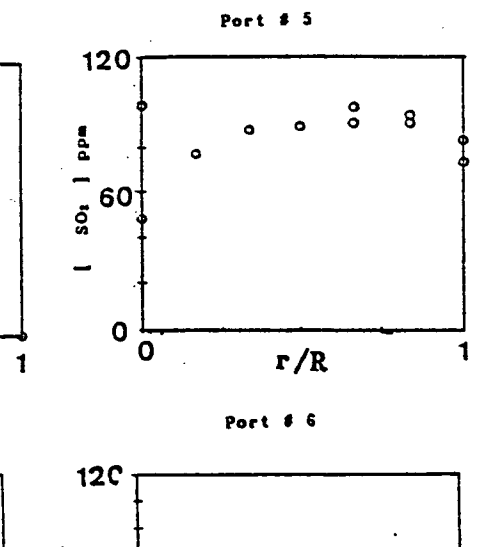
Port # 5
[SO2] ppm
120
60
0
0
r/R
1

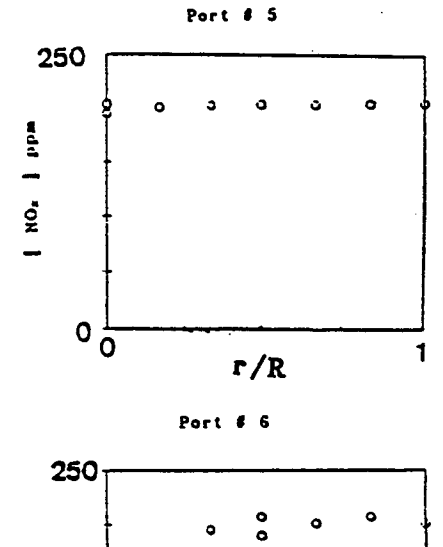
Port # 5
[NO2] ppm
250
0
0
r/R
1

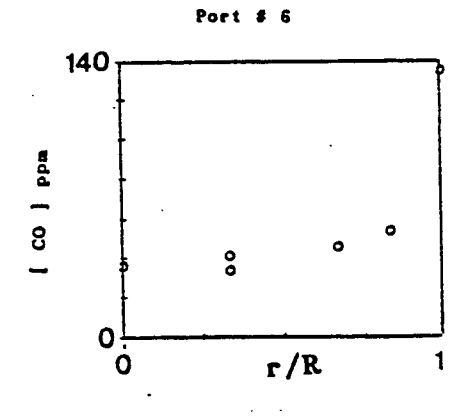
Port # 6
[CO] ppm
140
0
0
r/R
1

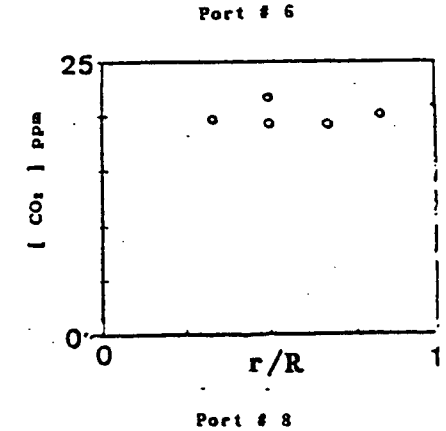
Port # 6
[CO2] ppm
25
0
0
r/R
1

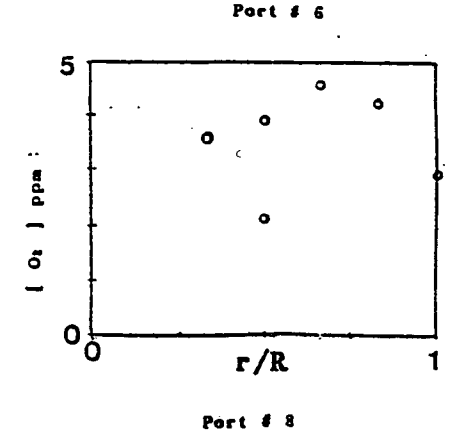
Port # 6
[O2] ppm
5
0
0
r/R
1

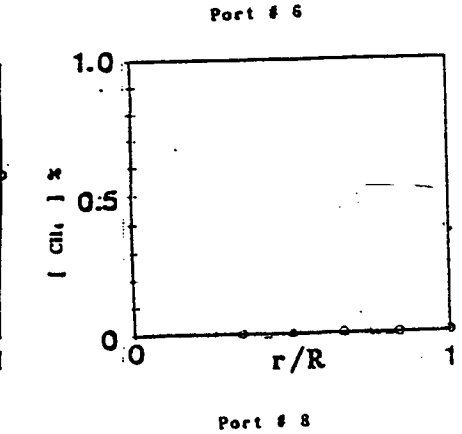
Port # 6
[CH4] %
1.0
0.5
0
0
r/R
1

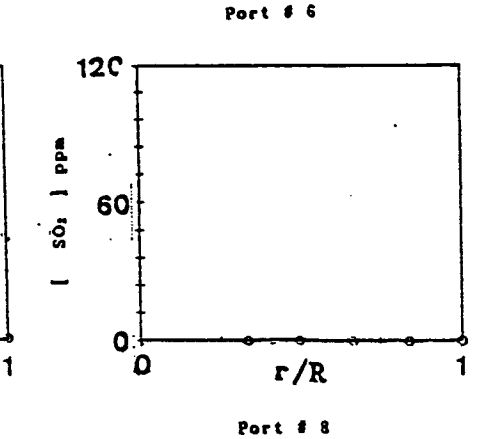
Port # 6
[SO2] ppm
120
60
0
0
r/R
1

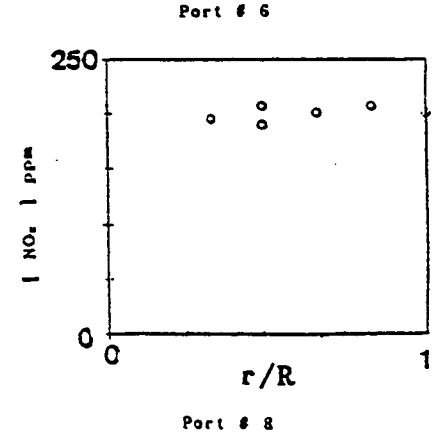
Port # 6
[NO2] ppm
250
0
0
r/R
1

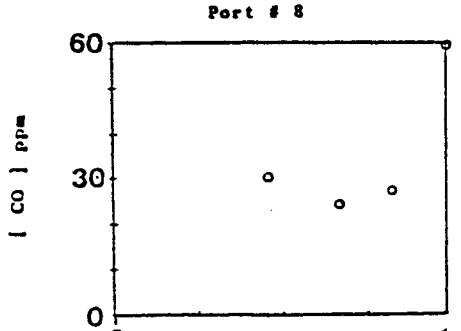
Port # 8
[CO] ppm
60
30
0
0
r/R
1

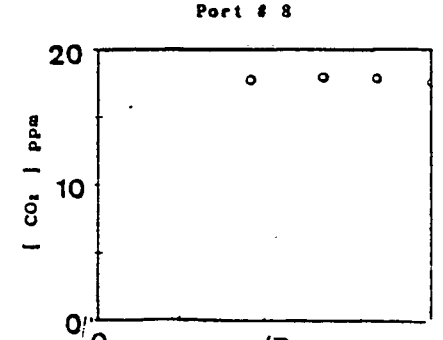
Port # 8
[CO2] ppm
20
10
0
0
r/R
1

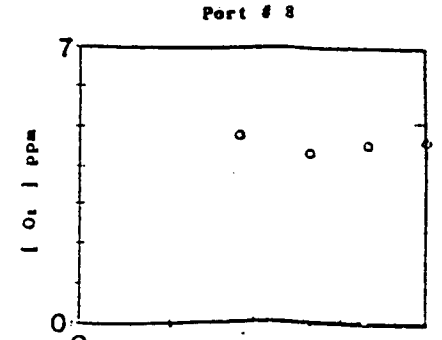
Port # 8
[O2] ppm
7
0
0
r/R
1

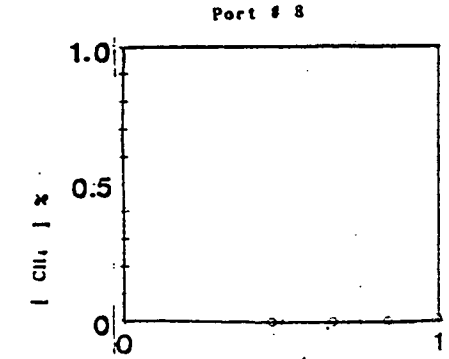
Port # 8
[CH4] %
1.0
0.5
0
0
r/R
1

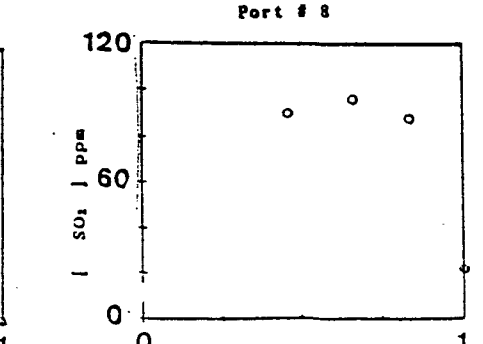
Port # 8
[SO2] ppm
120
60
0
0
r/R
1

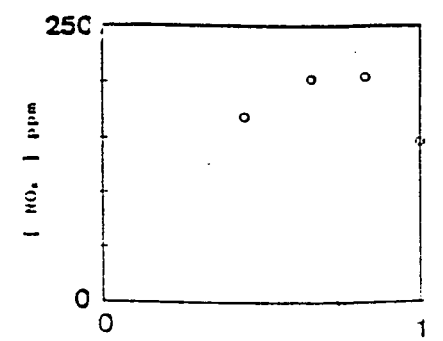
Port # 8
[NO2] ppm
250
0
0
r/R
1

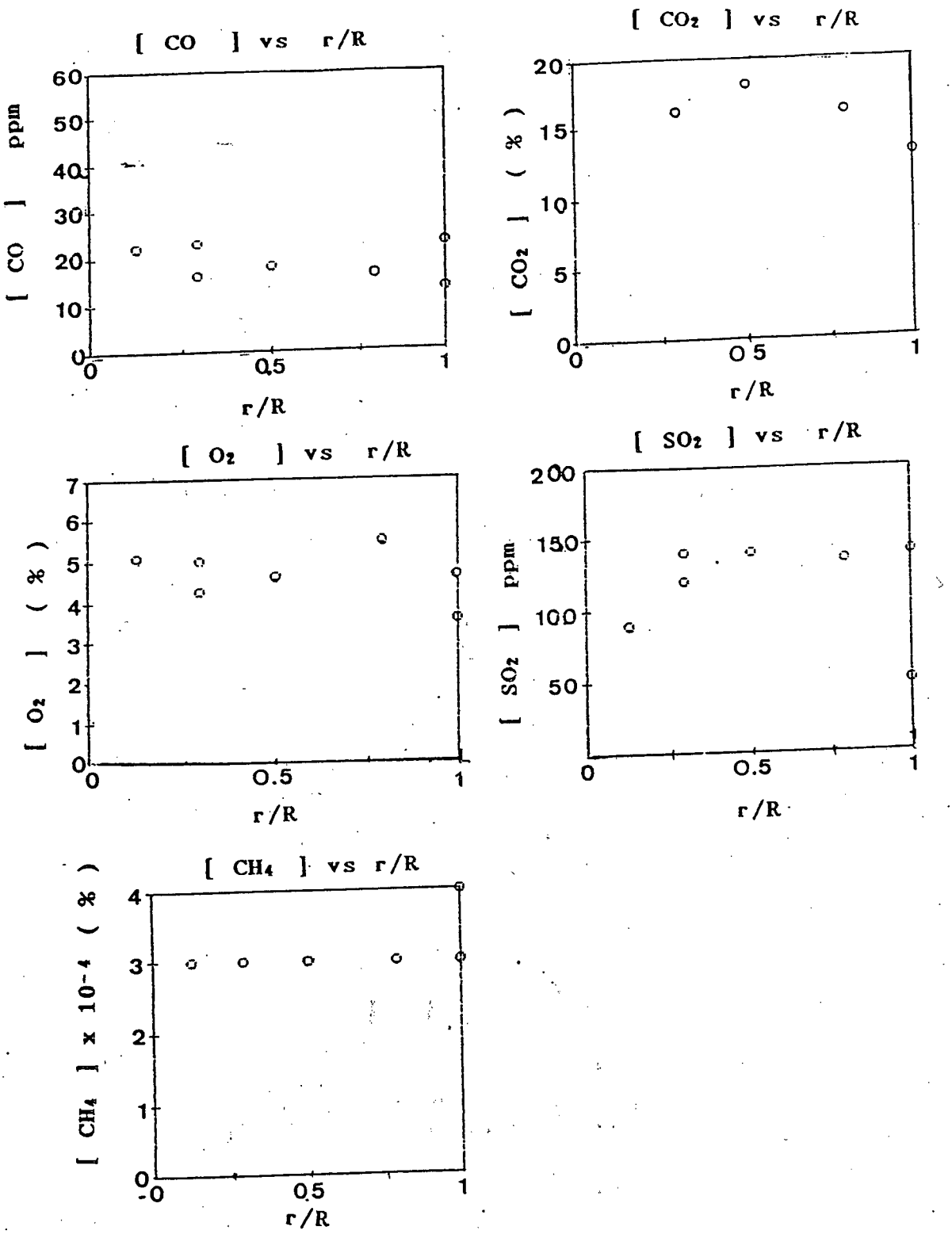

Figure 2.10 Gas Concentration Profiles for run 6.

port # 5

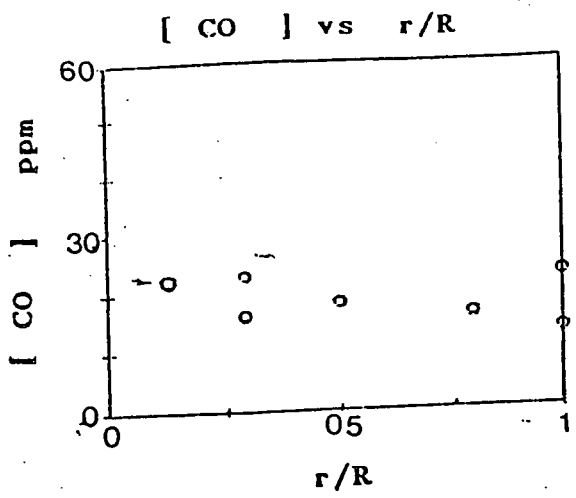

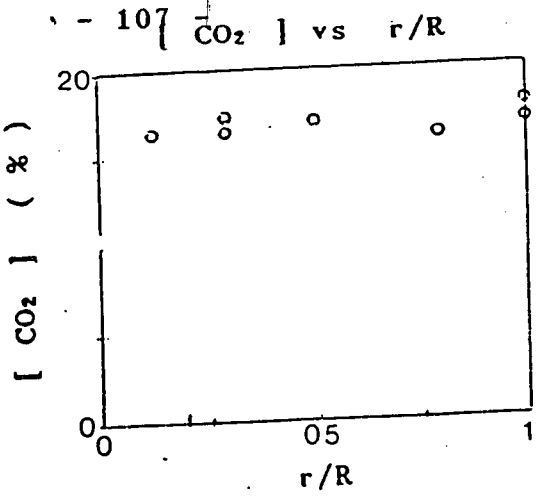

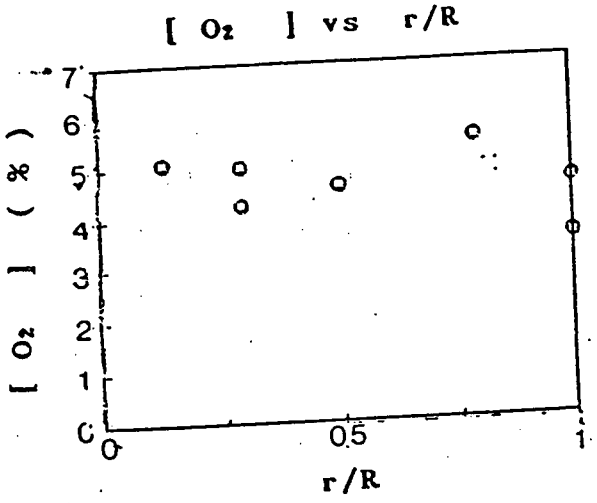

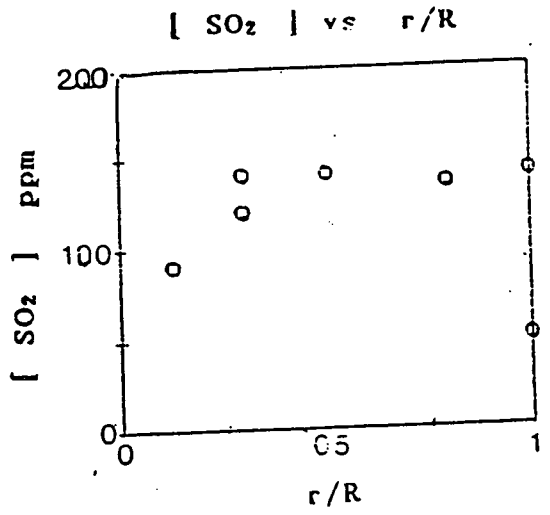

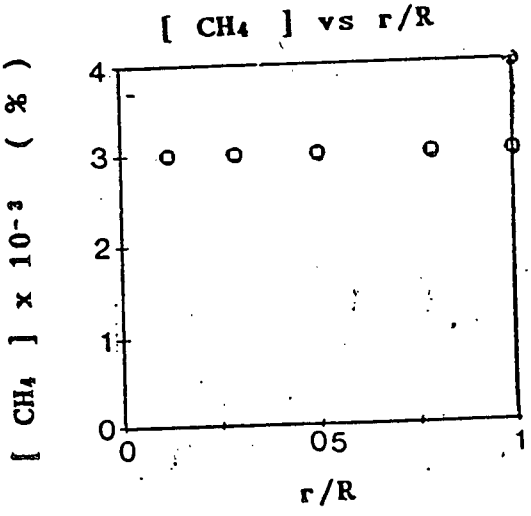

Figure 2.11 Gas Concentration Profiles for run 10.

port # 4

NO_x :

No radial trend for NO_x is apparent from the traverses performed in the five experiments. Values in the 200 to 225 ppm range were typical, with the exception of the traverse performed at port # 8 near the bottom of the cyclone. The discrepancy at this level is attributed to difficulties in maintaining flow at this port due to blocking by particles.

SO_2 :

Values between 0 and 140 ppm [SO_2] were observed within the cyclone, but with no evidence of a clear trend. In Figure 2.10 the lowest SO_2 concentrations were often observed near the wall, probably because of the denser solids region existing near the wall. While no sorbents were added during the runs, there may be sorption by calcium or other elements in the ash accounting for the reduced values.

CH_4 :

During most tests the gas analyses were unable to detect measurable [CH_4]. Only in runs 10 and 18 there were detectable values, these being of the order of 0.002 to 0.004 percent. No radial trend is evident.

CO_2 :

Values between 16.1 and 19.3 percent were measured within the cyclone and a slight radial trend is observed in

three of the traverses. Combusting char particles in the denser solids region near the wall are likely responsible for the observed small increase near the wall.

CO:

As with the [CO_2], [CO] tends to be somewhat greater at the wall than in the interior in five of the radial traverses. Four traverses show a doubling of the [CO], again indicating some char combustion inside the secondary cyclone.

O_2:

No clear trends in the [O_2] were seen in the profiles indicating that the extent of combustion occurring within the cyclone is rather small, at least for this fuel. Comparing the gas residence times of the cyclone and the riser it is clear that the cylone volume is less than that of the riser, approximately 60 % of the riser volume. As well because there is a greater chance for gas short circuiting in the cyclone than in the reactor the reduced extent of combustion is not surprising.

Gas sampling for each run lasted less than three hours and during that time the combustor was maintained as closely as possible at steady state conditions. The primary indication of steady operation was the flue gas O_2 concentration which was held between 3.5 and 6 percent for all readings, and 3.5 to 4.5 percent for more than 90% of

the time. Due to the nature of the experiments some scatter in the measured values was inevitable and clouded any subtle trends that may have existed. As well, the flow in a cyclone is very well mixed and any regional combustion activity would be difficult to detect. For example if combustion was preferred at a given radius, one would only expect to find increased combustion products concentrations if the flow was sufficiently segregated. This is not typically the case in cyclones as the flow is more turbulent and well mixed than segregated. An improved experiment would see continuous monitoring at several radial points simultaneously (rather than sequentially), with the focus being placed on the region near the wall.

2.5 Conclusions and Recommendations

The main features of part II of this work are as follows:

1. Radial gas concentration profiles within a secondary cyclone serving a high temperature Circulating Fluidized Bed Combustor operating with a low sulphur coal as fuel have been measured and presented.

2. Radial gradients in the gas concentration profile were negligible for [NO_x], [SO_2], [CH_4], and [O_2].

3. Near the wall [CO] levels increased, as did [CO_2], suggesting increased char combustion in this zone.

It is recommended that attempts be made to determine similar radial gas concentration profiles in the primary cyclone of the UBC pilot scale CFB combustor. This would require a probe capable of sampling gases in the much denser solids regions of the primary cyclone. It is also recommended that simultaneous monitoring at several radial points be performed as opposed to a sequential sampling. This would reduce the uncertainty imposed on the radial profiles due to the time varying nature of the species concentration within the gas flow (i.e. non-steady state operation). Profiles should be attained with a less reactive coal (e.g. anthracite) and a high sulphur coal (e.g. Minto). Cyclone reactions may play a more important role for these fuels.

NOMENCLATURE

a	Inlet depth (m)
A	Coefficient (-)
A_c	Centrifugal acceleration (m/s^2)
A_g	Gravitational acceleration (m/s^2)
A_i	Inlet area (m^2)
A_p	Particle Area (m^2)
b	Inlet width (m)
b_e	Inlet width (m)
b_i	Coefficient (m)
c_i	Fraction by mass for channel i of catch. (-)
c_m	Solids loading (g/m^3)
c_o	" Zero load " dust concentration ($grains/ft^3$, g/m^3)
c_a	Dust concentration ($grains/ft^3$)
C	Total mass caught (kg)
C'	Cunningham correction factor (-)
C	Dust concentration ($grains/ft^3$, g/m^3)
C_D	Drag coefficient (-)
d_{crit}	Critical particle diameter (m)
d_p	Particle diameter (um)
d_{pa}	Aerodynamic diameter (g/cm^3)$^{0.5}$
d_{pg}	Feed aerosol mass medial diameter (cm)
d_{p50}	Particle diameter caught with 50% efficiency (microns)
D	Body diameter (m)

D_b	Bottom diameter (m)
D_c	Cyclone diameter (m)
D_H	Hydraulic diameter of cyclone inlet (m)
D_o	Outlet diameter (m)
D_x	Imaginary cylinder diameter (m)
e_o	Zero load collection efficiency (%)
E	Collection efficiency (%)
$E_{corr.}$	Loading corrected collection efficiency (%)
$E_{exper.}$	Experimental collection efficiency (%)
E_i	Collection efficiency for channel i. (%)
E_o	Collection efficiency at low loading (%)
f_i	Feed mass for channel i (kg)
F_c	Centrifugal force (N)
F_D	Particle drag force (N)
G	Cyclone configuration parameter. (-)
Ga	Galileo number (-)
h_e	Inlet depth (m)
H_o	Overall height (m)
k_1	Coefficient (-)
k_{p1}	Restitution coefficient (-)
l_i	Fraction by mass for channel i of loss. (kg)
L	Experimental solids loading (kg/kg solids/air)
L_{B24}	Particle loading in run B24 (kg/kg solids/air)
L_{cy}	Cylinder length (m)
L_m	Total mass passing cyclone (kg)
L_o	Outlet length (m)
L_p	Particle loading ratio (kg/kg solids/air)
LFAC	Apparent gas viscosity coefficient (-)
m	Particle mass (kg)

n	Vortex exponent (-)
N	Particle path revolutions (-)
N_{Ref}	Flow Reynolds number (-)
N_{Rep}	Particle Reynolds number (-)
N_{Rerp}	Radial particle Reynolds number (-)
N_{St}	Stokes number (-)
N_{St50}	Stokes number for cut diameter (-)
$P(e)$	Probability associated with high loading E (-)
$P(E_o)$	Probability associated with low loading E (-)
Q	Gas flow (m^3/s)
Q_c	Gas split ratio (-)
r_a	cyclone radius (m)
r_i	Vortex finder radius (m)
R	Radial co-ordinate (m)
R_x	Radius of imaginary cylinder (m)
$S^{0.5}$	Dimensionless particle diameter (m)
SFACTOR	Saltation factor (-)
$T_A(x)$	Predicted collection efficiency (-)
V_e	Inlet Velocity (m/s)
V_i	Inlet velocity (m/s)
V_p	Radial particle velocity component (m/s)
V_{rp}	Radial particle velocity (m/s)
V_{rg}	Radial gas velocity (m/s)
V_{tp}	Tangential particle velocity (m/s)
V_s	Particle saltation velocity (m/s)

Greek symbols

ρ	Gas density (kg/m^3)
ρ_p	Particle density (kg/m^3)
x_G	Mass median particle diameter (m)
χ	Shape factor (-)
u_g	Gas viscosity (kg/ms)
u_{gapp}	Effective gas viscosity (kg/ms)

References

1. Sorbent optimization for FBC technology, Chatham Circulating Fluidized Bed Demonstration project, Energy Mines, and Resources report (May 1989).

2. Stairmand, C.J., "The design and performance of cyclone separators.," Trans. Instn. Chem. Engrs. (Vol. 29, 1951): pp. 357-383.

3. Beeckmans, J. M., Aerosol Measurement; Lundgren, D., Ed.; University at Florida Press, Gainsville, FL, 1979.

4. Calvert, S., Englund, H., Handbook of Air Pollution Technology, New York: John Wiley and Sons, 1984, pp. 320-329.

5. Strauss, W., Industrial gas Cleaning 2nd edition, New York: Pergamon Press, 1975, pp. 238-276.

6. Leith, D., Mehta, J., "Cyclone performance and Design," Atmospheric Environment (1973 Vol. 7): pp. 527-549.

7. Gauthier, T.A., Briens, C.L., Galtier, P., "Uniflow cyclone efficiency study," Dept. of Chemical and Biochemical Engineering, University of Western Ontario.

8. Ter Linden, A. J., Tonindustrie-Zeitung, 22(iii) 49 (1953).

9. Mukhopadhyay, S.N., Chowdhury, K.C. Roy, "The collecting efficiency of a cyclone separator," , Brit. Chem. Eng. (April 1970): Vol. 15, No. 4. pp. 529

10. Whitby, K.T., Lundgren, D.A., Jordan, R.C., J. Air. Pollution Control Association 11,(1961): pp. 503-504.

11. Parker, R., Jain, R., and Calvert,. "Particle collection in cyclones at a high temperature and pressure," Env. Sci. Tech. (1981): 15 (4) pp. 451-458.

12. Wheeldon, J. M., Burnard, J.K. "Performance of Cyclones in the Off-Gas Path of a Pressurized Fluidized Bed Combustor," Filtration and Separation (May June 1987): pp. 178-187.

13. Dietz, P.W., "Collection efficiency of cyclone separators," AIChE Journal. (1981), (Vol. 27, No. 6)

14. Gloger, J., Hanke, S., Energietechnik (1971): 21(4) 158-164.

15. Mothes, H., Löffler, F., "Motion and Separation of particle in a cyclone," Chem. Engg. Process. (1984) 18 pp. 323-331.

16. Abraham, F.F., Physics Fluids (1970): 13, pp. 2194-5.

17. " Cyclone Dust Collectors," API publication, A.P.I. New York (1955).

18. American Petroleum Institute (API) "Manual on Disposal of Refinery Wastes," API publication 931, Chp. 11 (1975).

19. Sproull, W.T., "Effect of Dust Concentration Upon the Gas Flow Capacity of a cyclonic Collector," J. Air Poll. Control Assn. 16 (8), pp. 439-441 (1966).

20. Massey, B.S., Mechanics of fluids, 4th ed. New York: Van Nostrand Reinhold Company, 1979 pp. 222 -227.

21. Abrahamson, J., Allen, R.W.K., "The efficiency of conventional reverse return cyclones at high temperatures," ChemE SYMPOSIUM Series No. 99. (1988).

22. Ogawa, A., " Theoretical approach with Markov Process Model to Seperation Processes of Cyclone dust collector depending on feed dust concentration," J. Coll. Engineering, Nihon Univ., A-26, (March 1985). Note: Referenced in 41.

23. Masin, J.G., Kock, W.H., "Cyclone Efficiency and Pressure Drop Correlations in Oil Shale Retorts," Environmental Progress Vol 5, No. 2, (May 1986), pp. 116 -122.

24. Mothes, M., LÖffler, F., "Motion and deposition of particle in cyclones," Ger. Chem. Eng., 8 (1985,) pp. 223 -233.

25. Boysan, F., Ayers, W.H., Swithenbank, J., "A Fundamental Mathematical Modelling Approach to Cyclone Design," Trans. IChem Engg. Vol. 60, 1982.

26. Laurendeau, N. M., "Heterogeneous Kinetics of coal char gasification and combustion," Prog Energy Combust. Sci, Vol.4, pp. 221-270 (1978).

27. Grace, J.R. and Lim C.J., " Circulating Fluidized Bed Combustion of Coal, Woodwastes and Pitch," Final report prepared for Energy, Mines and Resources Canada, under contract 24ST.23440-6-9007 (1987).

28. A.S.H.R.A.E., "Flow measurements, instruments and apparatus," ASME Power Test Codes, Part 5 of Ch. 4. (1959).

29. J. R. Grace, C.M.H. Brereton, C.J. Lim, R. Legros, R.C. Senior, R.L. Wu, J.R. Muir, R. Engman "Circulating Fluidized Bed Combustion of Western Canadian Fuels," Final report prepared for Energy Mines and Resources Canada, under contract 52 SS.23440-7-9136 August 1989.

30. R. Legros, C.M.H. Brereton, C.J. Lim, H. Li, J.R. Grace and E.J. Anthony . "Combustion characteristics of different fuels in a Pilot Scale Circulating Fluidized Bed Combustor," Proc. Conference on Fluidized Bed Combustion, 661-666 (1989)

31. Wu, L. R., PhD. thesis, "Heat Transfer in Circulating Fluidized Beds" University of British Columbia, Department of Chemical Engineering (1989).

32. M. F. Couturier, B. Doucette and S. Poolpal, " A Study of Gas concentration, Solids Loading and Temperature profiles within the Chatham CFB Combustor," a report to ENERGY MINES AND RESOURCES CANADA, (Nov. 1989).

33. Stern, A.C., gen. ed., Air Pollution 3rd edition, New York: Academic Press, 1977, chapter 3, pp. 98-136.

34. Razgaitis, R., Guenther, D.A., "Separation Efficiency of a Cyclone Separator with a Turbulence-Suppressing Rotating Insert," Transactions of the ASME Vol. 103, (July 1981).

35. M.F. Couturier, Professor,Department of Chemical Engineering University of New Brunswick, Personnel communication.

36. Sucec, J., Heat Transfer, WM.C.Brown Publishers: Dubuque, Iowa (1985), p. A11

37. Seville, J., et al., (1984) Particle Characterization Vol. 1, no.1 Weinheim, Federal republic of Germany (July 1984)

38. J. Zhao, J. R. Grace, C.J. Lim, C.M.H. Brereton, R. Legros, and E.J. Anthony "NO_x emissions in a pilot scale circulating fluidized bed combustor," in Proceedings of EPRI/EPA 1989 Joint Symposium on Stationary Combustion NO_x Control.

39. Leith,D., W. Licht, "The Collection Efficiency of Cyclone Type Particle Collectors-A New Theoretical Approach," Air Pollution and It's Control, AIChE Symposium Series 126,68, 1972.

40. Turner

41. Patterson, P.A., PhD. Thesis, "High Temperature Cyclones", Department of Chemical Engineering, McGill University, Montreal (1989).

APPENDIX

PRELIMINARY TESTS

PART I

CONDITIONS

SOLIDS: 11 um mean dia. flyash.
Inlet velocity: 4.45 m/s
Configuration: C1 (base case)
variable vortex finder length.

V.F. position L/D (FULLY ADJUSTABLE V.F.)	L/H	collection efficiency
0.12	0.11	50.0
0.59	0.54	73.9
0.81	0.74	96.3

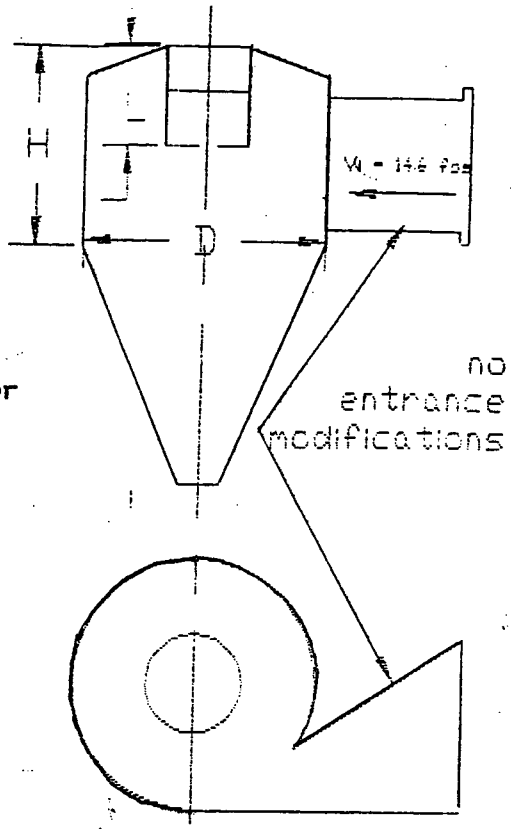

PART II

CONDITIONS

SOLIDS: 50 um mean dia. flyash.
Inlet velocity: 5.4 m/s
Configuration: 1. C3 without extended vortex finder.

2. variable vortex finder length.

V.F. position	L/D	L/H	collection efficiency
EXISTING	0.31	0.28	41 %
PROPOSED	0.63	0.57	47 %

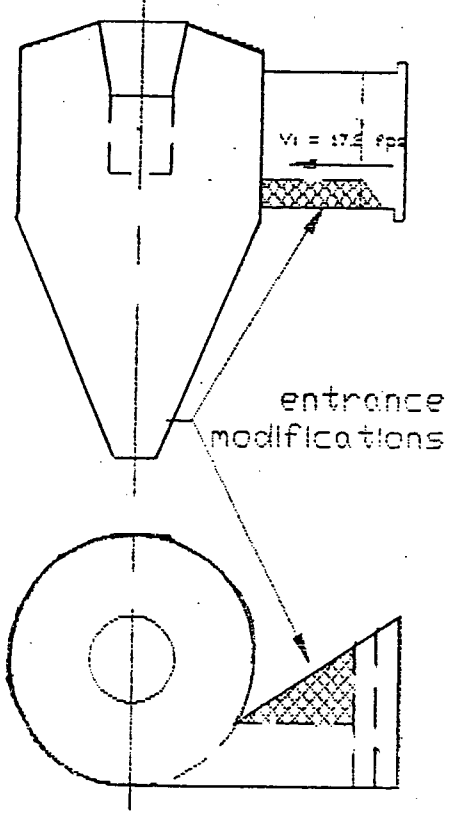

FIGURE A1 Shake down test summary. All runs performed before run B1.

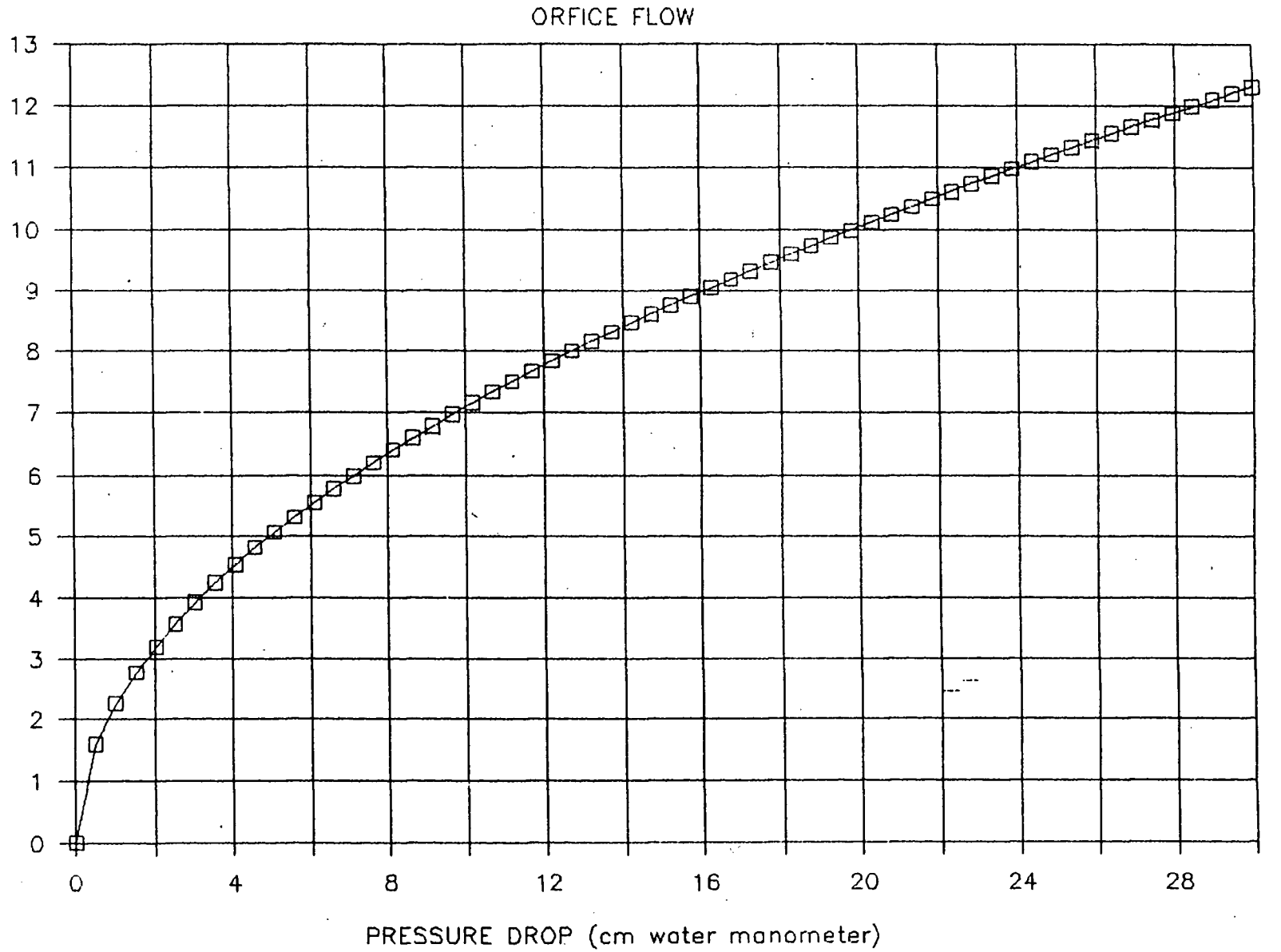

FIGURE A2 Orifice flow curve. M^3/s vs pressure drop.

Figure A3 Data logging program serving UBC model cyclone apparatus.

```
REM  PROGRAM FOR INSTANTANEOUS SAMPLING OF LOAD CELLS
     OPEN "cyco.OUT" FOR OUTPUT AS #2
     OPEN "COM1:9600,N,8,1,CS,DS" FOR RANDOM AS #1
     INPUT "run number?", n$
     PRINT #2, "run number = ", n$
2    hh = 0

3    TIME$ = "00:00:00"
5    ta$ = TIME$
7    seconds = VAL(MID$(ta$, 1, 2)) * 3600 + VAL(MID$(ta$, 4, 2)) * 60 + VAL(MID$(ta$, 7, 2))
9     IF (seconds - hh) = 1 THEN 20


20   PRINT "logging data"
     hh = seconds
     PRINT #1, "2";
     INPUT #1, b$
     PRINT #1, "3";
     INPUT #1, c$
     PRINT #2, VAL(MID$(b$, 5, 6)), VAL(MID$(c$, 5, 6))
     PRINT VAL(MID$(b$, 5, 6)), VAL(MID$(c$, 5, 6))
     GOTO 5

30   END
```

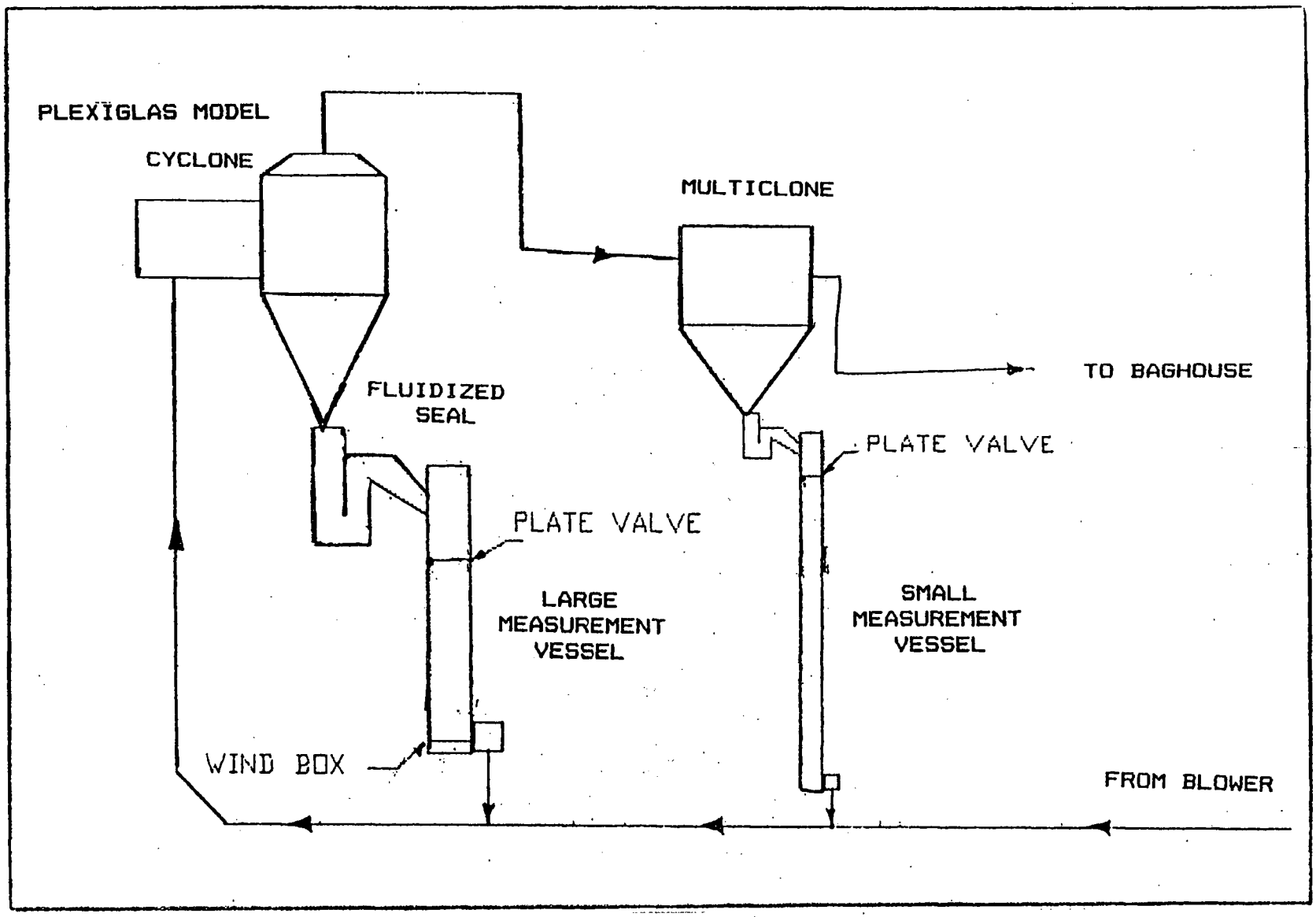

Figure A4 Schematic of attempted recycle system schematic showing a high solids loading feed and measurement vessels, multiclone and bag filter arrangements.

PAGE 125 INSERTED FOR
PAGE NUMBER CONTINUITY

Figure A6 UBC CFBC solid fuel analysis for run B17 (29).

Proximate and Ultimate Analyses of Solid Fuel

	Highvale Coal
Proximate Analyses (as received)	
Volatile Matter	30.5
Fixed Carbon	42.1
Ash	12.2
Moisture	15.2
Ultimate Analyses (dry basis)	
Carbon	62.4
Hydrogen	3.6
Nitrogen	0.8
Sulphur	0.2
Oxygen (by difference)	18.7
Ash	14.3
Higher Heating Value (MJ/kg)	24.0

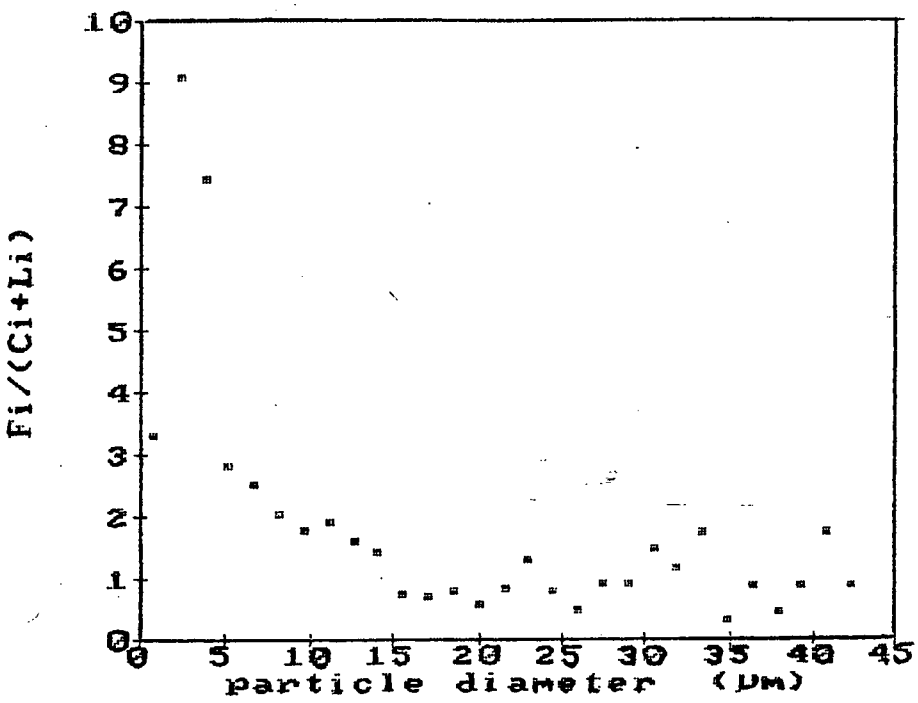

Figure A7 Mass balance, as performed on a per channel basis for run B10. Image analysis particle size distributions. Fines loss (below 15 microns) attributed to filter inefficiency.

Figure A8 Temperature data for Part I experiments.

RUN #	Dry bulb temperature °C	Wet bulb temperature °C
B1	12	10
B2	15	11
B3	12	8
B4	11	7
B5	11	7
B6	16	12
B7	16	12
B8	16	12
B9	19	15
B10	19	15
B11	22	18
B12	18	15
B13	18	15
B14	18	15
B15	18	15
B16	18	15
B17	18	15
B18	18	15
B19	18	15
B20	18	15
B21	22	19
B22	22	19
B23	22	19
B24	22	19
B25	22	19
B26	22	19
B27	22	19
B28	22	19
B29	22	19
B30	22	19
B31	22	19
B32	15	11
B33	15	11
B34	15	11
B35	15	11

FIGURE A9 COLLECTION EFFICIENCY DATA

RUN B4 size microns	efficiency %
7.7	0
7.9	0
8.11	35
8.32	32
8.53	39
8.75	35
8.98	32
9.21	44
9.45	46
9.69	48
9.94	49
10.2	54
10.46	54
10.73	65
11.01	62
11.29	69
11.58	71
11.88	75
12.19	80
12.5	78
12.82	86
13.16	88
13.49	89
13.84	90
14.2	92
14.57	94
14.94	95
15.53	93
15.72	96
16.13	99
16.54	99
16.97	99
17.41	100
17.86	98
18.32	98
18.79	100
19.28	99
19.77	100
20.28	98
20.81 to 86.4	100

RUN B10 size microns	efficiency %
0.74	25
2.23	10
3.71	11
5.2	32
6.68	37
8.16	47
9.65	54
11.13	51
12.62	62
14.1	70
15.59 to 46.76	100

FIGURE A9 DATA SUMMARY FOR PARTS I AND II (CONTINUED)

CHATHAM COLLECTION EFFICIENCY DATA

DATA size MICRONS	LOSS FRACTION	CATCH FRACTION	EFFICIENCY %
7.32	0.00E+00	0.00E+00	0.00
7.51	5.97E-05	0.00E+00	0.00
7.70	5.97E-05	0.00E+00	0.00
7.90	9.42E-05	0.00E+00	0.00
8.11	6.59E-05	0.00E+00	0.00
8.32	9.89E-05	0.00E+00	0.00
8.53	9.89E-05	0.00E+00	0.00
8.75	1.04E-04	0.00E+00	0.00
8.98	1.08E-04	0.00E+00	0.00
9.21	1.44E-04	0.00E+00	0.00
9.45	1.51E-04	0.00E+00	0.00
9.69	1.51E-04	0.00E+00	0.00
9.94	1.96E-04	5.55E-06	0.00
10.20	2.45E-04	0.00E+00	0.00
10.46	2.45E-04	5.77E-06	0.00
10.73	2.97E-04	0.00E+00	0.00
11.01	3.52E-04	6.21E-06	0.00
11.29	3.96E-04	0.00E+00	0.00
11.58	5.01E-04	0.00E+00	0.00
11.88	5.65E-04	0.00E+00	0.00
12.19	7.30E-04	0.00E+00	0.00
12.50	7.79E-04	6.88E-06	0.00
12.82	9.55E-04	0.00E+00	0.00
13.16	1.12E-03	0.00E+00	0.00
13.49	1.30E-03	0.00E+00	0.00
13.84	1.65E-03	0.00E+00	0.00
14.20	2.03E-03	7.99E-06	0.00
14.57	2.21E-03	0.00E+00	0.00
14.94	2.73E-03	0.00E+00	0.00
15.33	3.31E-03	0.00E+00	0.00
15.72	3.86E-03	0.00E+00	0.00
16.13	4.70E-03	9.10E-06	0.00
16.54	5.34E-03	0.00E+00	0.00
16.97	6.82E-03	0.00E+00	0.00
17.41	7.94E-03	0.00E+00	0.00
17.86	9.61E-03	9.99E-06	0.00
18.32	1.16E-02	1.27E-06	0.00
18.79	1.34E-02	0.00E+00	0.00
19.28	1.61E-02	0.00E+00	0.00
19.77	1.88E-02	1.09E-05	0.00
20.28	2.19E-02	0.00E+00	0.00
20.81	2.58E-02	1.46E-06	0.00
21.34	2.85E-02	0.00E+00	0.00
21.89	3.23E-02	0.00E+00	0.00
22.46	3.69E-02	1.57E-06	0.22
23.04	3.95E-02	0.00E+00	0.00
23.63	4.26E-02	1.63E-06	0.19
24.24	4.62E-02	7.25E-06	0.78
24.87	4.73E-02	0.00E+00	0.00
25.51	4.72E-02	1.76E-06	0.17
26.17	4.92E-02	1.65E-05	1.58
26.84	4.78E-02	3.69E-06	0.34
27.54	4.71E-02	1.93E-06	0.19
28.25	4.74E-02	1.04E-05	1.00
28.97	4.54E-02	3.97E-06	0.38
29.72	4.34E-02	4.13E-06	0.42
30.49	3.69E-02	1.34E-05	1.40
31.28	3.39E-02	6.53E-06	0.81
32.08	2.69E-02	1.39E-05	1.85
32.91	2.25E-02	1.14E-05	1.92
33.76	1.67E-02	1.71E-05	3.37
34.63	1.22E-02	1.20E-05	3.20
35.52	8.94E-03	2.28E-05	7.95
36.44	7.80E-03	2.61E-05	11.84
37.38	6.05E-03	2.93E-05	14.7205
38.35	5.33E-03	3.29E-05	19.9943
39.33	3.38E-03	6.93E-05	37.4109
40.35	4.00E-03	6.57E-05	47.1316

CHATHAM COLLECTION EFFICIENCY DATA

DATA size MICRONS	LOSS FRACTION	CATCH FRACTION	EFFICIENCY %
41.39	3.10E-03	8.50E-05	49.40
42.46	3.19E-03	1.14E-04	62.84
43.55	2.22E-03	1.07E-04	60.67
44.68	2.13E-03	1.12E-04	69.80
45.83	1.62E-03	9.92E-05	68.17
47.01	1.85E-03	9.76E-05	73.40
48.23	9.58E-04	1.31E-04	76.48
49.47	9.73E-04	2.14E-04	91.12
50.75	1.41E-03	2.29E-04	91.53
52.05	1.02E-03	2.95E-04	90.59
53.40	4.24E-04	3.67E-04	94.29
54.78	6.50E-04	4.12E-04	97.81
56.19	1.33E-03	5.10E-04	97.30
57.64	1.14E-03	6.55E-04	95.77
59.13	1.17E-03	8.23E-04	97.08
60.65	7.16E-04	9.92E-04	97.50
62.22	9.86E-04	1.28E-03	98.79
63.82	1.00E-03	1.63E-03	98.70
65.47	1.04E-03	2.12E-03	98.98
67.16	2.39E-03	2.82E-03	99.21
68.89	5.43E-04	3.39E-03	98.49
70.67	1.68E-03	4.53E-03	99.74
72.49	1.14E-03	6.18E-03	99.41
74.36	0.00E+00	7.78E-03	99.68
76.28	1.51E-03	9.23E-03	100.00
78.25	1.55E-03	1.07E-02	99.69
80.26	1.89E-03	1.27E-02	99.74
82.34	6.53E-04	1.39E-02	99.70
84.46	1.66E-03	1.57E-02	99.91
86.64	2.40E-03	1.67E-02	99.78
88.87	1.05E-03	1.68E-02	99.69
91.17	1.08E-03	1.93E-02	99.88
93.52	0.00E+00	1.83E-02	99.87
95.93	2.27E-03	1.90E-02	100.00
98.41	1.56E-03	1.76E-02	99.72
100.95	0.00E+00	1.53E-02	99.78
103.55	0.00E+00	1.50E-02	100.00
106.22	0.00E+00	2.06E-02	100.00
108.96	0.00E+00	2.52E-02	100.00
111.77	0.00E+00	3.10E-02	100.00
114.66	0.00E+00	3.12E-02	100.00
117.62	0.00E+00	3.61E-02	100.00
120.65	0.00E+00	4.43E-02	100.00
123.76	0.00E+00	4.97E-02	100.00
126.96	0.00E+00	5.09E-02	100.00
130.23	0.00E+00	4.60E-02	100.00
133.59	0.00E+00	4.66E-02	100.00
137.04	0.00E+00	4.76E-02	100.00
140.57	0.00E+00	5.63E-02	100.00
144.20	0.00E+00	6.14E-02	100.00
147.92	0.00E+00	6.24E-02	100.00
151.74	0.00E+00	6.36E-02	100.00
155.65	0.00E+00	4.27E-02	100.00
159.67	0.00E+00	3.38E-02	100.00
163.79	0.00E+00	7.40E-03	100.00
168.01	0.00E+00	8.33E-03	100.00

GAS CONCENTRATION DATA FOR RUN 17

READING	r/R	O2 %	CO PPM	CO2 %	SO2 PPM	CH4 %	NOX PPM
1	0.33	4	41	20	107	0	209
2	0.50	3	48	21	297	0	214
3	0.67	4	47	20	305	0	219
4	0.83	4	46	20	297	0	214
5	1.00	3	165	20	132	0	209
6	0.50	4	41	20	109	0	211
7	0.83	4	41	20	205	0	215
8	0.33	4	42	20	130	0	214
9	0.67	4	41	20	203	0	215
10	1.00	4	134	20	66	0	215
11	0.50	4	31	20	53	0	216
12	0.83	4	37	20	155	0	216
13	1.00	3	88	21	176	0	203

GAS CONCENTRATION DATA FOR RUN 18

reading #	r/R	O2 %	CO ppm	CO2 %	SO2 ppm	CH4 %	NOX ppm
1	0	4	36	20	0	0	196
2	0	4	34	19	0	0	207
3	0	5	41	19	0	0	201
4	1	4	46	20	0	0	207
5	1	3	54	21	0	0	201
6	1	2	134	22	0	0	190

Radial Gas Concentration profiles RUN 5 PORT 2

r/R	O2	CO	CO2	SO2	CH4	NOX
1.0	4.1	35	18.4	50	0	198
0.8	4.1	20	18.4	116	0.002	195
0.7	4	20	18.4	113	0.002	195
0.5	4	19	18.5	114	0.002	190
0.3	3.9	20	18.5	112	0	190
0.2	3.9	22	18.4	104	0	185
0.0	3.9	24	18.4	101	0	180
0.0	3.9	26	18.3	90	0	180
0.3	4.3	21	18.4	112	0	185
0.7	4.1	20	18.6	120	0	200
0.2	4.2	21	18.5	116	0	200
1.0	4.3	39	18.3	40	0	200
0.5	4.3	21	18.5	101	0	189
0.0	4.3	21	18.3	111	0	201
1.0	4.2	50	18.5	40	0	205

Radial Gas Concentration profiles, Run 5 Port 4

r/R	O2	CO	CO2	SO2	CH4	NOX
0.4	4.7	25	17.8	78	0	201
0.6	4.5	33	18	89	0	204
0.8	4.2	34	18.1	41	0	202
0.9	4.4	40	17.8	34	0	201
0.9	4.3	42	18.1	10	0	200
1.0	4.3	51	17.8	10	0	200

Figure A9 Data summary for Parts I and II.
Note: All gas concentration data in ppm except values for O_2, CH_4, and CO_2.

Radial Gas Concentration profiles, Run 5 Port 5

r/R	O2	CO	CO2	SO2	CH4	NOX
0.1	5.7	24	17.1	40	0	120
0.0	4.6	25	17.9	48	0	195
0.2	4.5	22	17.8	77	0	201
0.3	4	19	17.9	87	0	202
0.5	4.5	18	18.1	89	0	203
0.7	4.6	17	18.1	90	0	203
0.8	4.5	19	18.1	90	0	204
1.0	4.7	20	18.1	73	0	205

GAS CONCENTRATION DATA RUN 5, PORT 6

r/R	O2	CO	CO2	SO2	CH4	NOX
0.33	3.58	35.76	19.78	0.00	0.00	195.59
0.50	3.91	33.53	19.34	0.00	0.00	206.76
0.67	4.58	41.35	19.22	0.00	0.00	201.18
0.83	4.25	45.82	20.01	0.00	0.00	206.76
1.00	2.91	53.65	20.90	0.00	0.00	201.18
0.50	2.12	134.12	21.57	0.00	0.00	190.00

GAS CONCENTRATION DATA RUN 5, PORT 8

#	r/R	O2	CO	CO2	SO2	CH4	NOX
1	0.46	4.8	30	17.7	90	0	170
2	0.67	4.3	24	17.9	96	0	202
3	0.83	4.5	27	17.8	88	0	203
4	1.00	4.6	59	17.5	22	0	145

RUN # 6 RADIAL GAS CONCENTRATION DATA

r/R	O2	CO	CO2	SO2	CH4	NOX
1.00	4.10	63.00	17.30	0.00	0.00	175.00
0.83	4.20	39.00	17.00	0.00	0.00	225.00
0.67	4.20	32.00	16.90	0.00	0.00	220.00
0.33	4.40	31.00	17.20	0.00	0.00	225.00
0.17	5.20	29.00	16.40	0.00	0.00	230.00
0.00	4.00	40.00	17.60	0.00	0.00	230.00
0.00	2.80	48.00	18.40	0.00	0.00	230.00
1.00	NA	78.00	18.40	0.00	0.00	220.00

GAS CONCENTRATION DATA FOR RUN 6

RUN #	r/R	O2	CO	CO2	SO2	CH4
2	1.00	4.6	23	16.8	50	0.004
6	0.29	5	23	16.4	120	0.003
8	0.50	4.6	18	16.9	140	0.003
10	0.79	5.5	16	16.1	135	0.003
12	0.13	5.1	22	16.4	90	0.003
14	1.00	3.5	13	17.8	140	0.003
16	0.29	4.25	16	17.3	140	0.003

Figure A9 Data summary for Parts I and II.
Note: All gas concentration data in ppm except values for O_2, CH_4, and CO_2.